



**UiT** The Arctic University of Norway

Faculty of Science and Technology

Department of Geosciences

**Sedimentology and architecture of a deep-water turbidite system;  
Kongsfjord Formation, Finnmark, northern Norway**

Lucie Alain

Master's thesis in Geology, GEO-3900

May 2022



## Abstract

The Kongsfjord Formation is a Late Precambrian deep-marine sedimentary succession exposed along the northern coastline of the Varanger Peninsula, northern Norway. Several studies in the 1970s and 1980s led to the recognition of the Formation as an ancient submarine fan system and to the identification of several architectural elements, including lobes and channels. However, there are no published work documenting bed type variability in detail and recent investigations of the lobes are lacking. This study is based on outcrop data, including stratigraphic logs and digital outcrop models collected in three localities. The recognition of eight bed types suggests that the Formation was deposited by various sediment density flows including high- and low-density turbidity flows, transitional flows and cohesive debris flows. The investigated outcrop sections comprise stacked lobes that record deposition in unconfined settings. Lobes have a two-fold architecture with a thin-bedded lower part and a thick-bedded upper part that record deposition in lobe fringe, off-axis and axis settings. Lobes commonly show thickening upward trends interpreted as recording lobe progradation. In the most proximal investigated areas, scours record sediment bypass and deposition in confined and semi-confined settings. Hybrid event beds interpreted as being deposited by transitional flows that transformed from turbulent to laminar flow conditions, occur in lobe fringe and lobe off-axis settings of the most distal areas. Two sub-types of hybrid event beds are observed throughout the Formation, suggesting that different mechanisms led to flow transformation. The distribution of hybrid event beds throughout the Kongsfjord Formation may reflect periods of slope disequilibrium and the dominant stacking patterns of lobes. Differences in lobe dimensions and stacking patterns between the investigated outcrop sections indicate differences in flow evolution and feeder channel geometry and stability. Thin, aggradationally to compensationally stacked lobes are deposited in slope-proximal settings. Thick, aggradationally to compensationally stacked lobes are deposited in distal basin-floor settings. The Kongsfjord Formation accumulated in a rift basin as part of N–NE prograding slope to basin-floor system comprising the overlying fluvio-deltaic successions of the Båsnæringen Formation. High sedimentation rates and slope instability are likely to be the main controls for the deposition of the Kongsfjord Formation turbidite system as coalescent lobes on the basin-floor.



## Foreword

I would like to thank my supervisor Sten-Andreas Grundvåg for supervision during the entire process of working on this thesis. I really appreciated your guidance and feedback. I would also like to thank my co-supervisor Julian Janocha for valuable help with the outcrop models and for feedback on my thesis.

I would like to thank Weiwei Shuai for assistance during long and rainy days in the field. I am very grateful for your help.

Thanks to my family and friends in Tromsø, France and elsewhere for the support and good time throughout my studies.

Lucie Alain

Tromsø, May 2022



# Table of Contents

1	Introduction .....	1
2	Geological framework.....	5
2.1	Tectonic development of the Varanger Peninsula.....	6
2.1.1	Rifting and basin development.....	6
2.1.2	The Trollfjorden–Komagelva Fault Zone .....	8
2.1.3	Timanian orogeny .....	8
2.1.4	Caledonian orogeny.....	9
2.2	Stratigraphy of the Varanger Peninsula.....	10
2.2.1	Stratigraphy of the Barents Sea Group.....	11
2.2.2	Stratigraphy of the Løkvikfjellet Group.....	12
2.3	The Kongsfjord Formation .....	12
3	Data and methods .....	14
3.1	Datasets.....	14
3.2	Methods .....	15
3.2.1	Fieldwork .....	15
3.2.2	Facies analysis and bed types.....	15
3.2.3	Processing of the DOMs .....	16
4	Results .....	18
4.1	Facies analysis and bed types .....	18
4.1.1	BT 1: Amalgamated turbidite beds .....	23
4.1.2	BT 2: Coarse-grained turbidite beds .....	24
4.1.3	BT 3: Thick-bedded turbidite beds.....	26
4.1.4	BT 4: Medium-bedded turbidite beds .....	28
4.1.5	BT 5: Thin-bedded turbidite beds .....	29

4.1.6	BT 6: Fine-grained turbidite beds .....	32
4.1.7	BT 7: Hybrid event beds .....	33
4.1.8	BT 8: Debrite beds .....	34
4.2	Depositional architecture and depositional environments.....	40
4.2.1	Architectural elements.....	40
4.2.2	Bed type associations .....	41
4.2.3	Nålneset.....	44
4.2.4	Veidnes.....	49
4.2.5	Seglommen.....	58
5	Discussion .....	65
5.1	Depositional sub-environments .....	65
5.1.1	Slope-proximal settings.....	65
5.1.2	Basin-floor settings .....	68
5.2	Distribution of hybrid event beds .....	72
5.2.1	Origin of HEBs.....	72
5.2.2	Controls on HEBs deposition.....	74
5.3	Controls on lobe deposition.....	76
5.3.1	Lobe dimensions .....	77
5.3.2	Lobe stacking patterns.....	79
5.4	Depositional model for the Kongsfjord Formation .....	81
5.5	Comparison with other submarine fan systems.....	83
6	Conclusions .....	87
7	Future research .....	89
	References .....	90
	Appendix 1: Stratigraphic logs.....	104
	Appendix 2: Digital outcrop models .....	106





# 1 Introduction

Subaqueous sediment density flows are volumetrically the most important flow process for transporting sediments across the surface of Earth (Talling et al., 2015). They contribute to the formation of canyons and channel-levee systems and deposit submarine fan systems that can extend far into the deep ocean. Their deposits are valuable records of climatic, eustatic and tectonic changes and may form important hydrocarbon reservoirs that are targets for exploration. Sediment density flows are difficult to monitor directly due to their location and unpredictable occurrence. Few direct measurements of sediment density flows have been obtained by cable breaks and instruments (e.g., the 1929 Grand Banks event, the 1979 Nice event, the 2006 Pingtung event offshore SW Taiwan; Mulder et al., 1997; Piper et al., 1999; Hsu et al., 2008). Therefore, much of the present understanding of sediment density flows and their deposits comes from modern sea floor studies (e.g., Normark, 1970, 1978; Mulder et al., 1997; Wynn et al., 2002; Gervais et al., 2006; Deptuck et al., 2008) or from preserved ancient outcrops (e.g., Bouma, 1962; Mutti & Ricci Lucchi, 1972, 1978; Hodgson et al., 2006; Tinterri & Tagliaferri, 2015).

The description of deep-marine graded sandstone beds in the northern Apennines by Kuenen and Migliorini (1950) led to a revolution in the field of deep-water research. These beds were interpreted as deposited by turbidity currents defined as sediment-laden flows that travel down current due to their excess densities. The term ‘turbidites’ was introduced by Kuenen (1957) to describe these deposits. These revolutionary works led to numerous studies of subaqueous sediment density flows and their deposits. Combined field studies and laboratory experiments resulted in several facies schemes (e.g., Bouma, 1962; Mutti & Ricci Lucchi, 1972; Middleton & Hampton, 1973; Walker, 1978; Lowe, 1982). Based on these studies, the concept of turbidity current progressively evolved to include a wide range of flow types that occur in deep-water systems such as high- and low-density turbidity flows, debris flows (Middleton & Hampton, 1973; Carter, 1975; Lowe, 1982) and more recently slurry and transitional flows (Lowe & Guy, 2000; Haughton et al., 2003; Baas & Best, 2008; Haughton et al., 2009). The study of both modern and ancient submarine fan systems also led to the construction of several predictive depositional models for sediment density flows. Amongst the most influential fan models are the ones developed by Normark (1970) based on modern submarine fan systems offshore California and Mexico and by Mutti and Ricci Lucchi (1972, 1975) and Walker (1978) based

on outcrop studies of preserved ancient submarine fan systems in the Apennines, Pyrenees, Appalachians and in California. These models led to the recognition of different architectural elements: lobes, channels, interchannels; and of distinct sub-environments: inner, middle and outer fan. In the following years, these models formed the basis of the study of submarine fan systems.

High resolution bathymetric and seismic studies have provided valuable information on the morphology of submarine fan systems and enabled the recognition of architectural elements based on the identification of their geometries (Normark, 1978; Pickering et al., 1995; Prather et al., 2000; Sprague et al., 2005; Gervais et al., 2006; Deptuck et al., 2008). However, the development of bathymetric and seismic studies also led to the questioning of the classical submarine fan models because of the difficulties in comparing modern and ancient systems (e.g., Bouma et al., 1985; Mutti & Normark, 1987; Mutti & Normark, 1991; Piper & Normark, 2001). Submarine fan systems can differ greatly from each other and their characteristics depend on the interaction of several factors such as basin morphology, tectonics, sediment supply, eustasy and climate (Bouma, 2004; Mutti et al., 2009). Thus, detailed stratigraphic analysis of individual submarine fan system is necessary to understand their deposits and associated formative processes. Recent studies of ancient submarine fan systems focus on the recognition of the hierarchic order of depositional elements and their facies associations (e.g., Amy & Talling, 2006; Hodgson et al., 2006; Prélat et al., 2009; Cunha et al., 2017; Tinterri & Piazza, 2019; Piazza & Tinterri, 2020). These studies showed that detailed facies analysis combined with stratigraphic analysis is a key to understanding ancient submarine fan systems and the controls on their formation.

In the last decades, lobes have been extensively studied across various submarine fan systems (e.g., Deptuck et al., 2008; Prélat et al., 2009; Bourget et al., 2010; Grundvåg et al., 2014; Marini et al., 2015; Brooks et al., 2018b; Piazza & Tinterri, 2020; Zhang & Li, 2020; Rohais et al., 2021). Lobes are the most down-dip elements and the largest depositional bodies of submarine fan systems and record changes in climatic, eustatic and tectonic conditions (Mulder & Etienne, 2010; Prélat et al., 2010). Seismic and bathymetric studies have provided better insight to the internal architecture of lobes and resulted in several hierarchical classifications (e.g., Gervais et al., 2006; Deptuck et al., 2008). However, these studies are limited by the low-resolution of seismic data and often lack the high-resolution documentation of facies

distributions permitted by outcrop studies. Recent outcrop studies have particularly focused on lobe stacking patterns and documented thickening and coarsening upward trends (e.g., Prélat et al., 2009; Macdonald et al., 2011a). These trends can be used to understand the evolution of lobe deposition through time and space. It has been observed that lobes can have complex geometries, depositional architectures, facies distribution and stacking patterns (e.g., Gervais et al., 2006; Hodgson et al., 2006; Deptuck et al., 2008; Prélat et al., 2009; Prélat et al., 2010; Etienne et al., 2012; Grundvåg et al., 2014; Piazza & Tinterri, 2020). These characteristics can vary consequently even within a single submarine fan system (Deptuck et al., 2008; Etienne et al., 2012; Marini et al., 2015) and give insights to the factors controlling the deposition of lobes.

This study investigates the Kongsfjord Formation, a Neoproterozoic deep-marine sedimentary succession that crops out on the Varanger Peninsula, northern Norway (Fig. 2.1). The Formation consists mainly of interbedded sandstone and mudstone and has been interpreted as an ancient submarine fan system by several authors (Pickering, 1985; Drinkwater et al., 1996). The Formation has been extensively studied in the 1970s and 1980s (Siedlecka, 1972; Pickering, 1979, 1981, 1982a, 1983). These studies recognised different architectural elements including channels and sheets and interpreted depositional sub-environments such as middle, transitional and outer fan areas. The Formation has also been used as an analogue for hydrocarbon reservoirs (Drinkwater & Pickering, 2001). However, these studies were most likely influenced by the classical submarine fan models of Mutti and Ricci Lucchi (1972) and Walker (1978). Since these descriptions, major advances in the understanding of subaqueous sediment density flows and their deposits have been made, particularly with the increased understanding of flow behaviour, flow transformation leading to the deposition of hybrid event beds, and lobes and their internal architecture. Thus, a re-investigation of the Kongsfjord Formation is needed in order to put the succession within the perspective of the state-of-art of deep-water research. The objectives of this thesis are therefore the following:

- Investigate the sedimentology and architecture of the Kongsfjord Formation and determine the processes under which the succession accumulated. What types of sediment density flows deposited the succession? Did the entire Formation deposit under turbidity flows or are there signs of flow transformation and deposition by other types of sediment density flows?

- Identify and characterise the architectural elements of the Kongsfjord Formation and determine their origin. What are their internal architecture and their depositional environments?
- Characterise lobes of the Kongsfjord Formation and determine what factors controlled their internal architecture. Is there cyclicity in lobe stacking patterns? Do lobes show similar characteristics across the Formation? What are the controls on their deposition?

## 2 Geological framework

The Varanger Peninsula is located in north-eastern Finnmark, in northern Norway (Fig. 2.1A). It is bounded by Tanafjorden to the west, the Barents Sea to the north, and Varangerfjorden to the south and to the east. The Varanger Peninsula comprises well exposed sedimentary successions (Fig. 2.1B). These successions most likely accumulated in rift-basins during the Late Precambrian (Drinkwater et al., 1996; Roberts & Siedlecka, 2002; Røe, 2003; Nystuen, 2008). They were later affected by several episodes of deformations during the Timanian and particularly the Caledonian orogeny (Herrevold et al., 2009). The present-day geology of the Varanger Peninsula thus reflects a complex tectonic and stratigraphic history outlined in the following sections.

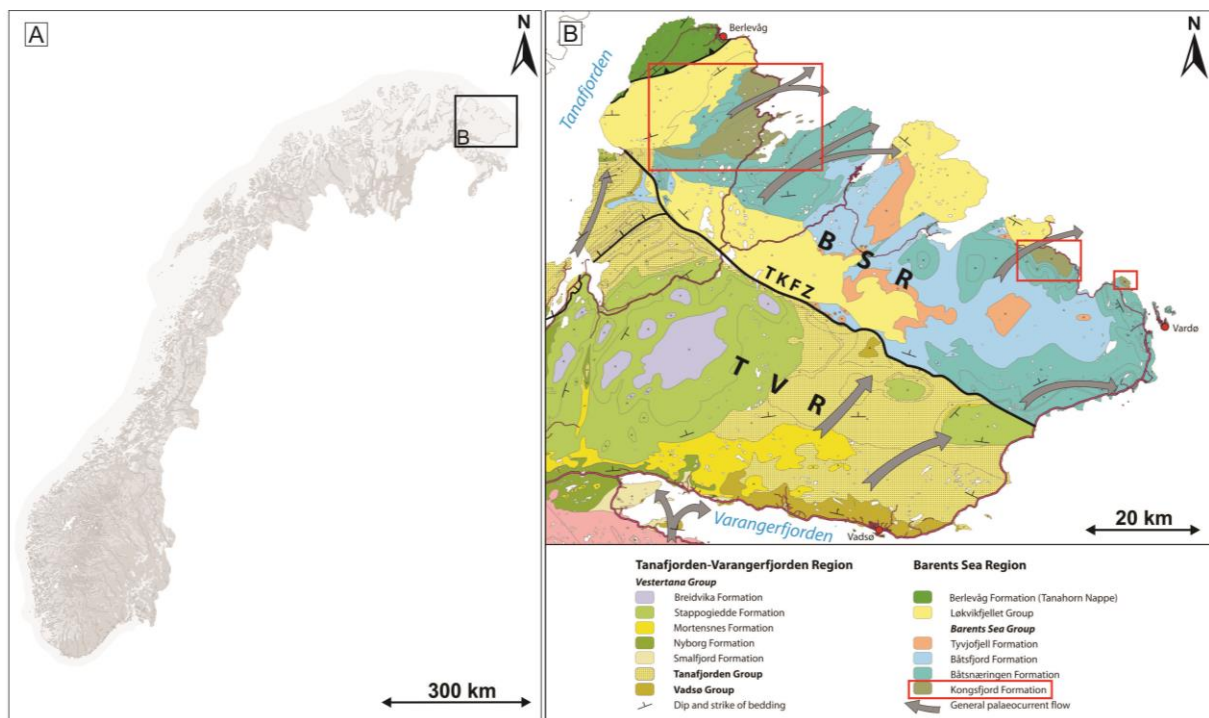


**Figure 2.1:** (A) Topographic map of Norway showing the location of the Varanger Peninsula. Source map: NMA (2021a). (B) Simplified geological map of the Varanger Peninsula. The principal paleocurrent directions are indicated by grey arrows. TKFZ - Trollfjorden–Komagelva Fault Zone; BSR- Barents Sea Region; TVR-Tanafjorden–Varangerfjorden Region. Red squares highlight the main outcrop areas of the Kongsfjord Formation. Modified after Roberts and Siedlecka (2012).

## **2.1 Tectonic development of the Varanger Peninsula**

### **2.1.1 Rifting and basin development**

The sedimentary successions from the Varanger Peninsula most likely accumulated in a passive, extensional margin on the northeastern margin of Baltica during the break-up of the late Precambrian supercontinent Rodinia (Roberts & Siedlecka, 2002; Nystuen et al., 2008). Rodinia presumably formed during the Meso-Proterozoic after the collision of the existing cratons and existed from ca. 1100 Ma until ca. 860 Ma when the cratons started to break apart (Li et al., 2008; Bogdanova et al., 2009). The break-up of the supercontinent was possibly initiated by a superplume that led to continental arching and rifting (Li et al., 1999; Li et al., 2008; Bogdanova et al., 2009). During the rifting phase, several basins formed on the future margins of the cratons. The active rift basins gradually turned into passive margins during the Mesoproterozoic, allowing considerable volumes of sediment to be deposited, including the successions cropping out in the Varanger Peninsula (Drinkwater et al., 1996; Nystuen et al., 2008).

Meso- and Neoproterozoic sedimentary successions can be followed from the Varanger Peninsula to the Timan Range in western Russia through the Rybachi and Kanins Peninsulas constituting the 1800 km long, NW–SE trending Timan–Varanger Belt (Roberts & Siedlecka, 2002). These successions accumulated in two distinct active domains along the northeastern faulted margin of Baltica, one of Rodinia's cratons (Siedlecka & Roberts, 1992; Roberts & Siedlecka, 2012). On the Varanger Peninsula, the sedimentary successions from the two domains are separated by a major regional lineament: the Trollfjorden–Komagelva Fault Zone (TKFZ). On the southwestern part of the fault zone, sediments accumulated in a pericratonic domain (the Tanafjorden–Varangerfjorden Region, TVR, in Fig. 2.1B), while successions from the northeastern part of the fault (the Barents Sea Region, BSR, in Fig. 2.1B) accumulated in a basinal domain (Siedlecka & Roberts, 1992; Drinkwater et al., 1996; Roberts & Siedlecka, 2002; Nystuen et al., 2008).

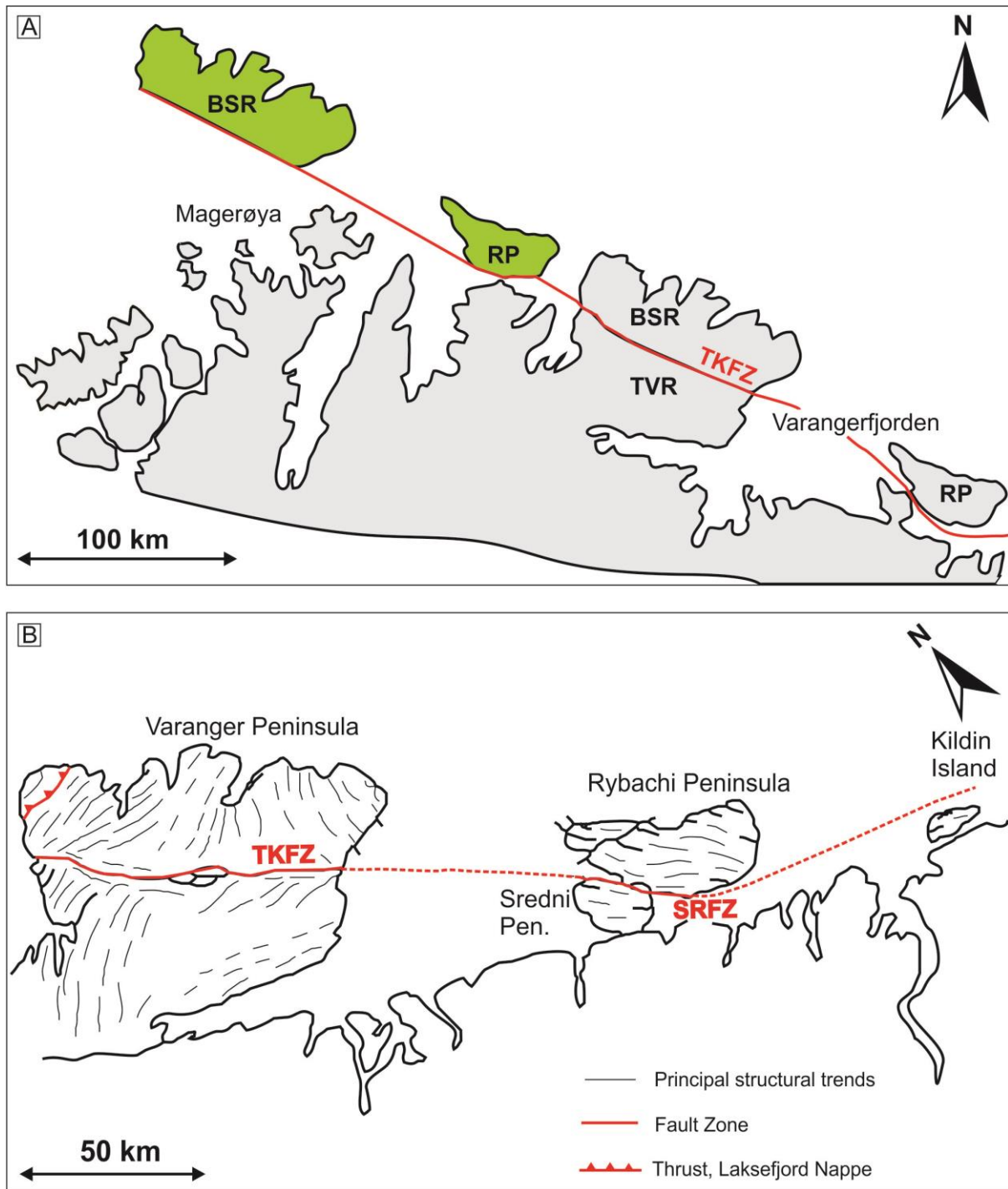


**Figure 2.2:** (A) Outline map showing the inferred original locations of the Barents Sea Region (BSR) and the Rybachy Peninsula (RP) prior to translation (in green) along the Trollfjorden–Komagelva Fault Zone (TKFZ) and juxtaposition with the Tana–Varangerfjorden Region (TVR) during the Caledonian deformation event. Redrawn from Roberts and Siedlecka (2012). (B) Outline map showing the principal structural trends (mostly axial surfaces of folds) of the Varanger, Rybachy and Sredni Peninsulas. Redrawn from Roberts and Siedlecka (2002).



### **2.1.2 The Trollfjorden–Komagelva Fault Zone**

The NW–SE trending TKFZ is one of the most prominent structural features of the Varanger Peninsula, forming a more than 75 km long and up to 5 km wide lineament which separates the TVR to the south of the fault from the BSR to the north of the fault (Figs. 2.1B and 2.2). The TKFZ extends north-westwards to the south of the Nordkinn Peninsula and offshore onto the shelf north of Magerøya (Fig. 2.2A; Gabrielsen et al., 1987). To the southeast, the fault zone can be traced in western Russia between the Rybachi and Sredni Peninsulas linking up with the Sredni–Rybachi Fault Zone (Fig. 2.2B; Siedlecka & Roberts, 1992; Roberts, 1995). The fault most likely originated during the Archean time so it probably played an active role in the formation of rift basins along the margins of Baltica during the break-up of Rodinia (Herrevold et al., 2009). It functioned as a normal fault during the passive sedimentation in the Meso- and Neoproterozoic and was later reactivated during several tectonic episodes from Precambrian to Cenozoic times (Siedlecka & Siedlecki, 1967; Herrevold et al., 2009).

The TKFZ is currently considered to be a major dextral strike-slip lineament which experienced significant offset during the Caledonian orogeny (Fig. 2.2A; Rice et al., 1989; Roberts & Siedlecka, 2012). The structural deformation is different in the northern and southern regions. In the BSR, north of the TKFZ, three main sets of fractures striking NW–SE, N–S and ENE–WSW are recognised while in the TVR, south of the fault zone, the three main sets of fractures strike NNE–SSW, NW–SE and WNW–ESE (Fig. 2.2B). These structures have been attributed to several deformational episodes of which two major events correspond to the Timanian and the Caledonian orogeny (Roberts & Siedlecka, 2002; Herrevold et al., 2009). Two additional sets of faults and deformations are also seen and attributed to later reactivation episodes along the TKFZ (Herrevold et al., 2009; Roberts & Siedlecka, 2012).

### **2.1.3 Timanian orogeny**

A major set of NW–SW to NNW–SSE trending faults, mainly observed north of the TKFZ, has been attributed to contractional deformation during the Timanian Orogeny (Fig. 2.2B; Herrevold et al., 2009). The Timanian orogeny is a major collisional event that occurred mainly during the Ediacaran from ca. 600 Ma to 560 Ma (Roberts & Siedlecka, 2002; Roberts et al., 2004). The sedimentary successions deposited along the margin of Baltica were involved in a

collisional event against this same northeastern margin. It coincides with the conversion of the passive margin of Baltica in which sedimentary successions accumulated into an active, compressional margin (Roberts & Siedlecka, 2002). This resulted in several tectonic deformation structures visible along the Timan–Varanger Belt. The Timanian orogeny also resulted in arc magmatic intrusions from which remnants can be found in the eastern part of the Timan–Varanger Belt (Roberts & Siedlecka, 2002). In the Varanger Peninsula, the deformations mostly occur in the northeastern part of the Peninsula (Herrevold et al., 2009).

#### **2.1.4 Caledonian orogeny**

A major set of structures trending NE–SW to ENE–WSW observed across the Varanger Peninsula has been attributed to a second major deformational episode during the Caledonian orogeny (Fig 2.2B; Herrevold et al., 2009). The Caledonian Orogeny started in the early Ordovician and culminated during the Mid Silurian to Early Devonian (Gee et al., 2008). In the Varanger area, the Caledonian deformation caused dextral strike-slip displacement along the TKFZ (Rice & Frank, 2003; Nystuen et al., 2008; Herrevold et al., 2009; Roberts & Siedlecka, 2012). Sedimentary successions of the BSR were displaced along the TKFZ to their present-day location and juxtaposed with successions of the TVR (Fig. 2.2A). The displacement was first estimated to be of the order of 500–1000 km by Kjøde et al. (1978) on the basis of paleomagnetic data and then reviewed to approximately 250 km by Bylund (1994).

The Caledonian Orogeny also corresponds with the intrusion of several mafic dykes that cut into Formations of the Varanger Peninsula (Beckinsale et al., 1976; Rice & Frank, 2003; Rice et al., 2004; Herrevold et al., 2009; Nasuti et al., 2015). These dykes mainly occur in the BSR and have been dated of Late Proterozoic and Early Cambrian ages (Siedlecka & Roberts, 1992). They were probably emplaced prior to the deformation or during the initial phase of the Caledonian orogeny. A set of cleavages and folds in the sedimentary successions have also been attributed to the Caledonian Orogeny (Herrevold et al., 2009). Rice and Frank (2003), based on Ar/Ar ages, estimated cleavages in the mudstones of the Løkvikfjellet Group to be of Late Ordovician age.

Sedimentary successions of the BSR and the TVR were affected by possibly several episodes of reactivation after the Caledonian orogeny through the Late Palaeozoic and the Mesozoic

(Siedlecka et al., 2004; Nystuen et al., 2008; Herrevold et al., 2009). Some of these episodes probably caused the intrusion of younger dolerite dykes. Roberts (2011) re-interpreted U-Pb ages on zircons from a dolerite dyke cutting sandstones of the Løkvikfjellet Group in Hamningberg to be of Late Devonian age. This dyke, similar to other dolerite dykes from the Varanger and the Rybachi Peninsulas was thus interpreted as having formed during an episode of post Caledonian deformation.

## **2.2 Stratigraphy of the Varanger Peninsula**

The Tanafjorden–Varangerfjorden Region (TVR), southwest of the TKFZ, consists of ca. 4000 m thick sedimentary successions resting unconformably on crystalline Precambrian bedrock (Siedlecka & Roberts, 1992; Røe, 2003; Roberts & Siedlecka, 2012). The successions are autochthonous to para-autochthonous and comprise three stratigraphic groups deposited in fluvial to shallow-marine environments: the Vadsø Group, the Tanafjorden Group, and the Vestertana Group. The Vestertana Group comprises two tillite-bearing horizons, including the renowned Bigganjargga tillite, indicating periods of glaciation (Siedlecka & Siedlecki, 1967; Siedlecka & Roberts, 1992; Røe, 2003). These units are not considered further in this thesis.

Northeast of the TKFZ, the Barents Sea Region (BSR) consists of a ca. 15000 m thick regressive sequence of mainly deep-marine to shallow-marine and fluvio-deltaic deposits including the Barents Sea Group and the Løkvikfjellet Group (Fig. 2.3). On the western side of the Varanger Peninsula, a NE–SW oriented thrust zone separates the Løkvikfjellet Group from the overlying Berlevåg Formation (Fig. 2.2B). The Berlevåg Formation which consists of low-grade green-schist-facies has been suggested to be part of the Laksefjord Nappe Complex which was thrust upon successions of the BSR during the Caledonian orogeny (Kirkland et al., 2008). The successions from the TVR and the BSR are in contact on the western side of the peninsula where formations of the Vadsø Group unconformably overly formations of the Barents Sea Group (Rice, 1994).

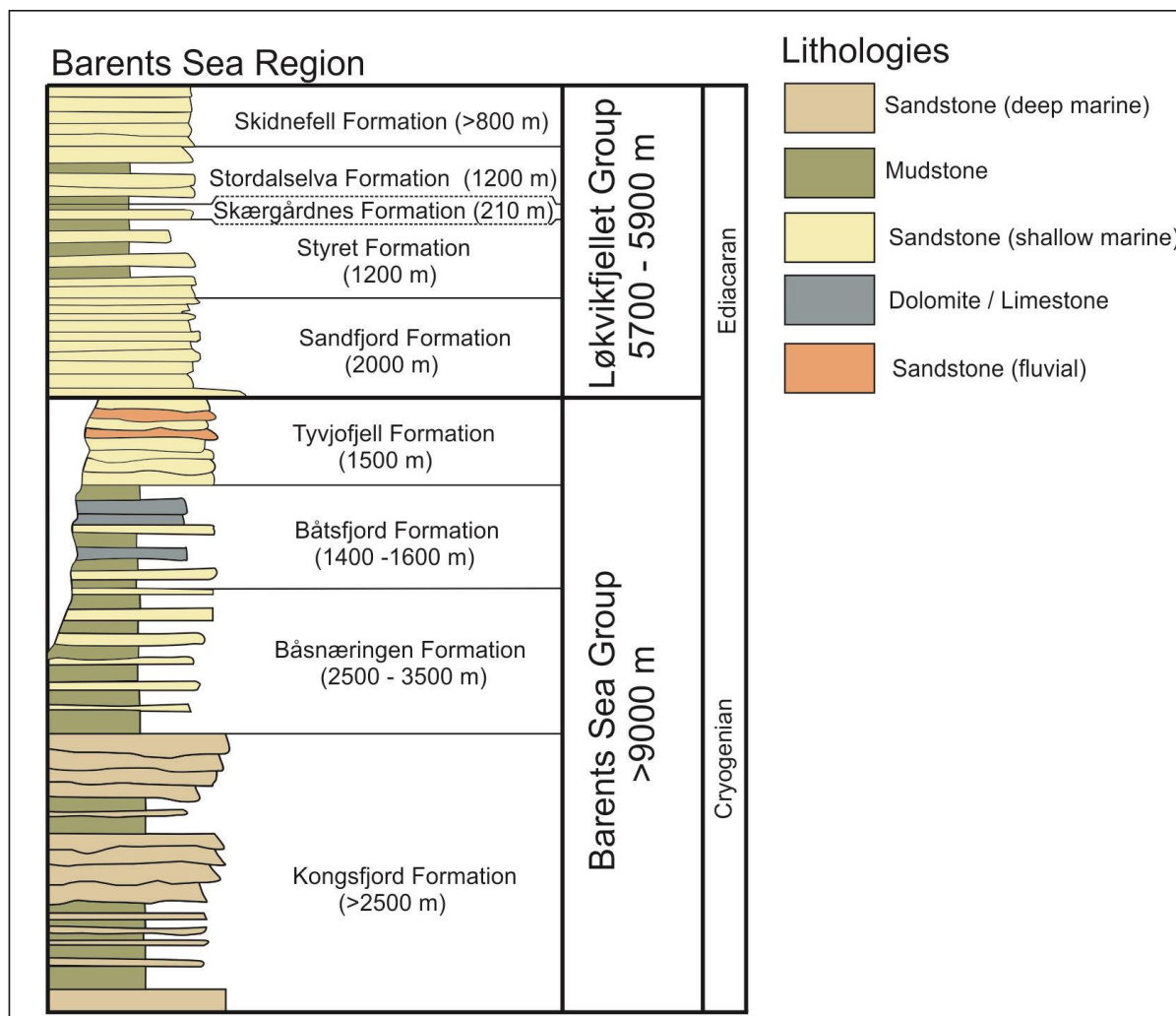


**Figure 2.3:** Lithostratigraphy of the Barents Sea Region. Redrawn from Nystuen (2008).

### 2.2.1 Stratigraphy of the Barents Sea Group

The lowermost unit of the BSR, the Barents Sea Group is an approximately 9000 m thick succession which has been subdivided into four formations (Fig. 2.3). The Kongsfjord Formation, the focus of this thesis, is the lowermost unit of the group. It consists mainly of interbedded sandstone and mudstone which was deposited as a series of submarine fans on the basin floor (Pickering, 1979, 1981, 1982a, 1983, 1985; Drinkwater & Pickering, 2001). The base of the formation is not exposed anywhere and its thickness has been first approximated to 4500 m by Siedlecka and Siedlecki (1967) but has later been re-estimated to ca. 3200 m by Pickering (1979). The Båsnæringen Formation which overlies the Kongsfjord Formation is an approximately 3500 m thick succession of interbedded sandstones and mudstones interpreted

as having accumulated in prodelta, delta front and delta plain environments (Fig. 2.3). The whole succession thus represents the progradation of the Båsnæring Formation delta system probably feeding and later prograding across the underlying submarine fans of the Kongsfjord Formation (Siedlecka & Edwards, 1980; Pickering, 1982b, 1984; Siedlecka et al., 1989; Hjellbakk, 1993; Hjellbakk, 1997). The 1500 m thick succession of interbedded sandstone and mudstone, dolomite and stromatolite-bearing limestone of the Båtsfjord Formation overlies conformably the Båsnæringen Formation (Fig. 2.3). The succession consist of shallow marine and tidally influenced deposits (Siedlecka & Roberts, 1992). The overlying Tyvjofjell Formation shows predominantly sandstone beds interpreted as representing deposition in a shallow-marine environment with possible fluvial incursions (Siedlecka & Roberts, 1992).

### **2.2.2 Stratigraphy of the Løkvikfjellet Group**

The Løkvikfjellet Group overlays unconformably the successions of the Barents Sea Group. It is approximately 5700 m thick and comprises the Sandfjorden, Styret, Skjærgårdnes, Stordalselva, and Skidnefjellet Formations (Fig. 2.3). It consists predominantly of cross-bedded and wave-rippled sandstones interbedded with siltstones and mudstones interpreted as shallow-marine deposits with subordinate fluvial deposits (Siedlecki & Levell, 1978; Siedlecka & Roberts, 1992). This group is not considered further in this thesis.

## **2.3 The Kongsfjord Formation**

The first description of the successions of the Varanger Peninsula was done by Holtedahl (1918) who identified rocks in the Kongsfjord area as a series of shales, the “Kongsfjords skiferserie” (p. 188). No work was done until the mid-1960s, when in an attempt to describe the lithostratigraphic successions of the Varanger Peninsula, Siedlecka and Siedlecki (1967) described the Kongsfjord Formation as a series of mudstones, slates and sandstones showing a variety of sedimentary features such as graded beds, load casts, ripple marks. The first interpretation of the formation was made by Siedlecka (1972) who described the Kongsfjord Formation as a flysch sequence comprising graded sandstone and mudstone beds deposited by turbidity currents. Later in the 1970s and 1980s, a massive step forward in the understanding of the unit was made after a series of papers by Pickering (1979, 1981, 1982a, 1983, 1985).

Based on field investigations, he described the formation as a 3.2 km succession of sediment density flow deposits. Pickering was the first author to recognise the Kongsfjord Formation as an ancient submarine fan system and identified several distinct sub-environments. Based on the differences in sedimentary features and analogy with other ancient submarine fans systems, Pickering (1985) defined inner, middle, outer and transitional fan environments. Additional field investigations were carried out by Drinkwater et al. (1996) and Drinkwater and Pickering (2001) who identified architectural elements within the Kongsfjord Formation submarine fan system, including sheets and channels. Drinkwater and Pickering (2001) also discussed the possible application of the Kongsfjord Formation as an analogue for hydrocarbon reservoir modelling.

### 3 Data and methods

#### 3.1 Datasets

The dataset consists of 29 stratigraphic logs, detailed photographic coverage and digital outcrop models (DOMs), including one gathered by Julian Janocha (UiT) using a DJI Mavic 2 Pro drone. Fieldwork was carried out in three localities where the Kongsfjord Formation crops out along coastal sections: Seglodden in the eastern/northeastern part of the Varanger peninsula, and the Veidnes and Nålneset locations to the north/northwest of the peninsula (Fig. 3.1). The three localities allow detailed description of sedimentological features from laminae- and bed-scale to macro-scale depositional elements. Because many outcrops are structurally deformed (tilted, faulted, folded, etc.), partially eroded or scree covered, the selection of the measured sections was mainly based on the visually determined quality of the outcrop.

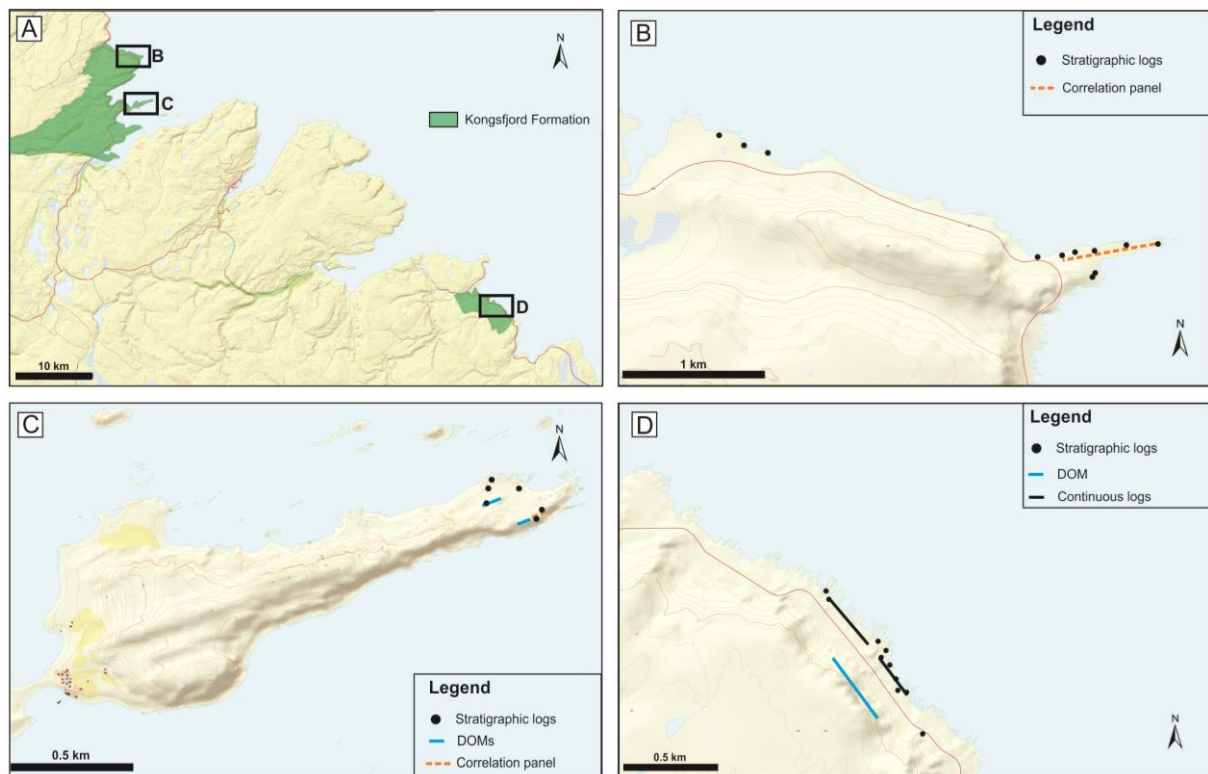


**Figure 3.1:** (A) Study area showing the three studied localities. Green area represents the outcrop area of the Kongsfjord Formation. Details of the datasets in (B) Nålneset; (C) Veidnes; and (D) Seglodden. Background maps: NMA (2021b).

## **3.2 Methods**

### **3.2.1 Fieldwork**

Fieldwork consisted in measuring stratigraphic logs and acquiring extensive photographic coverage in the three outcrop localities. The stratigraphic logs record lithology and facies, grain size (based on field observations), sedimentary structures, sorting, bed geometry and bed thickness.

In Nålneset, five logs from the eastern sector have been used to construct a 680 m long correlation panel of the NE–SW oriented section with particular focus on the lateral thicknesses and grain size variations (Fig. 3.1B). The lateral correlation panels were constructed based on the recognition of key units (i.e., thick-bedded and amalgamated units) and bed by bed correlation. In Veidnes, two logs measured along the southern coastline have been used to construct a 30 m long correlation panel of a SW–NE oriented section (Fig. 3.1C). In addition, overlapping photos were acquired to construct two DOMs in order to document the lateral changes in bed thickness and grain size (see Fig. 3.1C for location). The photos were taken with sufficient overlap (> 80 %) to ensure a good resolution of the model. In Seglodden, the excellent exposure along the coastline allowed the documentation of vertical changes and trends in bed thickness, grain size, degree of amalgamation and scouring along two continuous logs covering ca. 250 and ca. 310 m of stratigraphy each (Fig. 3.1D).

### **3.2.2 Facies analysis and bed types**

Based on field observations and post-fieldwork analysis of the stratigraphic logs, a series of recurrent sedimentary facies have been recognised in the Kongsfjord Formation (Table 1). These facies represent the basic building block of individual event beds (Table 2). The recognition and division of event beds follow well-established principles from the literature (e.g., Haughton et al., 2009; Muzzi Magalhaes & Tinterri, 2010; Cunha et al., 2017; Pierce et al., 2018; Tinterri & Piazza, 2019). This allowed to deduct a number of characteristics for each locality including sandstone/mudstone percentage, percentage of bed types (by occurrence and thickness), and percentage of beds exhibiting sole marks. The sandstone/mudstone percentage was based on grain size analysis reported from field observations. Potential sources of errors in the bed type identification might be induced by altered outcrop quality due to weathering and



post-deformational structures that resulted in poor outcrop description. In addition, the division into bed types have to a certain degree a subjective component to it, which may result in biased observations and bed type classifications.

### **3.2.3 Processing of the DOMs**

The DOMs from Veidnes and Segludden (the latter was processed by Julian Janocha) were constructed using Agisoft Metashape Professional software. The processing was done in several steps. The first step is the alignment of the photos where Metashape matches feature points along the photos to generate a sparse point cloud (Fig. 3.2A and B). Then, Metashape extends the sparse point cloud to a dense point cloud based on estimations of the camera positions (Fig. 3.2C) and then generates a mesh (Fig 3.2D). Finally, a texture layer is generated by projection of the photos to the mesh (Fig. 3.2E). Because the photos used to construct the models from Veidnes are not georeferenced, geographic coordinates were added to the DOM at a later stage based on field measurements.

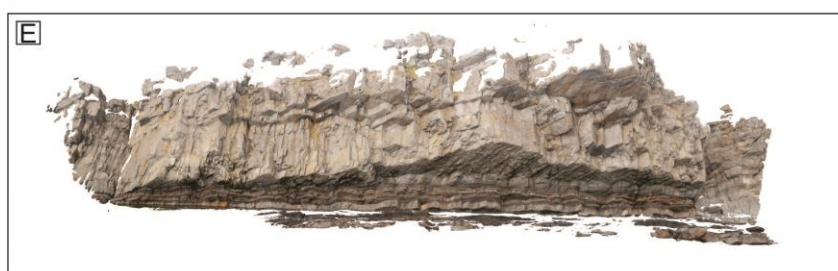
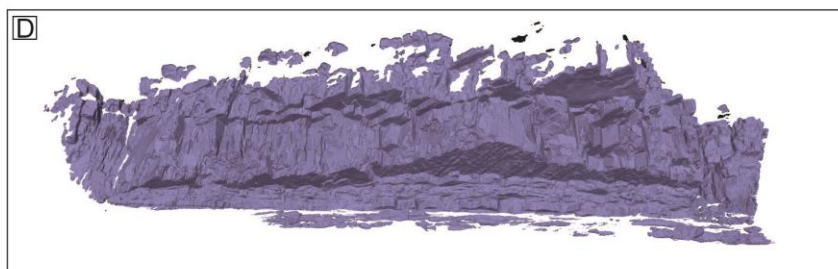
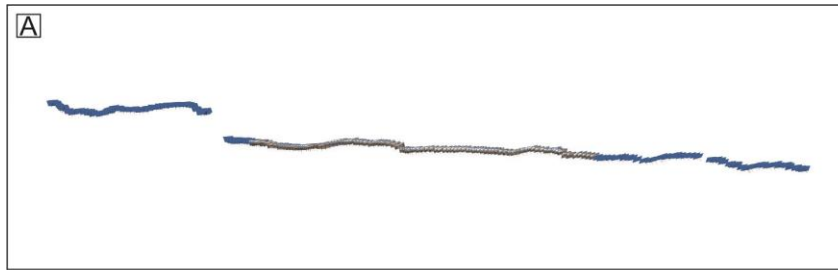


**Figure 3.2:** Step by step processing of the DOMs in Agisoft Metashape illustrated using one of the Veidnes DOM. (A) Aligned photos indicated by blue squares. (B) Sparse point cloud. (C) Dense point cloud. (D) Mesh. (E) Textured model.

## **4 Results**

### **4.1 Facies analysis and bed types**

At outcrop scale, facies divisions record changes in grain size, lithology and sedimentary structures and thus reflect changes in flow conditions. A total of 11 sedimentary lithofacies have been recognized in the Kongsfjord Formation whose characteristics are given in Table 1.

Beds have been identified based on the recognition of bounding surfaces. The contact above and below is either an accretionary or an erosional bounding surface (Campbell, 1967). In the Kongsfjord Formation, beds have been categorized into eight bed types mainly based on their different lithofacies assemblages and thicknesses (see Fig. 4.1 and Table 2). Four main categories are observed: amalgamated beds or units, turbidite beds, hybrid-event beds (HEBs) and debrite beds. Amalgamated beds may result from more than a single flow but are used when the recognition of bounding surfaces and the identification of single beds is problematic in the field due to a high degree of amalgamation. Turbidite beds are sub-divided into five sub-categories (coarse-grained, thick-, medium- and thin-bedded and fine-grained) based on the difference in bed thicknesses and grain sizes, which reflect changes in flow conditions. HEBs are bipartite beds that record an abrupt or progressive change in flow behaviour from turbulent to cohesive flows. Debrite beds are clast-rich conglomerates that record deposition by cohesive debris flows.

**Table 1:** Summary of the sedimentary lithofacies recognised in the Kongsfjord Formation.







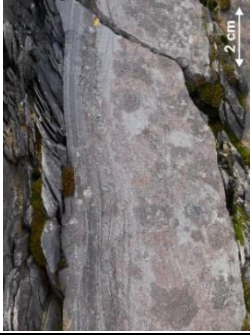
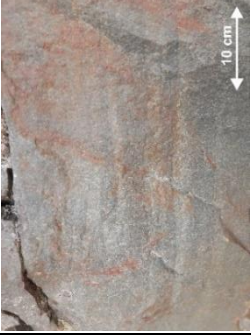
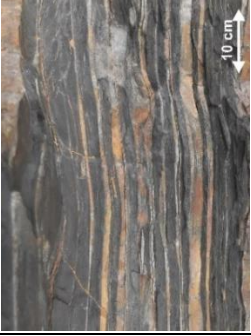
Facies	Lithology and grain size	Description	Process interpretation	References	Field expression
1	Matrix supported muddy conglomerate.	Mud-rich, very fine-grained sandstone matrix with various clasts. The majority of the clasts consists of quartz pebbles of highly variable roundness with no apparent orientation. Intraformational laminated mudstone clasts are abundant and larger clasts (up to 50 cm) occur occasionally.	<i>En masse</i> deposition by a cohesive debris flow.	Lowe (1982); Mulder and Alexander (2001).	
2	Matrix supported sandy conglomerate.	Medium to fine-grained sandstone matrix with various clasts. Clasts consist mainly of sub-horizontal oriented quartz pebbles to cobbles of variable roundness.	Traction deposition from a high-density turbidity flow or <i>en masse</i> deposition by a cohesive debris flow.	Corresponds to facies A1 of Mutti (1979).	
3	Clast supported conglomerate with medium-grained sandstone matrix.	Clasts consist mainly of quartz pebbles to cobbles of variable roundness and generally with no apparent orientation. Poorly developed imbrication occurs.	Traction deposition from a high-density turbidity flow.	Corresponds to the S1 division of Lowe (1982).	

Table 1: (continued)

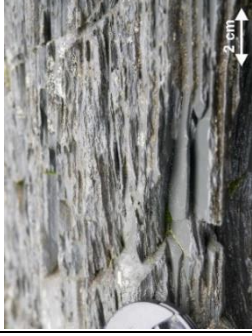

Facies	Lithology and grain size	Description	Process interpretation	References	Field expression
4	Very coarse- to medium-grained sandstone.	Plane-parallel stratified sandstone. The stratified layers of coarser sandstone are 5 to 15 cm. Occasionally, layers of aligned intraformational mudstone clasts occur.	Traction carpet underneath a high-density turbidity flow.	Corresponds to the S2 division of Lowe (1982).	
5	Coarse- to fine-grained sandstone.	Massive, ungraded to poorly graded, sharply based sandstone. The base of the bed is frequently loaded and/or exhibiting flute casts or groove casts. In places, mudstone clasts occur near the base of bed.	Rapid deposition by suspension settling from a high-density turbidity flow (Bouma, 1962; Lowe, 1982) or <i>en masse</i> deposition by a liquefied, sandy debris flow (Shanmugam, 1996).	Corresponds to the Ta division of Bouma (1962) and S3 division of Lowe (1982).	
6	Fine- to very fine-grained sandstone.	Plane-parallel laminated sandstone.	Traction deposition from a low-density turbidity flow under upper flow regime conditions.	Corresponds to the Tb division of Bouma (1962).	

**Table 1:** (continued)

Facies	Lithology and grain size	Description	Process interpretation	References	Field expression
7	Fine to very fine-grained sandstone.	Current ripple cross-laminated sandstone.	Traction deposition from a low-density turbidity flow under lower flow regime conditions.	Corresponds to the Tc division of Bouma (1962).	
8	Siltstone.	Undifferentiated massive to plane-parallel laminated siltstone. Locally, convolute laminations and soft sediment deformations occur.	Suspension settling from a fine-grained low-density turbidity flow.	Corresponds to the Td division of Bouma (1962) and to the T1 to T5 divisions of Stow and Shanmugam (1980).	
9	Siltstone to very fine-grained sandstone and interbedded mudstone.	Heterolithic units where the mudstone interbeds appear structureless and contain thin (0.5 to 1 cm), commonly convolute and irregular to planar siltstone laminae. Siltstone pseudonodules are locally embedded in the mudstone. Thicker (up to 2 cm) siltstone to sandstone beds show occasional internal plane-parallel or current ripple cross-lamination. Load casts occur locally.	Alternation between suspension settling of sand and silt from fine-grained low-density turbidity flows, occasionally with some traction, and mud fallout from mud-rich turbidity flows.	Corresponds to the Td division of Bouma (1962) and to the T1 to T5 divisions of Stow and Shanmugam (1980).	



**Table 1:** (continued)

Facies	Lithology and grain size	Description	Process interpretation	References	Field expression
10	Mudstone.	Undifferentiated massive to plane-parallel laminated mudstone.	Suspension settling by the dilute tail of a low-density turbidity flow or by hemipelagic fallout.	Corresponds to the Te division of Bouma (1962) and to the T6 to T8 divisions of Stow and Shanmugam (1980).	
11	Mud-rich sandstone.	Abundant load structures, folds, pseudonodules, various irregular sandstone patches and mudstone clasts in a heterogeneous mud-rich sandstone matrix.	<i>En masse</i> deposition by a cohesive debris flow.	Corresponds to the H3 division of Houghton et al. (2009).	

#### **4.1.1 BT 1: Amalgamated turbidite beds**

##### *Description*

This bed type consists mainly of thick (>1 m) sandstone beds with amalgamation surfaces being displayed either by a sharp grain size break (BT 1a); isolated mudstone clasts in the middle of the bed (BT 1b); or sharp breaks between successive interbeds (BT 1c; Fig. 4.1A). Type 1a beds consist of a basal sandstone unit (F5) overlain by a layer of clast supported conglomerate (F3). The transition between facies F5 and F3 shows an abrupt change in grain size across a sharp surface (Fig. 4.2A). Occasionally, the pebbly sandstone unit is grading upward into a finer, structureless sandstone (F5). Type 1b beds consist of very thick (> 3 m), ungraded massive sandstone beds (F5) exhibiting large isolated ‘floating’ mudstone clasts in the middle of the bed. Type 1c beds consist typically of two amalgamated, massive, ungraded sandstone interbeds (F5). The amalgamation surface is sharp and tabular, and the base of the upper sandstone is occasionally loaded (Fig. 4.2B). Typically, they form medium to thick beds (0.5 – 3 m).

##### *Interpretation*

These beds show signs of amalgamation between two and occasionally three sandstone beds. Because an amalgamation surface represents an erosive contact between two deposits, these amalgamated beds are deposited by a series of succeeding, highly erosive flows (Walker, 1966; Mattern, 2002). This bed type is dominated by massive medium- to fine-grained sandstone (F5) which suggests deposition by high-density turbidity flows (Bouma, 1962; Lowe, 1982). The clast supported conglomerate (F3) of BT 1a records traction deposition beneath a high-density turbidity flow (Lowe, 1982; Talling et al., 2012). Ho et al. (2018) suggested that pulses of increased velocity within a flow can result in coarsening intervals superimposed upon an overall normal graded profile. However, the distinction between amalgamated turbidites deposited by two or more erosive turbidity flows and multi-pulsed turbidites is challenging. BT 1b beds show isolated mudstone clasts in the middle of the bed, which presumably represent an amalgamation surface between two sandstone beds (Walker, 1966). However, Postma et al. (1988) showed that oversized floating mud clasts can glide along a rheological surface within a single high-density, bipartite turbidity flow. BT 1c beds record deposition by successive erosive high-density turbidity flows (Bouma, 1962; Walker, 1966).



#### **4.1.2 BT 2: Coarse-grained turbidite beds**

##### *Description*

Type 2 beds consist mainly of clast supported conglomerates and very coarse-grained sandstones. Two main sub-categories are observed (Fig. 4.1B). BT 2a beds consist of a graded sandstone division exhibiting a conglomerate base (F3) which passes upward into a coarse-grained sandstone division showing plane-parallel stratifications (F4; Fig 4.2C). Facies F4 locally includes layers of small (< 1 cm) aligned mudstone clasts (Fig. 4.1B). The upper part of BT 2a beds consists of finer-grained structureless sandstone (F5) occasionally grading into plane-parallel laminated sandstone (F6). This bed type is capped by a thin layer of mudstone (F10). BT 2a beds are typically very thick (>1 m). BT 2b beds consist of normal graded beds showing a basal interval of clast supported conglomerate (F3) passing upward into massive, coarse- to medium-grained sandstone (F5; Fig. 4.2D). These beds are typically thick (0.6 – 1 m). The base of the beds often exhibits flute casts.

##### *Interpretation*

These beds record the deceleration of high-density turbidity currents (Talling et al., 2012; Postma & Cartigny, 2014). The basal F3 facies, which is similar to the S1 division of Lowe (1982), suggests deposition by a dense basal layer in which turbulence is suppressed due to high sediment concentration. BT 2a beds exhibit a layer of stratified, very coarse- to coarse-grained sandstone above the basal conglomerate. These stratified layers are similar to the ‘spaced-lamination’ described by Hiscott and Middleton (1979, 1980) and the S2 division of Lowe (1982) and are interpreted as traction plus fallout deposition from high-density turbidity flows. Recent experimental studies showed that these spaced laminations reflect high basal sediment concentration and flow stratification (Cartigny et al., 2013; Postma & Cartigny, 2014). Thus, BT 2 beds record the deceleration of high-density turbidity flow, in which a dense basal layer deposits F3 and eventually F4 facies and the upper, more turbulent part of the flow deposits F5 facies.

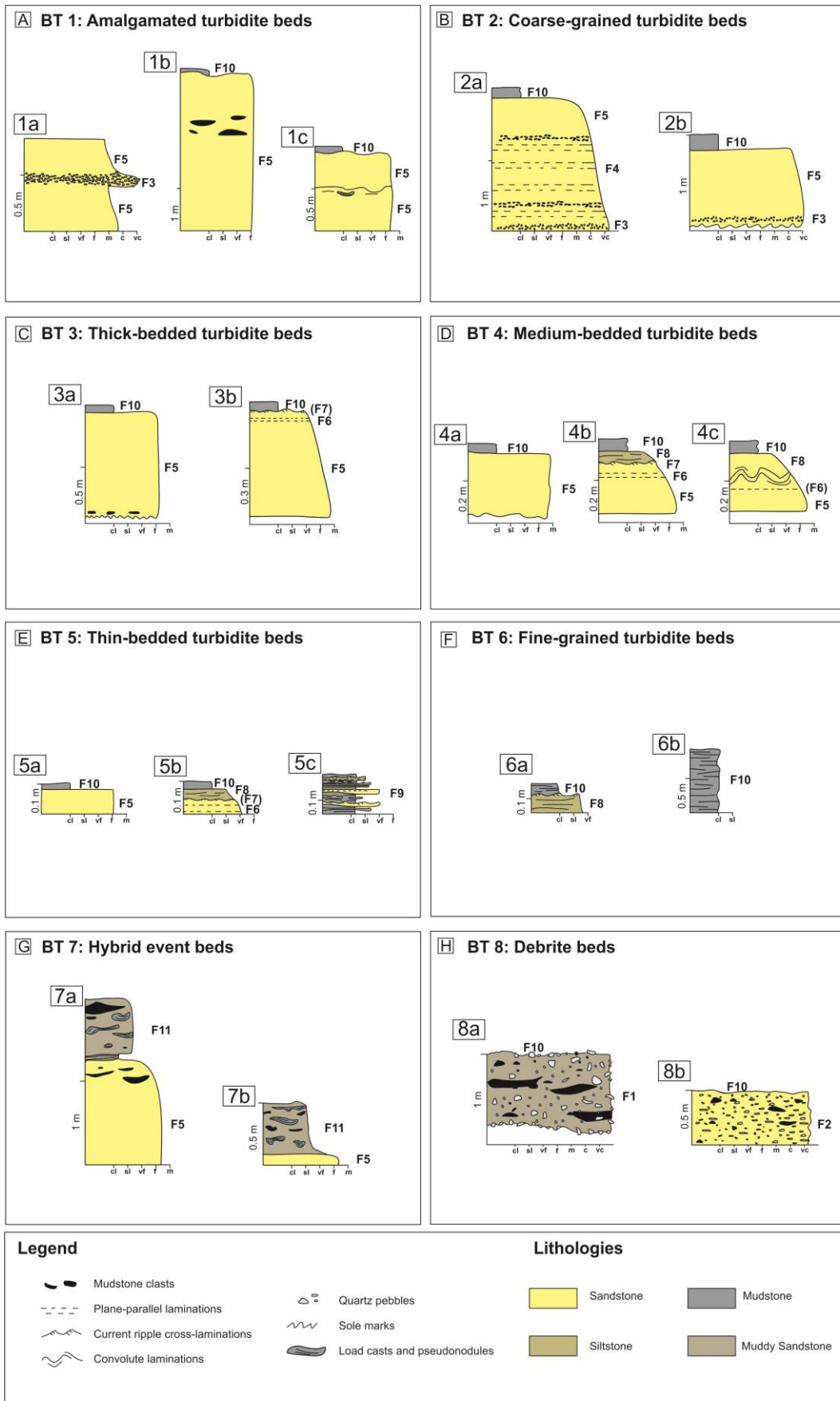


**Figure 4.1:** Sedimentary characteristics of the observed bed types of the Kongsfjord Formation including: (A) Amalgamated turbidite beds. (B) Coarse-grained turbidite beds. (C) Thick-bedded turbidite beds. (D) Medium-bedded turbidite beds. (E) Thin-bedded turbidite beds. (F) Fine-grained turbidite beds. (G) Hybrid event beds. (H) Debrite beds. See Table 2 for a descriptive summary of each BT.

### 4.1.3 BT 3: Thick-bedded turbidite beds

#### *Description*

Type 3 beds consist of thick (>0.5 m), medium- to fine-grained sandstone beds. They can be divided into 2 main sub-categories (Fig. 4.1C). BT 3a beds consist of thick, massive, ungraded medium- to fine-grained sandstones (F5) overlain by thin mudstone units (F10). The base of the beds is frequently loaded and exhibit various sole marks, mainly flute and groove casts. Frondescant marks, chevrons marks and groove casts showing twisted ends are also observed from several outcrops, in particular an impressive number of large sole marks at the base of a bed in Veidnes (Figs. 4.3A and C). Frequently, mudstone clasts are scattered near the base of the bed. BT 3a beds can be of great thickness (up to ca. 3 m). Conversely, BT 3b beds are thinner with a typical thickness of 60 - 80 cm. BT 3b beds are normal graded sandstones with a basal massive fine-grained sandstone (F5) passing upward into a plane-parallel sandstone (F6) and occasionally into a ripple cross-laminated sandstone unit (F7; Fig. 4.1C). The base of the beds also exhibits occasional sole marks.

#### *Interpretation*

The massive sandstone intervals are interpreted to have been deposited by high-density turbidity flows (Bouma, 1962; Lowe, 1982). The great thickness of this bed type and the frequent occurrence of sole marks and mudstone clasts suggest deposition by voluminous, highly erosive, high-density flows able to erode and transport coarse material and larger mud clasts (Talling et al., 2012). The plane-parallel laminated and current ripple cross-laminated intervals of BT 3b beds record traction plus fallout deposition from low-density turbidity flows. However, these laminated sandstone intervals are rarely observed in BT 3 suggesting high-fallout rates and rapid deposition (Middleton & Hampton, 1973; Talling et al., 2012). Alternatively, several studies proposed that massive sandstone beds result from *en masse* deposition by sandy debris flows (e.g., Shanmugam, 1996; Talling et al., 2012; Talling et al., 2013).

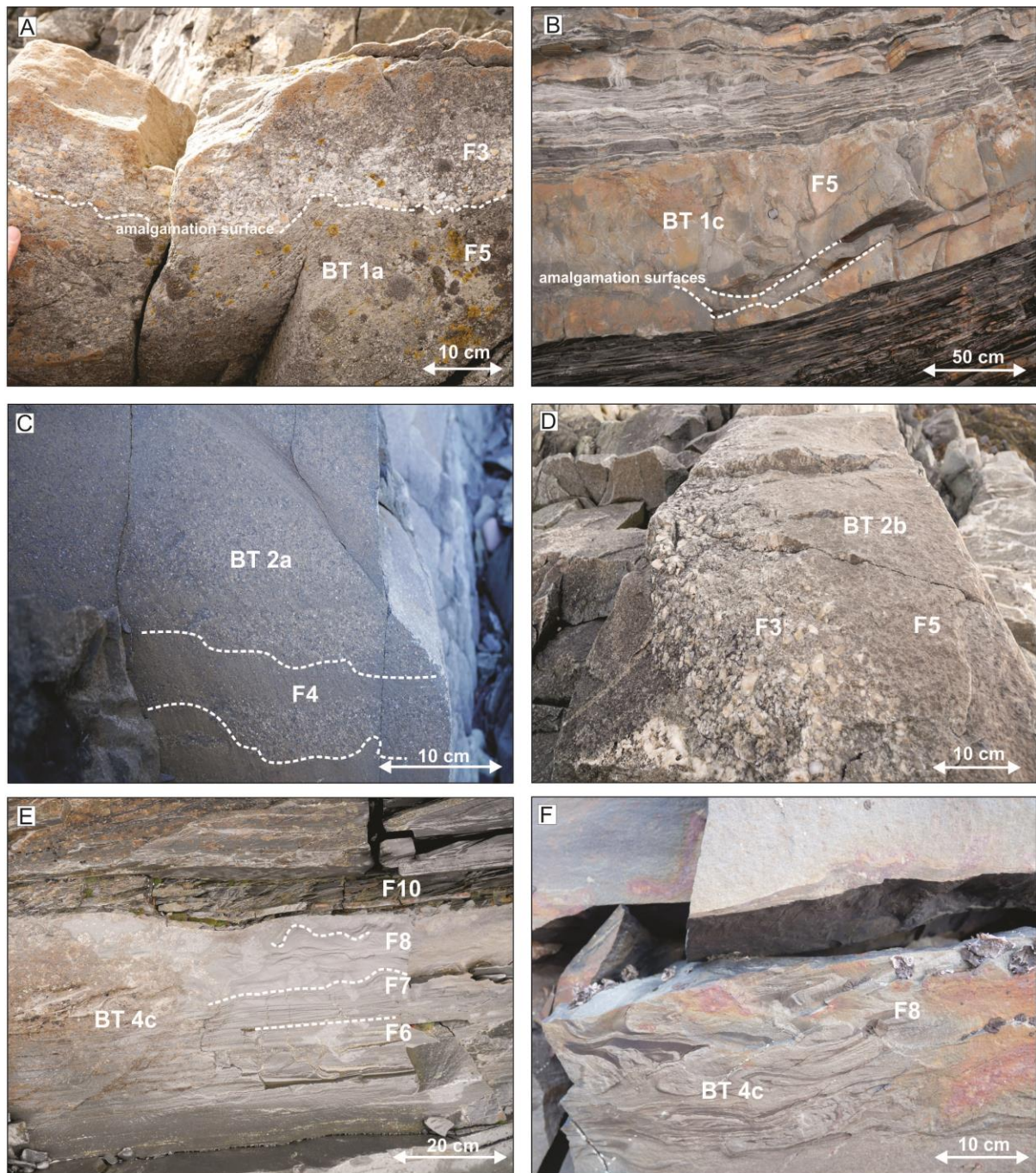


**Figure 4.2:** Details of the bed types observed within the 3 investigated localities. (A) Amalgamated turbidite bed (BT 1a). The amalgamation surface is displayed by an abrupt change in grain size across a sharp surface (stippled line). (B) Amalgamated turbidite bed (BT 1c) showing sharp amalgamation surfaces (stippled lines). (C) Coarse-grained turbidite bed (BT 2A) showing spaced stratifications (F4; stippled lines). (D) Coarse-grained turbidite bed (BT 2B) with clast-supported conglomerate division (F3) grading into a medium-grained sandstone (F5). (E) Medium-bedded turbidite bed (BT 4) showing plane-parallel lamination (F6) grading upward into current ripple cross-laminations (F7) and convolute laminations (F8). (F) Upper part of a medium-bedded turbidite bed (BT 4c) showing convolute laminations (F8).



#### 4.1.4 BT 4: Medium-bedded turbidite beds

##### *Description*

This bed type consists of medium-bedded (20 – 50 cm) sandstones to siltstones. BT 4 beds are subdivided into 3 sub bed types. BT 4a beds consist of ungraded, structureless sandstones (F5) overlain by a thin mudstone caps (F10; Fig. 4.1D). The base of the beds is occasionally loaded and/or exhibiting sole marks. Most frequently, the sole marks appear to be flute or groove casts occurring separately and rarely co-occurring. BT 4b beds are normal graded sandstones with a basal massive, fine-grained sandstone (F5) ideally grading upward into plane-parallel laminated (F6) and current ripple cross-laminated (F7) sandstone, and eventually siltstone (F8; Fig. 4.2E). This bed type is highly variable and often, one or several facies are missing from the ideal facies sequence. BT 4c beds exhibit convolute laminations in the upper part of the bed occurring in a confined interval (10 – 30 cm) above the ripple cross-laminated interval (F7) or the plane-parallel laminated interval (F6; Fig. 4.2E and F).



**Figure 4.3:** Details from the succession in Veidnes. (A) Digital outcrop model of lobe 1 (shown in log 1 of Fig. 4.11). Note how the channelised lobe axis deposits scour into the underlying lobe fringe deposits (white stippled line). (B) Lobe off-axis deposits of lobe 1. Note the two mud-rich HEBs (BT 7b; stippled).

lines) underlying the scoured base of the lobe axis deposits. (C) Frondescent marks and groove casts at the base of the channelised lobe axis deposits of lobe 1.

#### *Interpretation*

These bed types are very similar to BT 3a and 3b beds defined as thick-bedded turbidite beds. The massive sandstone intervals suggest deposition by high-density turbidity flows, whereas the finer grained sandstone to siltstone intervals record traction plus fallout from the waning, low-density part of the same turbidity flow (Bouma, 1962; Lowe, 1982; Talling et al., 2012). Sole marks occurring at the base of BT 4a record the bypass of an erosive, high-density turbidity flow. The difference in bed thickness with BT 3 could indicate lower fallout rates and thus deposition in more distal settings. BT 4c beds exhibit intervals of convolute laminated siltstone. Gladstone et al. (2018) investigated the formation of such intervals and suggested that they form due to a buoyancy-driven instability caused by the rapid deposition of a dense mud-rich interval on top of a less dense, sand-rich interval. Therefore, convolute laminations record rapid deposition under high-fallout rates.

### **4.1.5 BT 5: Thin-bedded turbidite beds**

#### *Description*

These beds consist of very thin to thin (0.5 – 20 cm), fine-grained sandstones to siltstones. This bed type has been subdivided into three main categories (Fig. 4.1E). BT 5a beds consist of thin massive fine- to very fine-grained sandstones (F5) overlain by mudstones (F10). Occasionally, the upper part of the beds exhibits a very thin interval of plane-parallel laminated sandstone (F6) above facies F5. BT 5b beds are normal graded, consisting of a very-fine grained plane-parallel laminated sandstone (F6) passing upward into a current ripple cross-laminated sandstone (F7) and massive or laminated siltstone (F8; Fig. 4.4A). Frequently, one or several facies are missing in sections of this bed type. BT 5c is a heterolithic bed type consisting of alternating layers of very-fine grained sandstone to siltstone and structureless mudstone (F9) forming thick bed sets (up to ca. 10 m; Fig. 4.4B and C). The fine-grained laminae are convolute and planar and show occasional internal plane-parallel laminations and/or current ripple cross-laminations. This bed type also exhibits occasional load casts and siltstone pseudonodules embedded in the mudstone (Fig. 4.4C).

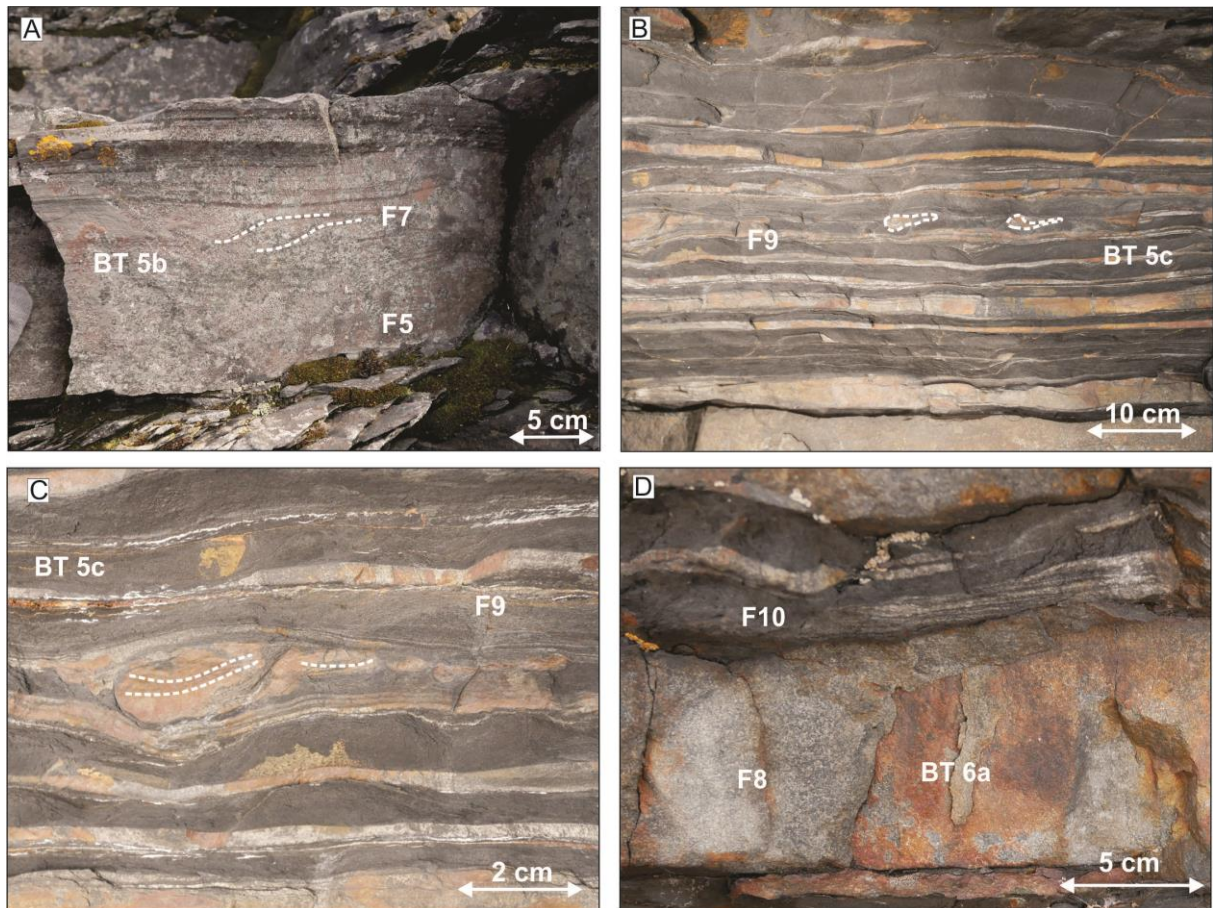


**Figure 4.4:** (A) Thin-bedded turbidite bed (BT 5b) showing current ripple cross-laminations (F7; stippled lines). (B). Bed set of thin-bedded turbidites beds (BT 5c). Note the sandstone pseudonodules embedded in the mudstone intervals (stippled lines). (C) Siltstone laminae and pseudonodules embedded in mudstone in thin-bedded turbidites beds (BT 5c). Note the laminations within the pseudonodules (stippled lines). (D) Fine-grained turbidite bed (BT 6a).

#### *Interpretation*

The massive sandstone intervals in BT 5a are interpreted to be deposited by a high-density turbidity flow, presumably of limited volumes in distal settings (Bouma, 1962; Lowe, 1982; Talling et al., 2012). The plane-parallel laminated sandstones and current cross-laminated sandstones of BT 5b and 5c beds record traction plus fallout deposition from low-density turbidity flows, whereas the siltstone intervals record deposition by fallout from the more dilute part of the flows (Bouma, 1962; Stow & Shanmugam, 1980; Talling et al., 2012). Collectively, these normal graded beds indicate deposition by depletive, waning, low-density turbidity flows. BT 5a and BT 5b beds are very similar to BT 4a and BT 4b beds and thus can be seen as a distal continuation of these bed types that are deposited in more distal settings where the fallout rates are lower.



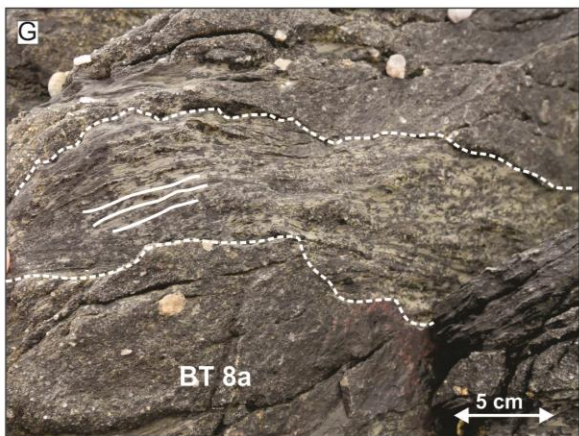
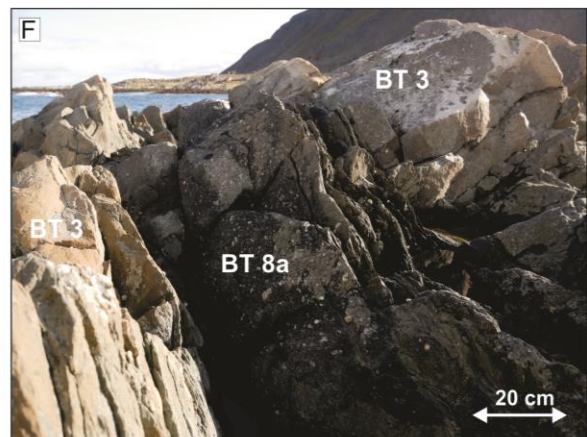
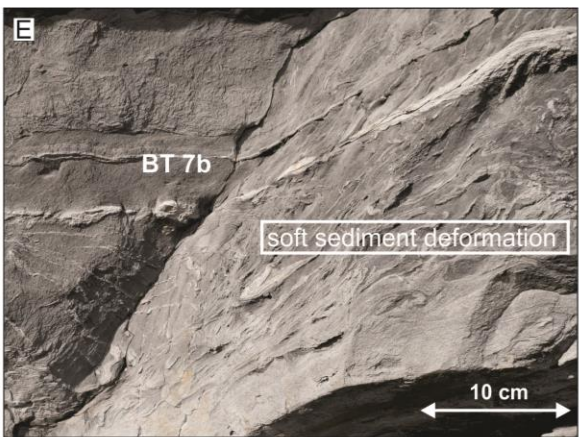
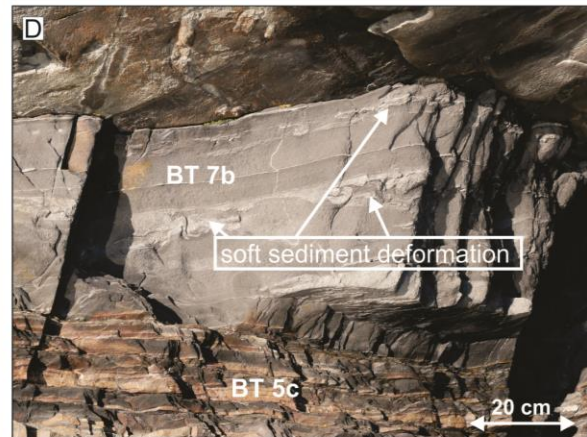
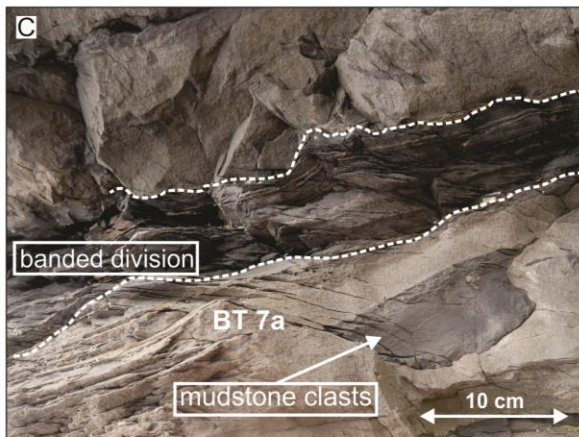
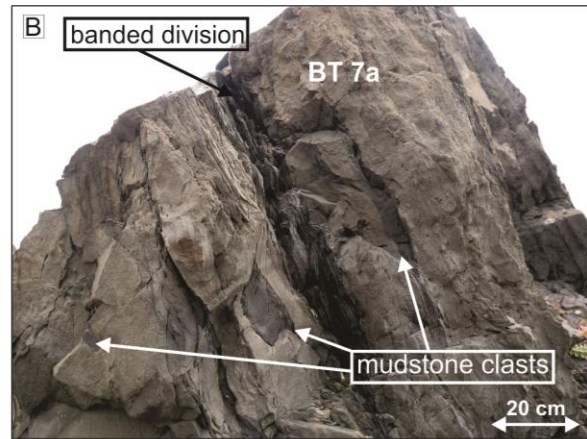
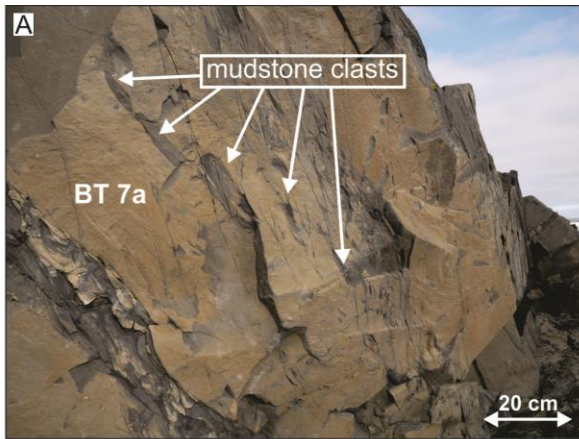




**Figure 4.5:** Details of the bed types. (A) Hybrid event bed (BT 7a) with a relatively sand-rich matrix containing abundant mudstone clasts. (B) Hybrid event bed (BT 7a). Note the large mudstone clasts. (C) Hybrid event bed (BT 7a) showing a banded mudstone division. (D) Hybrid event bed (BT 7b) overlying thin-bedded turbidite beds (BT 5c). Note the abundant soft sediment deformation. (E) Hybrid event bed (BT 7b). Note the abundant soft sediment deformation. (F) Debrite bed (BT 8a) with a mud-rich matrix containing large mudstone clasts. The bed is under- and overlain by thick-bedded turbidite beds (BT3). (G) Debrite bed (BT 8a). Note how the mudstone clast (stippled lines) is deformed and show internal laminations (plain lines). (H) Debrite bed (BT 8b) with a sand-rich matrix containing mainly sub-horizontal oriented pebbles and mudstone clasts.

BT 5c beds which show very-fine grained sandstone to siltstone laminae, are deposited by suspension fallout from dilute, low-density turbidity currents (Bouma, 1962; Stow & Shanmugam, 1980). When laminations occur, they record traction deposition from the coarser sand and silt grains, whereas the mudstone interbeds represent fallout of mud from the dilute tail of the fine-grained turbidity currents. These beds record frequent changes in flow velocity where very-fine grained sandstone and siltstones are deposited during period of higher energy and mud settles during period of reduced energy (Stow & Shanmugam, 1980). Thus, this bed type indicates deposition by successive, mud-rich, waning turbidity flows.

#### **4.1.6 BT 6: Fine-grained turbidite beds**

##### *Description*

This bed type consists of siltstone and mudstone beds forming two distinct subdivisions. BT 6a beds consist of thin- to medium-bedded (10 – 30 cm) siltstones (Fig. 4.1F). The beds are normal graded, exhibiting massive siltstone, plane-parallel laminations and occasionally current ripple cross-laminations that passes upward into structureless mudstone (Fig. 4.4D). Occasionally, convolute laminations occur in a confined interval near the top of the bed. Type 6b beds form mudstone units that can be up to ca. 50 cm thick (Fig. 4.1F). The mudstone is structureless or plane-parallel laminated. These beds are often partially eroded in the present-day landscape.

##### *Interpretation*

These beds have a higher mud proportion than other bed types indicating deposition by dilute, mud-rich turbidity currents. Type 6a beds show normal grading indicating the deceleration of dilute, mud-rich fine-grained turbidity flows (Bouma, 1962; Stow & Shanmugam, 1980). BT 6b beds which consist only of mudstone record deposition by hemipelagic fallout (if laminated)

or by rapid suspension fallout from dilute, mud-rich density currents (if structureless; Bouma, 1962; Stow & Shanmugam, 1980).

#### **4.1.7 BT 7: Hybrid event beds**

##### *Description*

Type 7 beds consist of bipartite sandstone beds showing a basal structureless sandstone division (F5) and an upper, clast-rich, heterogeneous sandstone division (F11; Fig. 4.1G). The heterogeneous sandstone divisions contain abundant mudstone clasts, pseudonodules and patches of sandstone loaded into a mud-rich matrix (Figs. 4.3B and 4.5A, B, C, D and E). Two main sub-categories have been observed: very thick to thick beds (BT 7a) and medium to thick beds (BT 7b). Type 7a beds are typically > 1 m thick and contain a thick basal sandstone division. The sandstone unit exhibits large, isolated mudstone clasts towards the top and is overlain by thin alternating layers of mudstone (banded division) passing upward into the mud-rich sandstone division containing large mudstone clasts (Fig. 4.5A, B and C). Conversely, BT 7b beds consist of a thin (< 20 cm) clean sandstone division directly overlain by the mud-rich, commonly soft-sediment deformed heterogeneous division (Figs. 4.3B and 4.5D and E). The mud-rich heterogeneous division contains less and smaller mudstone clasts than BT 7a.

##### *Interpretation*

These beds are interpreted to be the result of transitional flows where the lower structureless sandstone division is deposited incrementally by a high-density turbidity current, and the upper clast-rich division is deposited *en masse* by a cohesive debris flow. Similar bed types are described by numerous studies in several Formations and various sedimentary basins, particularly during the two last decades (Lowe & Guy, 2000; Haughton et al., 2003; Amy & Talling, 2006; Haughton et al., 2009; Pierce et al., 2018). According to Haughton et al. (2003), the systematic co-occurrence of these two units and the irregular boundary between the two units suggest that the processes are co-genetic. Several mechanisms have been invoked for the linkage of the two processes including flow transformation of a turbidity current by progressive entrainment of mud causing turbulence damping and transformation of the flow to a cohesive debris flow (Haughton et al., 2003; Haughton et al., 2009). In bed type 7a, the thin alternating finer grains layers (banded division) on top of the clean sandstone division could reflect

deposition by flows that are intermediate between turbulent and laminar flow conditions and thus suggest gradational flow transformation (Lowe & Guy, 2000; Haughton et al., 2009).

#### **4.1.8 BT 8: Debrite beds**

##### *Description*

This bed type consists of two distinct sub-types of clast-rich conglomerates observed in the Nålneset section (Fig. 4.1H). BT 8a beds consist of mud-rich, fine-grained sandstone matrix containing abundant clasts (F1; Fig. 4.5F and G). The clasts consist mainly of quartz pebbles to cobbles and larger laminated, yet deformed mudstone clasts, all embedded in the matrix (Fig. 4.5G). BT 8b beds consist of fine-grained sandstone matrix also containing abundant quartz pebbles and mudstone clasts (F2; Fig. 4.5H). However, the mudstone clasts are relatively smaller than in BT 8a and the quartz pebbles appear to have a preferred sub-horizontal orientation. BT 8 beds have only been observed in the Nålneset outcrop section and the lateral extension of these beds is very limited.

##### *Interpretation*

These beds are interpreted as deposited *en masse* unlike the turbidites beds deposited incrementally (Talling et al., 2012). BT 8a beds are interpreted as deposited by laminar cohesive flows in which turbulence is suppressed due to a high mud content or due to a high concentration of clasts (Mulder & Alexander, 2001; Talling et al., 2012). The presence of large laminated mudstone clasts chaotically dispersed in a mud-rich matrix suggests deposition by a high-strength muddy debris flow (Talling et al., 2012). The mudstone clasts also show evidence of internal shear (Fig. 4.5G). BT 8b resembles the A1 facies of Mutti (1979) interpreted to have been deposited by gravelly turbidity currents. In fact, the sandier aspect of the matrix and the preferred orientation of the clasts could suggest deposition by a high-density turbidity flow (Lowe, 1982). However, the presence of mudstone clasts showing evidence of internal shear and the chaotic aspect of the deposit suggest *en masse* deposition by a cohesive debris flow (Mulder & Alexander, 2001). Mulder and Alexander (2001) suggested that the concentration of coarse particles within horizons and their preferred orientation could be the result of pulsed shearing within a laminar flow.

**Table 2:** Description and interpretation of the bed types in the Kongsfjord Formation. See also Fig. 4.1.

Bed types		Grain sizes and bed thickness	Description	Process interpretation
<b>BT 1:</b> Amalgamated beds	Type 1a	Very coarse- to medium-grained sandstone. Very thick (> 1m) to thick (0.5 – 1 m).	Normal graded sandstone (F5) transitionally to abruptly overlain by layer of graded coarser pebbly sandstone (F3) which typically pass upward into massive, medium-grained sandstone (F5).	These bed types show evidence of amalgamation and deposition by a series of succeeding high-density turbidity flows (Walker, 1966; Mattern, 2002), or from pulsating turbidity flows (Ho et al., 2018).
	Type 1b	Coarse- to fine-grained sandstone. Very thick (> 3m)	Massive, ungraded sandstone (F5) showing floating mudstone clasts in the middle of the bed. Occasionally, the base of the bed exhibits sole marks.	
	Type 1c	Coarse- to fine-grained sandstone. Very thick (> 1 m) to thick (0.5 – 1 m).	Amalgamated units of massive, ungraded sandstone beds (F5). In a stacked, amalgamated series, the base of the lower sandstone bed is occasionally loaded.	
<b>BT 2:</b> Coarse-grained turbidite beds	Type 2a	Very coarse- to fine grained sandstone to mudstone. Thick (0.8 – 1.5 m).	Clast supported conglomerate (F3) grading upward into very coarse-grained plane-parallel laminated sandstone (F4) with aligned layers of mudstone clasts and/or horizons of coarse- to medium-grained sandstone (F5). Overlain by mudstone (F10).	Deposition by a waning high-density turbidity current. The conglomerate division (F3) records deposition by a dense basal layer, whereas facies F4 and F5 record traction deposition and fallout from the more dilute upper part of the flow (Lowe, 1982; Postma & Cartigny, 2014).
	Type 2b	Very coarse- to medium-grained sandstone. Thick (0.8 – 1.5 m).	Clast supported conglomerate (F3) grading upward into medium-grained sandstone (F5).	

**Table 2:** (continued)

Bed types		Grain sizes and bed thickness	Description	Process interpretation
<b>BT 3:</b> Thick-bedded turbidite beds	Type 3a	Medium to fine-grained sandstone to mudstone. Thick (0.8 – 3 m).	Massive, ungraded medium to fine-grained sandstone (F5). The base of the bed is typically loaded and exhibit groove casts and/or flute casts. Occasional mudstone clasts occur near the base of the bed.	Deposition by a waning high-density turbidity current with high-fallout rates (Bouma, 1962; Talling et al., 2012).
	Type 3b	Medium- to very-fine grained sandstone to mudstone. Thick (0.8 – 1 m).	Normal graded bed consisting of massive sandstone (F5) grading upward into plane-parallel laminated (F6) and occasionally current ripple cross-laminated sandstone (F7). Overlain by mudstone (F10).	
<b>BT 4:</b> Medium-bedded turbidite beds	Type 4a	Medium- to fine-grained sandstone to mudstone. Medium (20 – 50 cm).	Massive, ungraded medium to fine-grained sandstone (F5) overlain by mudstone (F10). The base of the bed is occasionally loaded.	Deposition by a depletive, waning high-density turbidity current with high-fallout rates (Bouma, 1962; Talling et al., 2012).
	Type 4b	Siltstone to medium- to fine-grained sandstone and mudstone. Medium (20 – 50 cm).	Normal graded bed consisting of massive, medium to fine-grained sandstone (F5) grading into plane-parallel laminated (F6), current ripple cross-laminated (F7) sandstone and siltstone (F8). One or several facies are commonly missing. Overlain by mudstone (F10).	

**Table 2:** (continued)

Bed types		Grain sizes and bed thickness	Description	Process interpretation
<b>BT 4:</b> Medium-bedded turbidite beds	Type 4c	Medium- to fine-grained sandstone to siltstone and mudstone. Medium (20 – 50 cm).	Normal graded bed consisting of massive, medium to fine-grained sandstone (F5) grading into plane-parallel laminated (F6), the upper division of the bed exhibits convolute lamination and abundant soft sediment deformation (F8). Overlain by mudstone (F10).	Deposition by a depletive, waning high-density turbidity current with high-fallout rates (Bouma, 1962; Talling et al., 2012). Convolute laminations suggest rapid loading (Gladstone et al., 2018).
	<b>BT 5:</b> Thin-bedded turbidite beds	Fine- to very-fine grained sandstone to mudstone. Thin to very thin (< 20 cm).	Massive, fine- to very fine-grained sandstone (F5) overlain by mudstone (F10). Plane parallel lamination may occur sporadically in the uppermost part of the sandstone.	Deposition by a depletive, waning low-density turbidity current (Bouma, 1962; Stow & Shanmugam, 1980).
	Type 5b	Siltstone to very fine-grained sandstone and mudstone. Thin to very thin (< 20 cm).	Normal graded bed consisting of very fine-grained plane-parallel laminated sandstone (F6) passing upward into current ripple cross-laminated sandstone (F7) and siltstone (F8). Overlain by mudstone (F10).	
	Type 5c	Siltstone to very fine-grained sandstone and mudstone. Thin to very thin (< 10 cm).	Structureless mudstone containing very thin interbeds of very fine-grained sandstone to siltstone laminae (F9). Siltstone interbeds show occasional internal plane-parallel or current ripple cross-laminations. Siltstone pseudonodules are locally embedded in the mudstone.	

**Table 2:** (continued)

Bed types		Grain sizes and bed thickness	Description	Process interpretation
<b>BT 6:</b> Fine-grained turbidite beds	Type 6a	Siltstone to mudstone. Medium (20 – 30 cm) to very thin (< 10 cm).	Massive siltstone beds occasionally grading into plane-parallel laminated siltstone and/or current ripple cross-laminated siltstone (F8).	Deposition by a dilute low-density turbidity current (Stow & Shanmugam, 1980).
	Type 6b	Mudstone. Medium (30 – 50 cm) to very thin (< 10 cm).	Undifferentiated massive to plane-parallel laminated mudstone (F10).	Deposition by suspension settling from the dilute tail of a low-density turbidity flow or by hemipelagic fallout (Bouma, 1962; Stow & Shanmugam, 1980).
<b>BT 7:</b> Hybrid event beds	Type 7a	Bipartite sandstone beds. Very thick (> 1m) to thick (0.5 – 1 m)	Bipartite beds composed of a thick, massive, ungraded to poorly graded basal sandstone division (F5) containing isolated floating mudstone clasts towards the top, overlain by thin, commonly convolute layers of mudstone passing upward into a heterogeneous muddy sandstone with abundant large mudstone clasts (F11).	Deposition by a hybrid sediment density flow in which the basal F5 facies is deposited by a turbidity current (presumably of high density) and the overlying F11 facies by a cohesive debris flow (Lowe & Guy, 2000; Haughton et al., 2009). The thin layers of mudstone between the two units indicates intermediate flow conditions (Haughton et al., 2009).

**Table 2:** (continued)

Bed types	Grain sizes and bed thickness	Description	Process interpretation
<p><b>BT 7:</b> Hybrid event beds</p>	<p>Bipartite sandstone beds. Thick (0.5 – 1 m) to medium (0.2 – 0.5 m).</p>	<p>Bipartite beds composed of a thin (&lt;10 cm), massive, ungraded to poorly graded basal sandstone unit (F5) passing gradually upward into a heterogeneous muddy sandstone with abundant sandstone pseudonodules, liquefaction structures and small mudstone clasts (F11).</p>	<p>Deposition by a hybrid sediment density flow in which the basal F5 facies is deposited by a turbidity current (presumably of high density) and the overlying F10 facies by a cohesive debris flow (Lowe &amp; Guy, 2000; Haughton et al., 2009).</p>
<p><b>BT 8:</b> Debrite beds</p>	<p>Mud-rich, very fine-grained sandstone matrix with mudstone clasts. Thick (0.8 – 1 m).</p>	<p>Massive, mud-rich, very fine-grained sandstone containing numerous, randomly oriented pebbles and large laminated mudstone clasts (F1).</p>	<p><i>En masse</i> deposition by a mud-rich cohesive debris flow (Mulder &amp; Alexander, 2001).</p>
<p>Type 8b</p>	<p>Very-fine grained sandstone matrix with mudstone clasts. Medium to thick (0.4 – 0.8 m).</p>	<p>Massive, very fine-grained sandstone matrix containing abundant clasts of variable roundness. Clasts consist of sub-horizontal oriented quartz pebbles to cobbles and small mudstone clasts (F2).</p>	<p><i>En masse</i> deposition by a cohesive debris flow (Mulder &amp; Alexander, 2001).</p>



## **4.2 Depositional architecture and depositional environments**

### **4.2.1 Architectural elements**

Based on the vertical and lateral distribution of bed types, two main distinct architectural elements have been identified in the Kongsfjord Formation: channels and lobes. Channels are negative, elongate features that represent long-term pathways for sediment transport (Mutti & Normark, 1991). Channels record sediment bypass and deposition in confined settings (Mattern, 2002; Sprague et al., 2005). In some outcrop studies, the recognition of channels was based on the identification of their lenticular geometries and the erosive relationship to their underlying and surrounding strata (Eschard et al., 2003; Gardner et al., 2003; Hubbard et al., 2008). However, in the Kongsfjord Formation, the plan-form geometries of channels have not been observed because of outcrop limitations. Instead, the recognition of channelised deposits is based on the following criteria: (i) recognition of an erosive base, commonly with abundant flute and scour marks; and (ii) a high degree of amalgamation (i.e., a high proportion of BT 1 beds, which are interpreted to record deposition in confined settings). In the Kongsfjord Formation, the observed channels are typically shallow (<1 m erosional relief) and consist of a high proportion of BT 1, BT 2, and BT 3. The channels are commonly referred to as scours due to their shallow erosional reliefs.

Lobes record unconfined deposition in front of channels (Normark, 1970; Mutti & Ricci Lucchi, 1972). Many hierarchical classifications have been proposed for lobes (see Cullis et al., 2018). Here, a four-order classification scheme similar to the scheme developed by Pr elat et al. (2009) for the Karoo Basin is adopted. The lowest hierarchical division, a bed, results from a single depositional event. Beds stack together into distinctive lobe elements. Compensational stacking of lobe elements forms lobate or lenticular bodies termed lobes. At larger scale, compensational stacking of genetically related lobes typically forms lobe complexes.

Traditionally, lobate and lenticular geometries have been an important recognition criteria for turbidite lobes (Gervais et al., 2006; Deptuck et al., 2008). However, the recognition of such architectural elements is difficult in many outcrop and subsurface data sets, especially as these geometries are best observed in outcrops of great lateral extent and those having a three-dimensional component. Thus, the term sheet/sheet-like have commonly been applied to

describe tabular units in numerous outcrop studies (Satur et al., 2000; Drinkwater & Pickering, 2001; Eggenhuisen et al., 2011; Cunha et al., 2017; Marini et al., 2020). In the Kongsfjord Formation, the recognition of lobes has been based on two main criteria: (i) the systematic vertical stacking of beds into tabular-shaped, composite units of variable thicknesses exhibiting a thin-bedded lower part and a thick-bedded upper part, and which internally may comprise a series of smaller coarsening and thickening upward sub-units. These sub-units are interpreted as compensationally stacked lobe elements, which together form thicker composite units representing lobes; (ii) the recognition of sharp facies breaks, such as an abrupt transition from thick-bedded upward into thin-bedded turbidites, that demarcate stratigraphic surfaces interpreted as representing bounding surfaces between successive lobes (Prélat & Hodgson, 2013). The thin- to thick-bedded composite units representing lobes are 1.5 to 27 m thick, whereas its constituent lobe elements, if present and recognisable, are typically some few meters each (see Table 3 for a summary of lobe characteristics).

#### **4.2.2 Bed type associations**

The recognised lobes of the Kongsfjord Formation are characterised by a wide range of bed types (see Table 3). Based on vertical and lateral bed type distributions, three bed type associations are recognised and are interpreted to represent different depositional sub-environments: lobe axis, lobe off-axis and lobe fringe deposits. The recognition criteria for these sub-environments and their associated deposits are well-established in the literature and numerous studies documents and interpret deposits similar to those described below (e.g., Prélat et al., 2009; Etienne et al., 2012; Prélat & Hodgson, 2013; Sychala et al., 2015; Brooks et al., 2018b; Rohais et al., 2021; Sychala et al., 2021).

##### *Lobe axis*

Lobe axis deposits consist of amalgamated beds (BT 1), coarse-grained turbidite beds (BT 2) and thick-bedded turbidite beds (BT 3) and less frequently medium-bedded turbidite beds (BT 4) that are rarely separated by mudstone intervals (high sandstone/mudstone ratio). Beds are characterised by abundant erosive features and a high amalgamation degree (Figs. 4.3A and 4.6A). These deposits typically occur in the uppermost part of lobes.

**Table 3:** Summary of lobe characteristics for each locality.

Locality	Number of investigated lobes	Thickness	Architecture	Bed types	Stacking trends
Nålneset	10	1.5 to 5.5 m. 2.7 m on average.	Typically consists of a single lobe element.	Dominated by thin-bedded and fine-grained turbidite beds (BT 5 and BT 6) in its lower part (lobe fringe and lobe off-axis deposits) and amalgamated, coarse-grained and thick-bedded turbidite beds (BT 1, BT 2 and BT 3) in its upper part (lobe axis deposits).	Thickening upward.
Veidnes	5	5 to 11 m. 8 m on average.	Composite: consists of several stacked lobe elements.	Dominated by thin-bedded and fine-grained turbidite beds and hybrid event beds (BT 5, BT 6 and BT 7) in its lower part (lobe fringe and lobe off-axis deposits) and amalgamated and thick-bedded turbidite beds (BT 1 and BT 3) in its upper part (lobe axis deposits).	Thickening upward and thickening then thinning upward.
Segloddan	37	4 to 27 m. 12 m on average.	Composite: consists of several stacked lobe elements.	Dominated by thin-bedded and fine-grained turbidite beds (BT 5 and BT 6) in its lower part (lobe fringe and lobe off-axis deposits) and amalgamated and thick-bedded turbidite beds (BT 1 and BT 3) in its upper part (lobe axis deposits).	Thickening upward, constant, thickening then thinning upward; thinning then thickening upward; and thinning upward.

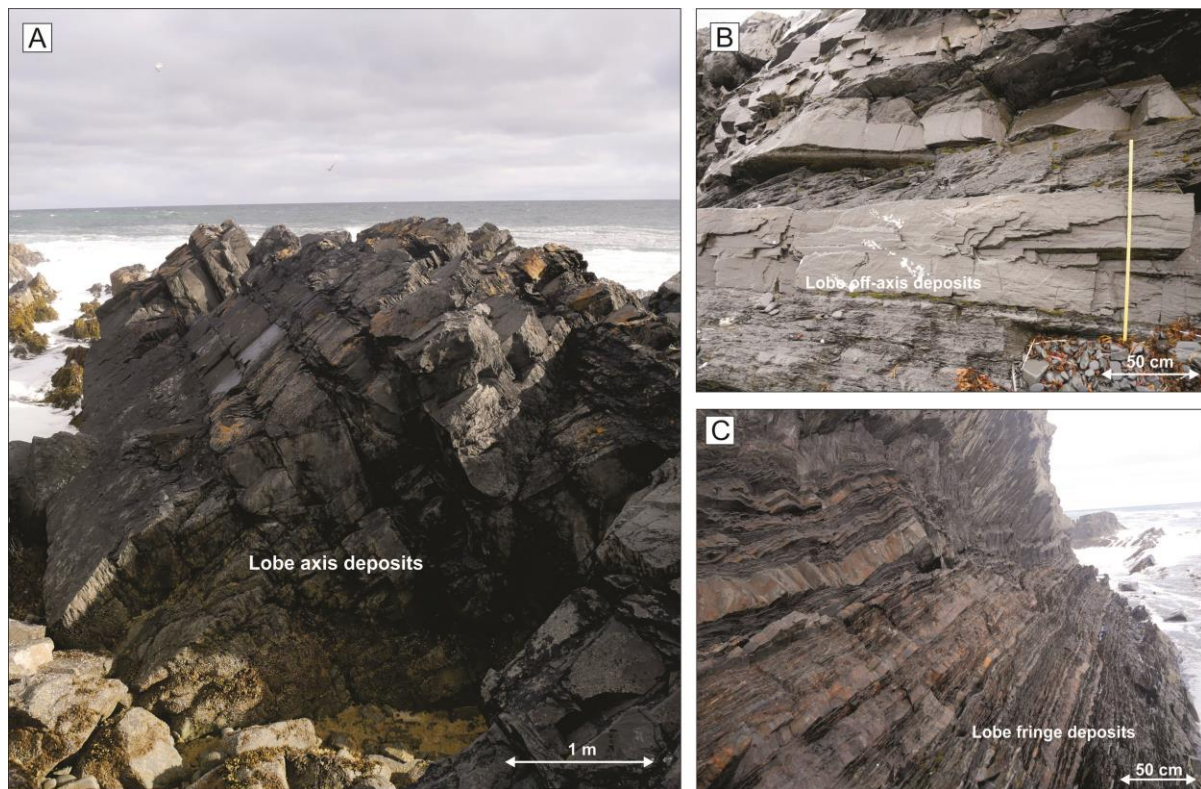


**Figure 4.6:** Outcrop photos of lobe sub-environments: (A) Lobe axis deposits (BT 1). (B) Lobe off-axis deposits (BT 4 and BT 6). (C) Lobe fringe deposits (BT 6).

#### *Lobe off-axis*

Lobe off-axis deposits are heterolithic and show a wide range of bed types including medium-bedded turbidite beds (BT 4), thin-bedded turbidite beds (BT 5), fine-grained turbidite beds (BT 6), HEBs (BT 7) and less frequently thick-bedded turbidite beds (BT 3). Beds are mostly medium- to thin-bedded and are often separated by thin mudstone intervals (Figs. 4.3B and 4.6B). These deposits typically occur below lobe axis deposits.

#### *Lobe fringe*

Lobe fringe deposits are characterised by thinly interbedded sandstone, siltstone, and mudstone. They comprise thin-bedded turbidite beds (BT 5), fine-grained turbidite beds (BT 6) and less frequently HEBs (BT 7) and medium-bedded turbidite beds (BT 4; Fig. 4.6C). Lobe fringe deposits have a higher mudstone percentage than lobe off-axis deposits (> 60%). These deposits typically occur in the lowermost part of lobes.

### 4.2.3 Nålneset

#### *Description*

The Nålneset section, located northwest of Kongsfjorden (Fig. 3.1A and B), consists of well exposed sandstone units separated by thin intervals of mudstone. The section consists of 85 % of very fine- to coarse-grained sandstone. Overall, the section is characterised by a high proportion of amalgamated sandstone beds (23.8 %) and of thick-bedded turbidite beds (23.7 %; Fig. 4.7A). Medium-bedded turbidite beds (18.2 %) and thin-bedded turbidite beds (17.3 %; Fig. 4.7A) also occur frequently. The average bed thickness is 37.8 cm.

A total of 10 stacked units, referred to as lobes, are recognised in the investigated succession (Fig. 4.8). Typically, the base of each lobe, consists of BT 5 and/or BT 6 beds separated by mudstone intervals (lobe fringe deposits) passing upward into BT 4, BT 5 beds eventually separated by thin mudstone intervals (lobe off-axis deposits). The upper parts of the lobes typically consist of one or more thick turbidite beds, often amalgamated (BT 1 or BT 3), referred to as lobe axis deposits (Fig. 4.9A, B, C and D). Beds are often amalgamated and therefore the recognition of lobe sub-environments is often problematic (Fig. 4.9A and B). The thicker sandstone beds (BT 1 and BT 3) commonly have erosive bases with sole marks (5 % of all the beds in the total section), commonly flutes casts and frequently exhibit rip-up mudstone clasts at their bases (Fig. 4.10A). Most of the lobes exhibit a clear thickening/coarsening upward trend passing from lobe fringe deposits in the lowermost part to lobe axis deposits in the uppermost part of the lobe (Figs. 4.8 and 4.9A, B and C). Lobes are typically 1.5 to 5.5 m thick and stack into a ca. 30 m thick succession that does not show any thick mudstone interval. (Fig. 4.8; Table 3).

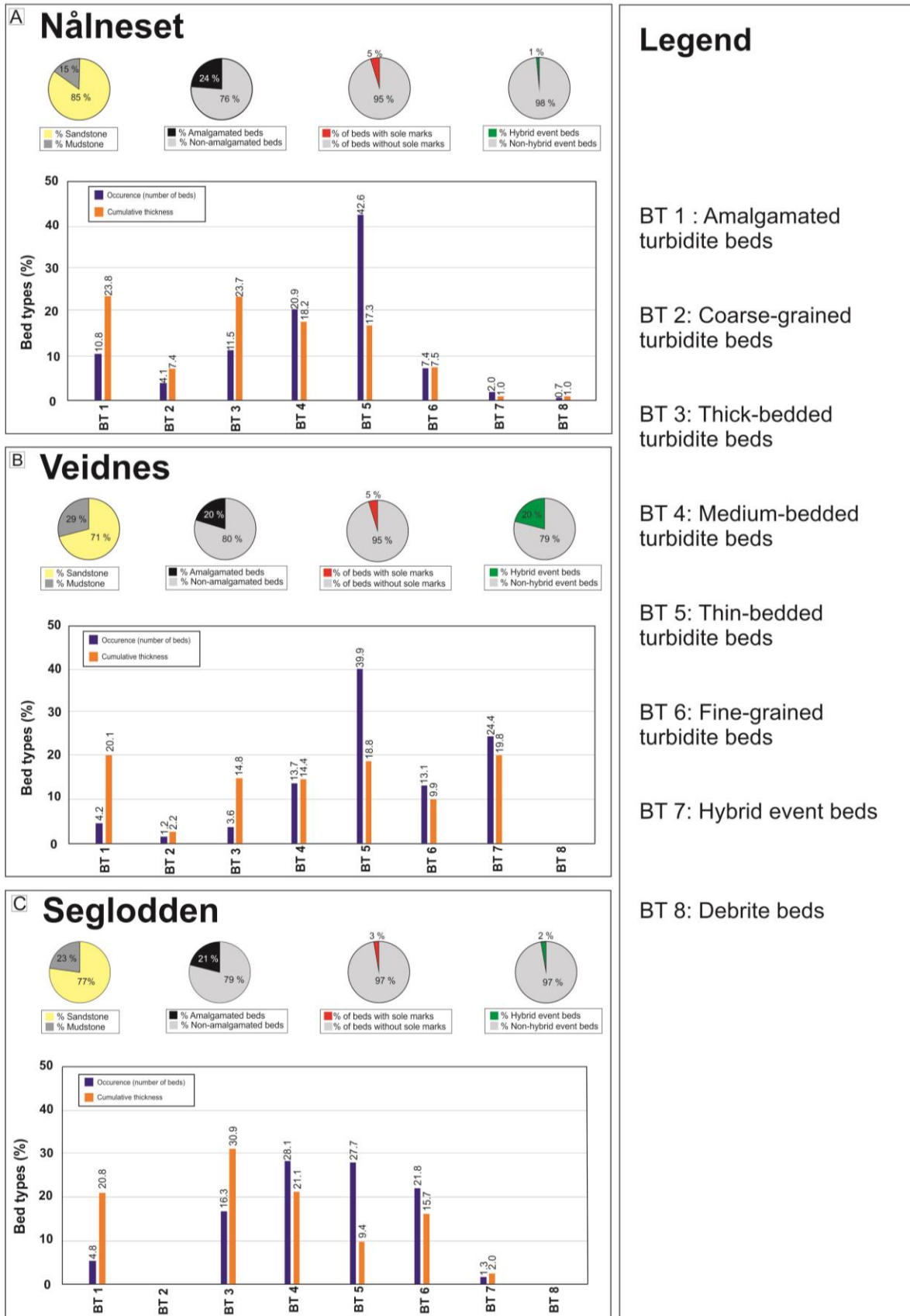


Figure 4.7: Diagrams showing the percentage of bed types by thickness and pie charts showing: (i) the sandstone/mudstone percentage; (ii) the degree of amalgamation; (iii) the proportion of beds showing

*sole marks (by number of beds) and; (iv) the proportion of HEBs (by thickness) for the (A) Nålneset, (B) Veidnes, and (C) Segludden outcrop sections.*

The good exposure and the tabular shape of the beds allowed the beds to be traced laterally for distances up to 680 m (Fig. 4.8). Some lobes exhibit lateral changes in thicknesses however, no pinch out is observed at the scale of the outcrops. Based on the correlated section, it seems that several lobes are thickening towards the southwest (e.g., lobes 7, 8 and 9 thicken of 3 m over a 680 m distance). The proportion of BT 2 beds increases towards the southwest where beds frequently display tractive structures. The thicknesses of the mudstone intervals separating turbidite beds seem to decrease towards the southwest, where there is a greater proportion of amalgamated turbidite beds. Shallow scours are abundant throughout the section. Typically, they cut less than one meter down into the underlying bed (Fig. 4.9E and F). One scour at the base of a sandstone bed in lobe 8, can be traced along the outcrop belt for approximately 200 m (from log 5 to log 7; Fig. 4.8).

HEBs are rare throughout the succession (only 1% of the total section) and cannot be traced laterally due to outcrop limitations. They typically contain small mudstone clasts (< 10 cm) dispersed in a mud-rich matrix (Fig. 4.10). Two debrite beds (BT 8a and BT 8b) are observed further west of the correlated logs (Fig. 4.5F, G and H). They contain abundant quartz pebbles and mudstone clasts dispersed in a mud-rich to sand-rich matrix. The debrite beds occur within lobes axis deposits and are bounded below and above by amalgamated and coarse-grained turbidite beds (BT 1 and BT 2). They cannot be traced laterally for a long distance (< 50 m).



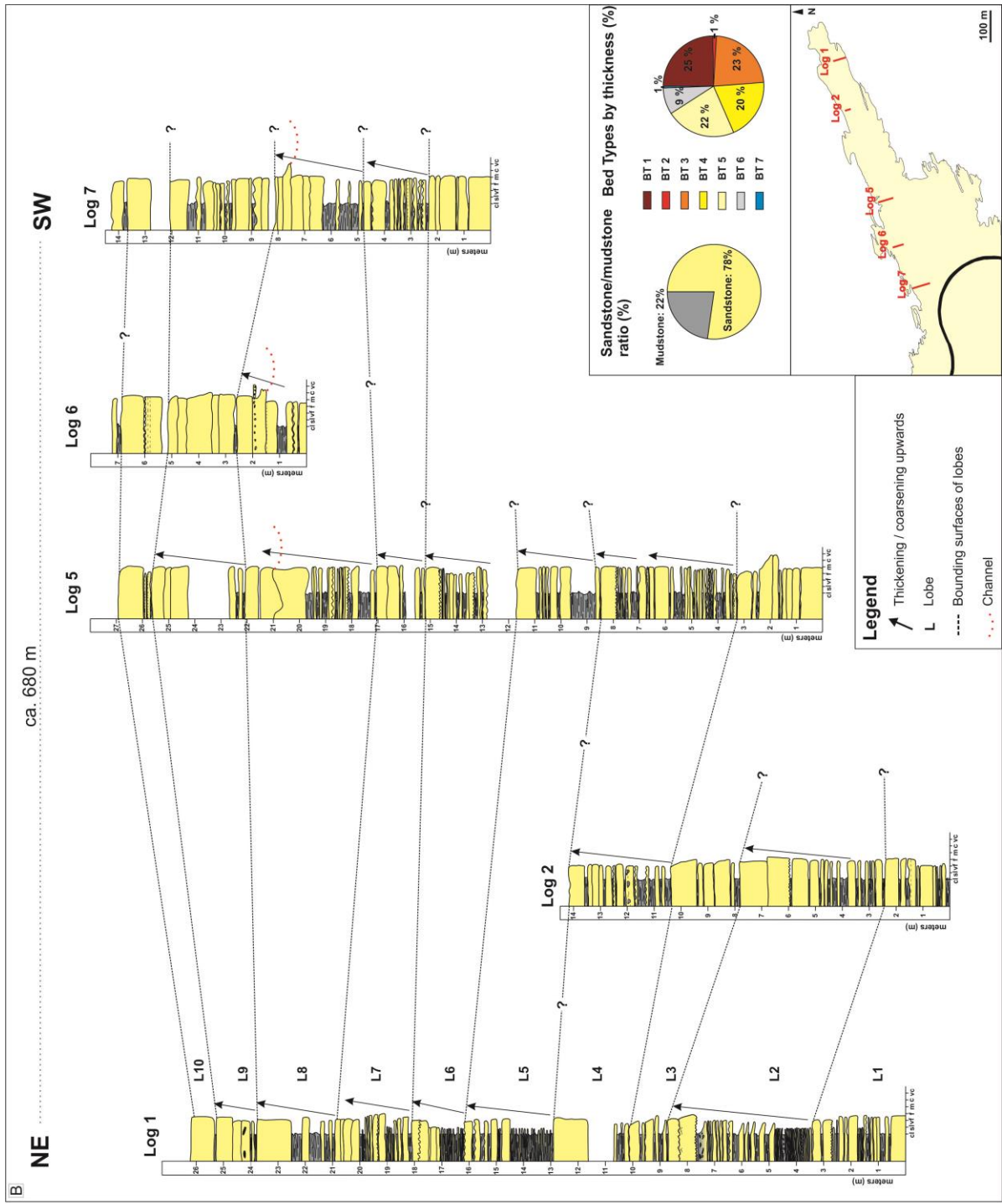
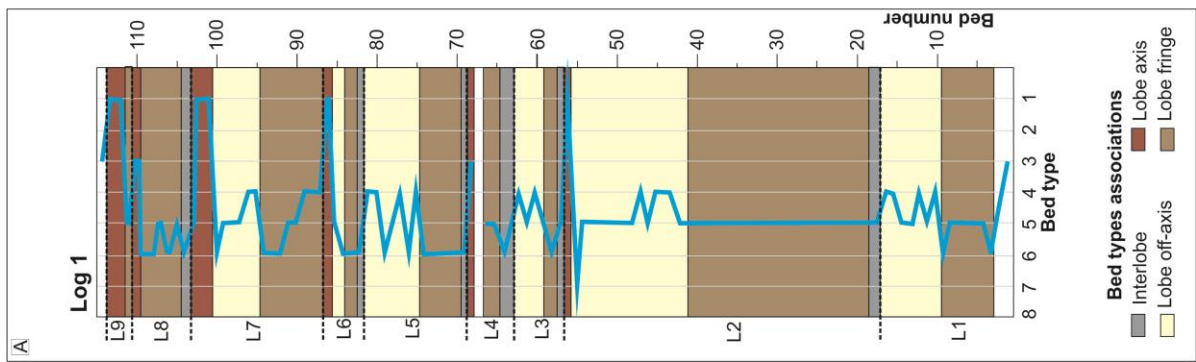




**Figure 4.8:** (A) Diagram illustrating the vertical variation and distribution of bed types (by bed number) for log 1. Note that the thicknesses of the bed type associations do not reflect the actual thicknesses of the deposits. (B) Tentative correlation panel of five stratigraphic logs in Nålneet, documenting the lateral development of ten vertically stacked lobes. Judging from the lateral thickness variations of the lobes, there seem to be a component of compensational stacking. Map showing the localities of the five correlated stratigraphic logs (logs 1, 2, 5, 6, and 7) on the Nålneet promontory. Pie charts showing (i) the sandstone/mudstone percentage, (ii) the bed type percentage (by thickness) for the five correlated logs.

#### *Interpretation*

Ten, relatively thin lobes are recognised in the Nålneet outcrop section (Fig. 4.8). The absence of thick mudstone intervals possibly representing interlobe complex deposits suggests that these lobes are part of the same lobe complex (Prélat et al., 2009). Lobes stack together and show repeated thickening upward packages from lobe fringe to lobe off-axis and lobe axis deposits. Thickening upward packages are widely recognised in lobes of many submarine fan systems, however their origin is still a matter of debate (e.g., Hiscott & Ghibaudo, 1981; Macdonald et al., 2011a). These trends are generally interpreted as the result of either lobe progradation (Ricci Lucchi, 1975; Grundvåg et al., 2014; Zhang & Dong, 2020) or the lateral shifts in lobe depocenters that form compensation cycles (Mutti & Sonnino, 1981; Prélat et al., 2009; Pyles et al., 2014). According to Macdonald et al. (2011a), lobe progradation results in repeated thickening upward packages across the fan system whereas compensational stacking results in varying thickness trends across the fan system. The repeated thickening upward packages observed in lobes of the Nålneet section suggest an upward increase in the degree of erosion and of degree of confinement at lobe scale due to the progradation of the lobes. Additionally, lateral changes in lobe thicknesses are documented from the correlated section (Fig. 4.8). Usually, stacking patterns of lobes are best documented in seismic datasets where lateral changes in lobe thicknesses are commonly attributed to the compensational stacking of lobes (Deptuck et al., 2008; Bourget et al., 2010). At outcrop scale, the lateral changes in lobe thicknesses could also suggest local compensational stacking of the lobes (Prélat et al., 2009).

The Nålneet section is characterised by a high proportion of amalgamated and thick-bedded turbidite beds suggesting deposition mainly by high-density turbidity flows (Walker, 1966; Lowe, 1982). Additionally, the frequent scouring, abundant rip-up mudstone clasts and erosive sole marks suggest deposition mainly by strong, highly erosive turbidity flows (Walker, 1966; Mattern, 2002). This could suggest deposition in semi-confined slope-proximal settings where

erosion is enhanced by the hydraulic jumps that passing flows experience when they travel from confined slope channels to unconfined basin floor areas or by the break-in slope associated with the abrupt decrease in slope angle at the transition to the basin floor (Komar, 1971; Macdonald et al., 2011b; Pohl et al., 2019; Soutter et al., 2021). The lateral increase in the amalgamation degree noted from the correlated logs, could indicate a gradual transition from unconfined deposition to deposition in more confined settings, such as the proximity to the terminus of channels (Mutti & Normark, 1991; Mattern, 2002; Wynn et al., 2002). The two debrite beds observed in the section record *en masse* deposition by cohesive debris flows (Mulder & Alexander, 2001). Even if debris flows deposits are occasionally reported from distal settings (e.g., Gee et al., 1999), these types of beds tend to occur mostly in proximal settings because they typically have shorter run-out distances than turbidity currents (Talling et al., 2012). Therefore, the Nålneset outcrop section represents deposition and stacking of lobes in a slope-proximal part of a lobe complex, or in the transition zone between the feeder channels and the proximal part of a lobe complex.

#### **4.2.4 Veidnes**

##### *Description*

The studied succession in Veidnes in Kongsfjorden consists of several small outcrops located on the northern and southern end of the peninsula (Fig. 3.1C). Overall, the succession consists of a high proportion of amalgamated beds (20.1 %), HEBs (19.8 %) and thin-bedded turbidites beds (18.8 %; Fig. 4.7B). Even if some coarse-grained turbidite beds (BT 2) have been observed in Veidnes, the succession consists mostly of fine-grained to medium-grained sandstone (71 % of sandstone). Beds have an average thickness of 33.6 cm.

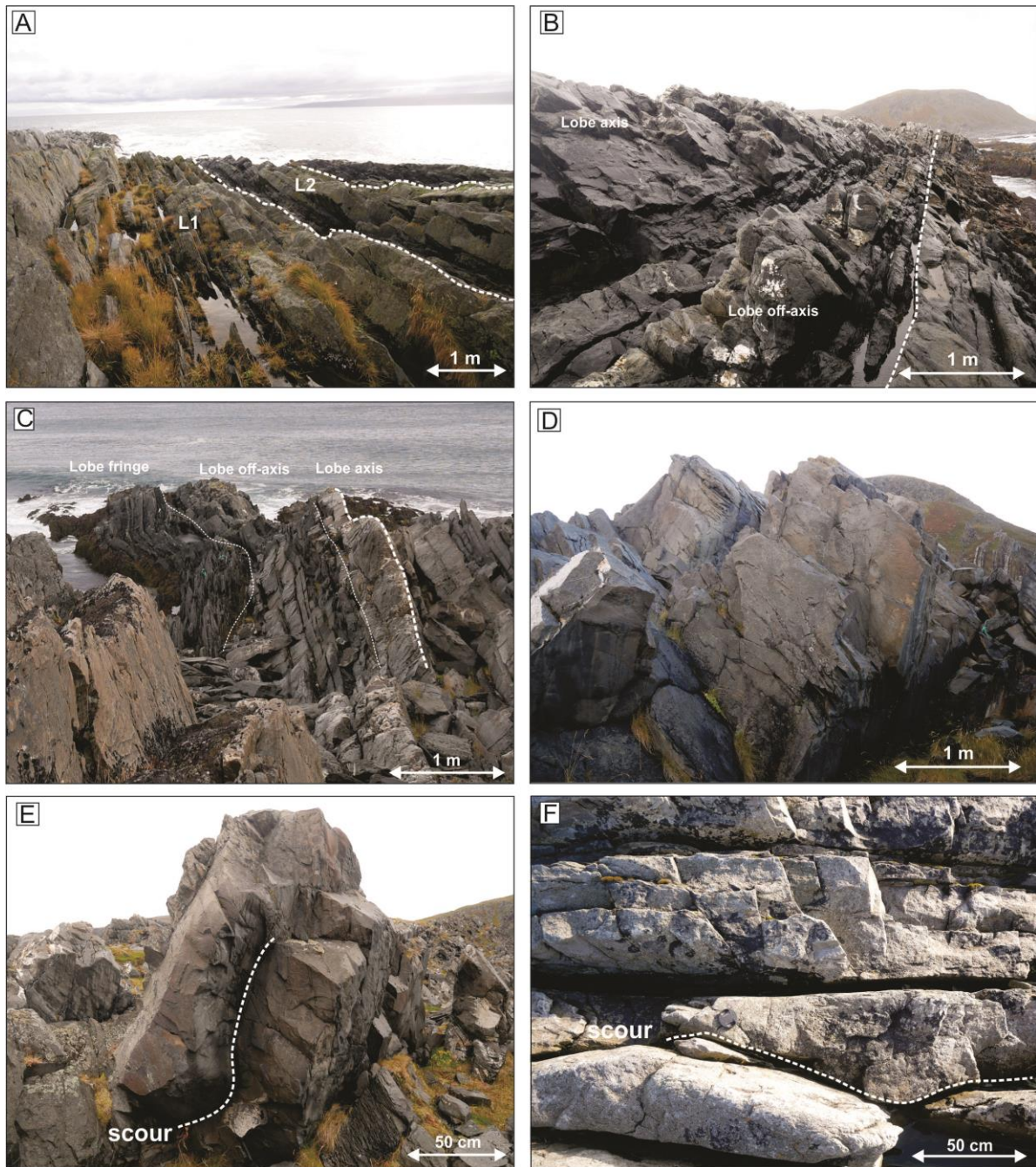


**Figure 4.9:** Details of the Nålneset outcrop section. (A) Outcrop photo of a part of the Nålneset section. Stippled lines indicate the bounding surfaces of lobes 1 and 2 (See Fig. 4.8). (B). Outcrop photo of a part of the Nålneset section. Stippled line indicates the bounding surface of a lobe (not logged). Note its two-fold architecture with a thin-bedded lower part (lobe off-axis deposits) and a thick bedded upper part (lobe axis deposits). (C) Outcrop photo of a lobe (not logged). Note its two-fold architecture with a thin-bedded lower part (lobe fringe and off-axis deposits) and a thick bedded upper part (lobe axis deposits). (D) Thick-bedded turbidite beds (BT 3; Lobe axis deposit). (E). Amalgamated turbidite bed (BT 1c) with a sharp amalgamation surface displaying a scoured base (stippled line). (F) Medium-bedded turbidite bed (BT 4a) exhibiting a scoured base.



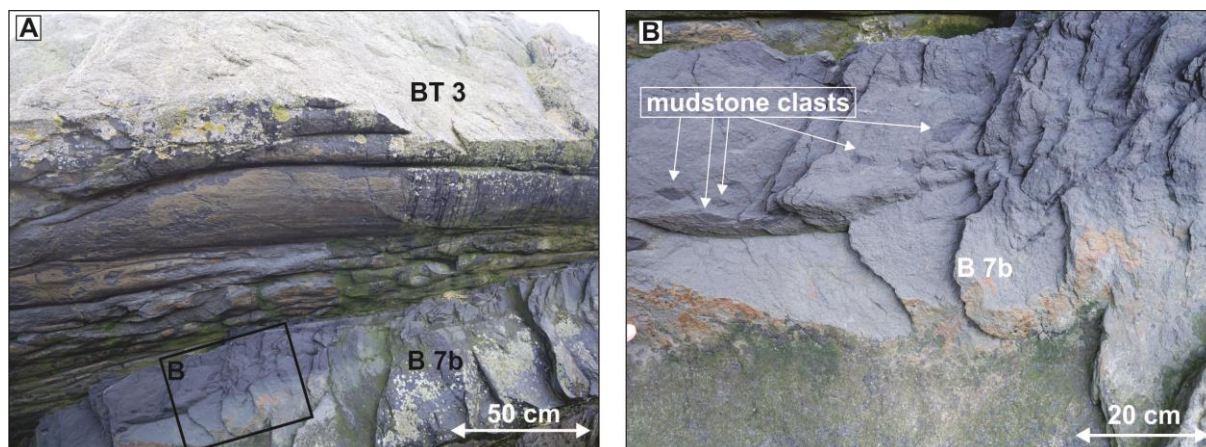


**Figure 4.10:** HEBs observed in the Nålneiset outcrop section. (A) HEB (BT 7b) under a thick-bedded turbidite bed (BT 3) showing sole marks. (B). HEB (BT 7b). Note the numerous small mudstone clasts dispersed in the mud-rich matrix.

The southern part of the peninsula is characterised by well exposed, laterally continuous beds that allowed correlation of two stratigraphic logs (for a total cumulative thickness of 31 m) and the recognition of four lobes (Fig. 4.11). Lobe 1 is 5 m thick and shows thickening and then thinning upward trends. The lowermost part of the lobe consists of lobe off-axis deposits (BT 4, BT 5, and BT 6, and BT 7) grading into lobe axis deposits in the uppermost part of the lobe (BT 1, BT 2 and BT 3; Figs 4.3 and 4.12). The lobe axis deposits have an erosive, channelised base with abundant sole marks (Fig. 4.3A and C) and are overlying two HEBs that pinch out towards the southwest. Lobe 2 is 8 m thick and shows a thickening and then thinning upward trend (Fig. 4.11). The thickest beds contain abundant intraformational mudstone clasts and various erosive features such as flutes (BT 2). Lobe 3 is 11 m thick and shows two thickening upward trends interrupted by a short interval showing a constant bed thickness. A thin interlobe deposit (BT 6) indicates the transition to lobe 4 (Fig. 4.11). Lobe 4 consists of heterolithic lobe fringe and lobe off-axis deposits (Fig. 4.13). Its thickness however is unknown due to outcrop limitations. The lobe consists of BT 4, BT 5 and BT 6 beds and a high portion of HEBs (BT 7; Fig. 4.13B).

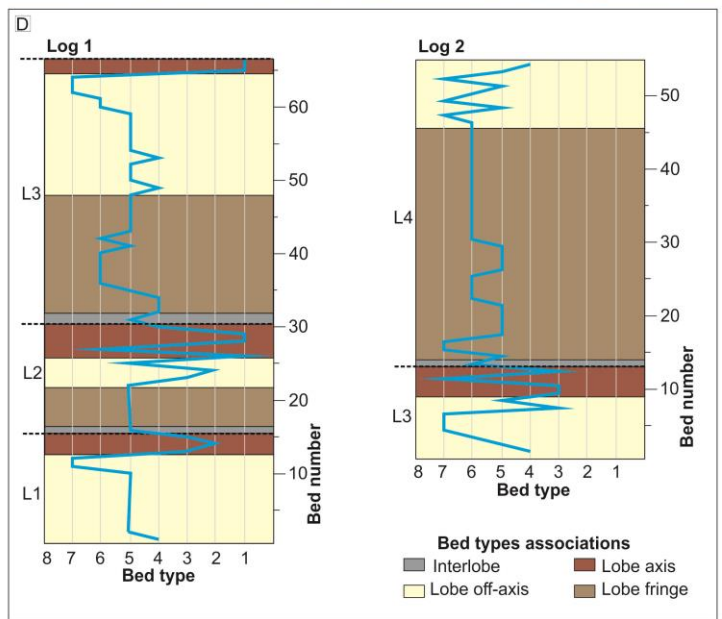
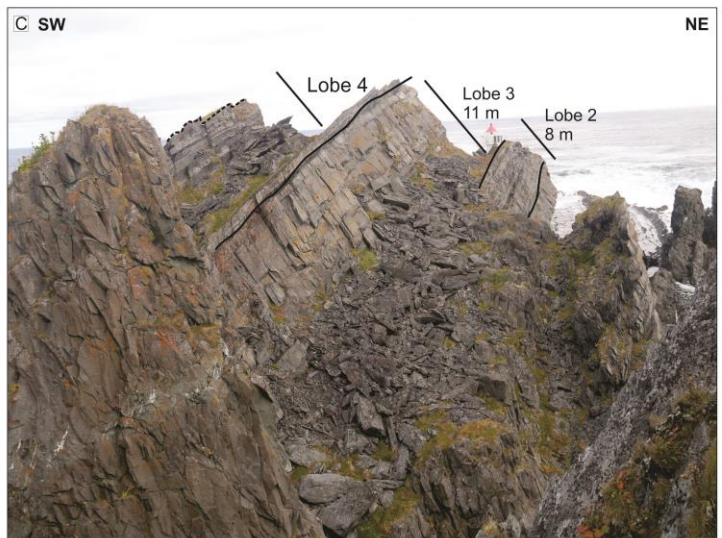
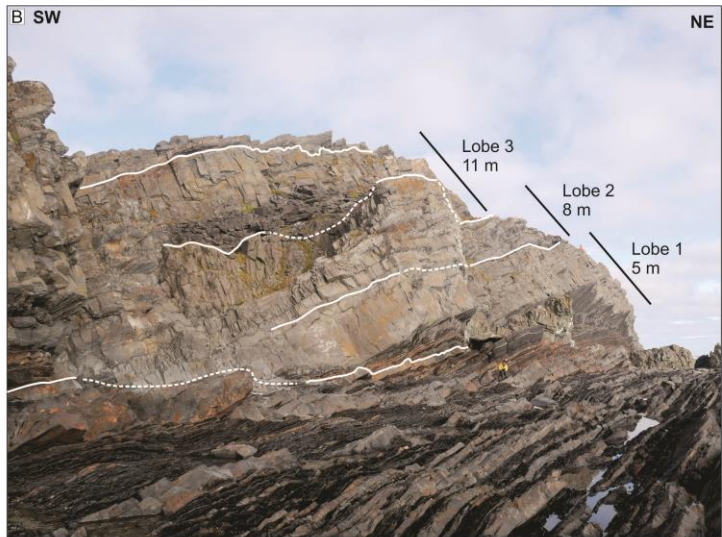
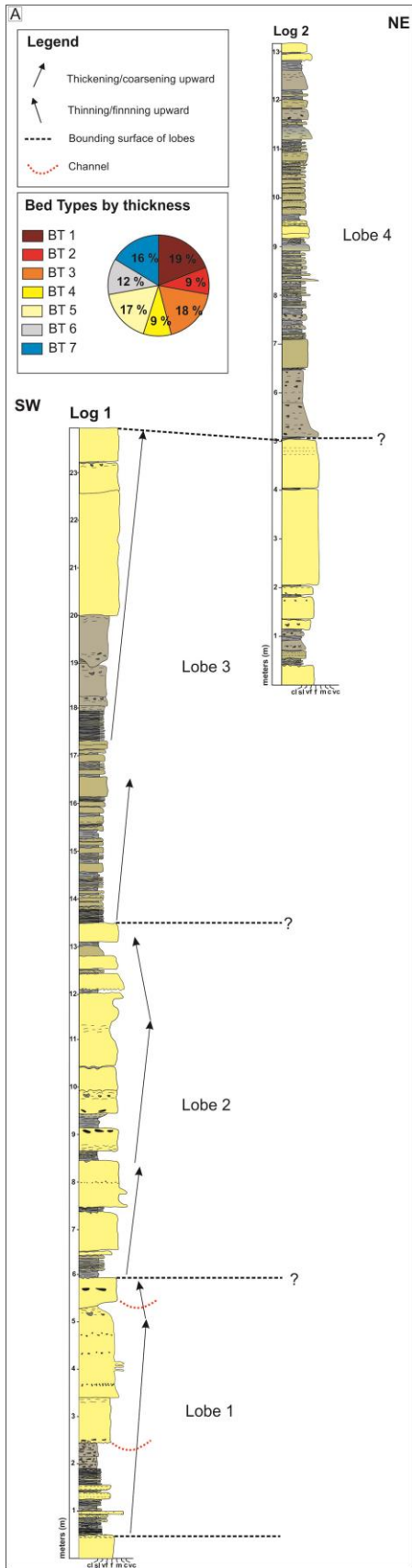




**Figure 4.11:** (A) Correlated stratigraphic logs from the southern part of Veidnes showing three well developed depositional lobes and the lower part of a potential fourth lobe. The pie chart illustrates the percentage of each bed type from the two stratigraphic logs (by thickness). (B) Outcrop photo showing the architecture of the first three stacked depositional lobes (lobes 1 to 3). (C) Outcrop photo of lobes 2, 3 and 4. (D) Diagrams illustrating the vertical variation and distribution of bed types (by bed number) for log 1 and log 2. Note that the thicknesses of the bed type associations do not reflect the actual thicknesses of the deposits.

The northern part of the peninsula consists of small, isolated outcrops that could not be correlated. However, they are all of excellent quality enabling detailed descriptions of bed types. A fifth lobe (lobe 5) showing a 3.5 m thick amalgamated lobe axis deposit overlying lobe off-axis deposits is recognised from a small outcrop (Fig. 4.14). However, the base of the lobe has not been clearly identified, therefore its thickness is unknown. The lobe off-axis deposits consist of BT 3, BT 4, BT 5 and BT 6 beds, some of which are thinning laterally (Fig. 4.14D).

The Veidnes outcrop section is characterised by a high proportion of HEBs (20 %; Figs. 4.7D and 4.15). The observed HEBs consist of BT 7b (i.e., exhibiting a thin basal sandstone unit). Their debris division contain numerous small mudstone clasts dispersed in a soft-sediment deformed mud-rich matrix (Fig. 4.15F). The HEBs are observed in lobe off-axis and lobe fringe deposits in the lower portion of the lobes (e.g., in lobes 1 and 3). Additionally, a well exposed outcrop in the northern part of the peninsula shows stacked HEBs (up to 2 m thick succession) that alternate with turbidite beds (Fig. 4.15).

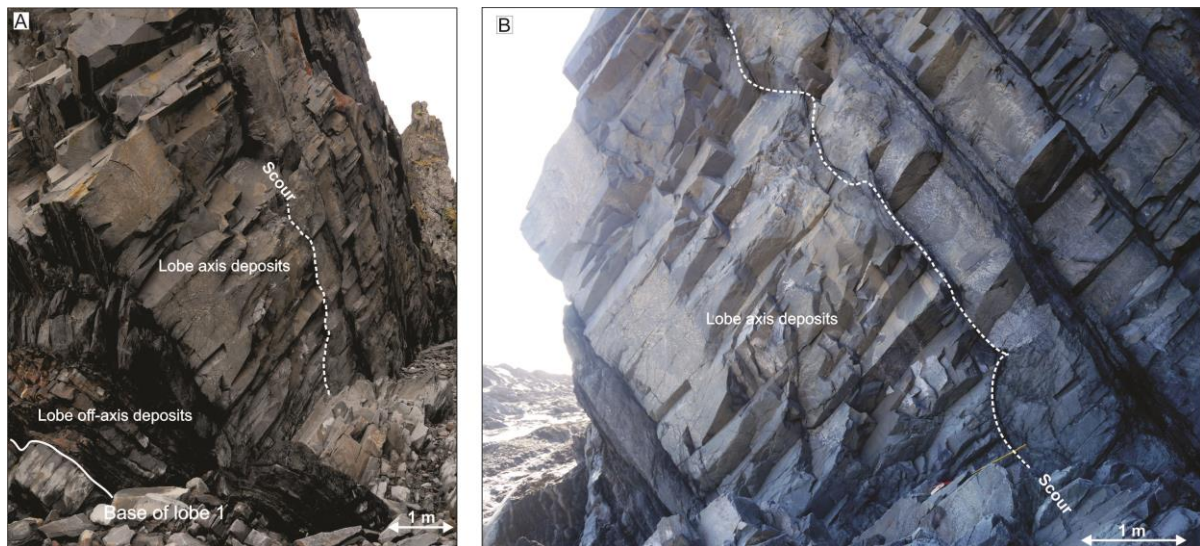


**Figure 4.12:** Outcrop photos of lobe 1 in Veidnes (see Fig. 4.11) showing: (A) Lobe off-axis and axis deposits. (B). Lobe axis deposits.



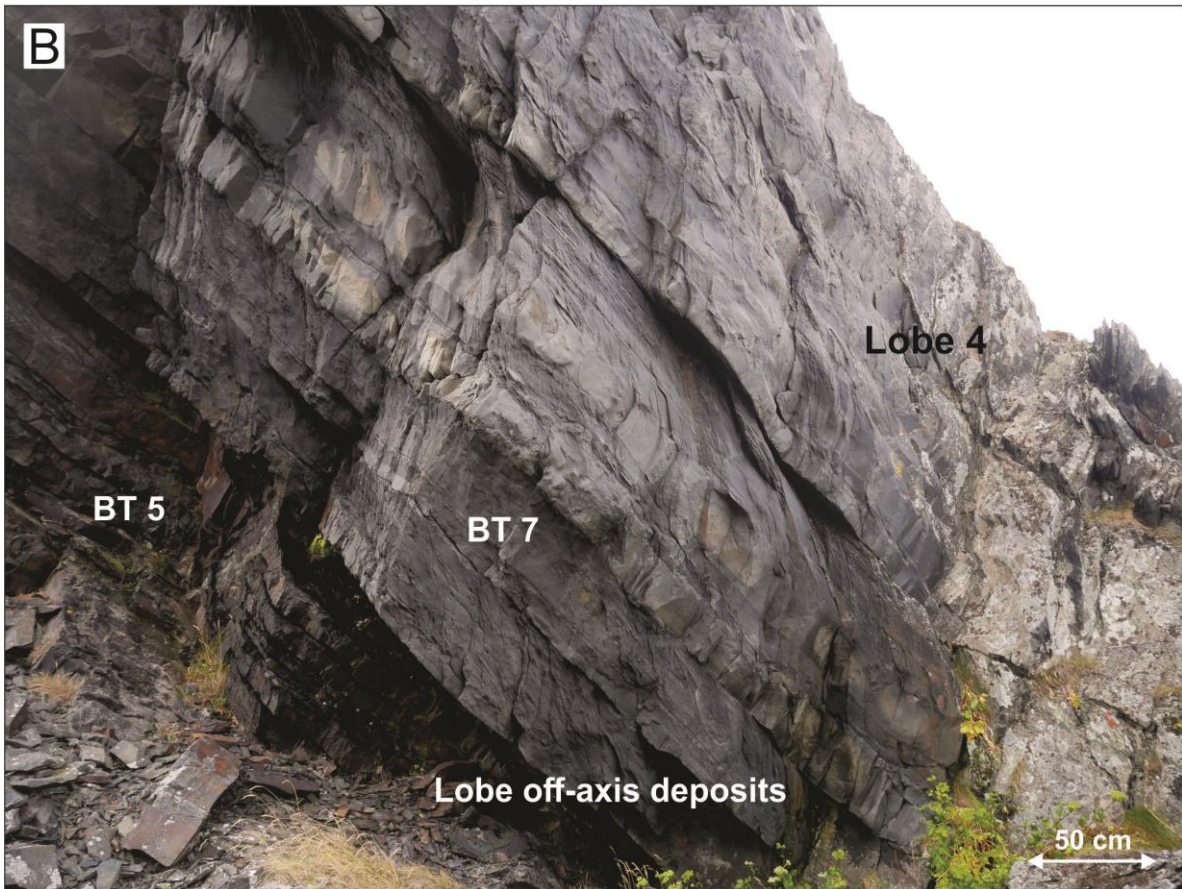
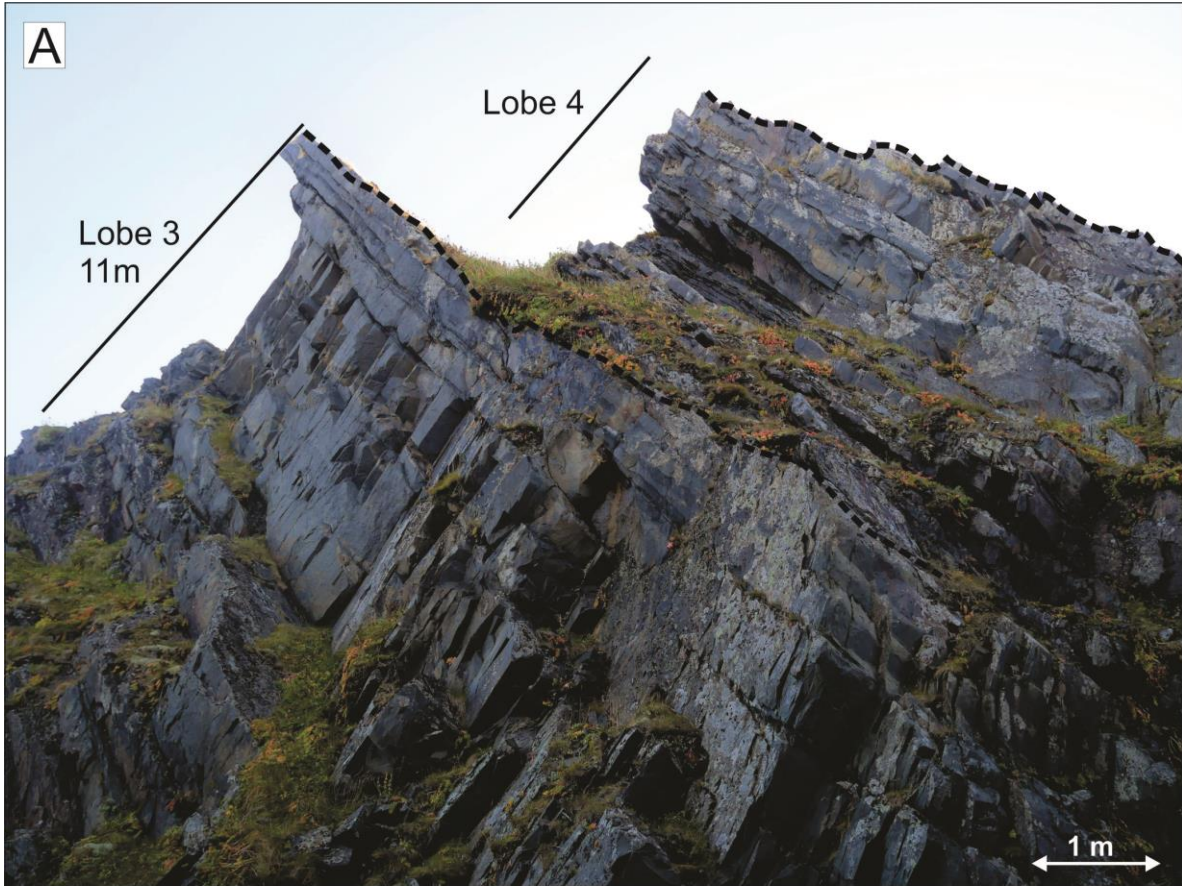




**Figure 4.13:** (A) Outcrop photo showing lobes 3 and 4 of the Veidnes outcrop section (see Fig. 4.11). (B) Outcrop photo showing the lobe off-axis deposits of lobe 4 consisting of thin-bedded turbidite beds (BT 5) in its lower part and HEBs (BT 7) in its upper part.

*Interpretation*

Five distinct lobes of approximately similar thicknesses (5 to 11 m) are recognised from the Veidnes outcrop section. Most of the lobes exhibit internal thickening upward cycles passing from lobe fringe deposits to lobe off-axis and lobe axis deposits that could suggest lobe progradation (Macdonald et al., 2011a; Grundvåg et al., 2014). However, some lobes also show thickening and then thinning upward trends. According to Macdonald et al. (2011a), progradation results in repeated thickening upward packages across the fan system whereas compensational stacking results in varying thickness trends across the fan system. Lobes showing different bed thickness patterns have been observed in several submarine fan systems (e.g., Prélat & Hodgson, 2013; Piazza & Tinterri, 2020). Prélat and Hodgson (2013) suggested that a wide range bed thickness patterns occur within lobes because sediment density flows tend to fill topographical lows resulting in shifts of the location of the lobe depocenter. Therefore, the different stacking trends observed in the lobes of the Veidnes outcrop section are interpreted as representing the compensational stacking of lobes.

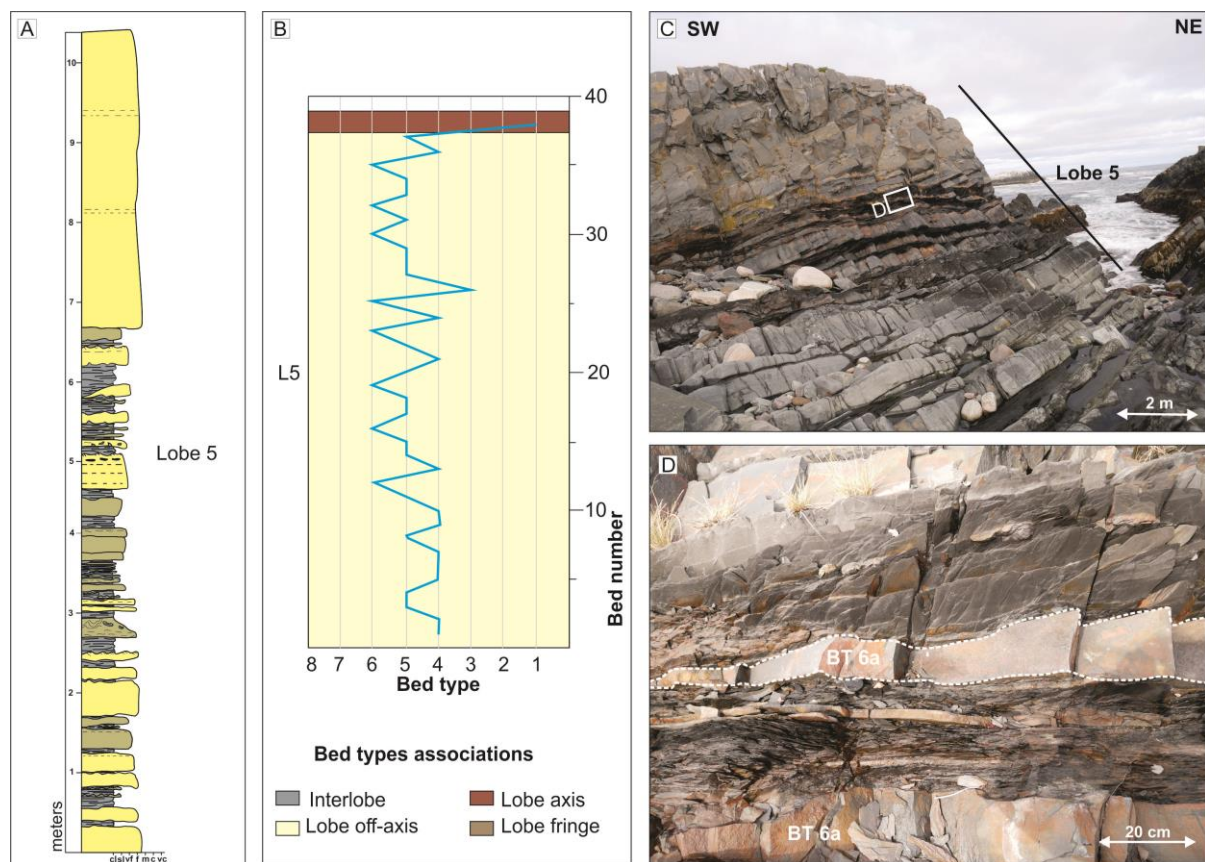




**Figure 4.14:** (A) Stratigraphic log of lobe 5 in the Veidnes outcrop section. (B) Diagrams illustrating the vertical variation and distribution of bed types (by bed number) for lobe 5. Note that the thicknesses of the bed type associations do not reflect the actual thicknesses of the deposits. (C). Outcrop photo of lobe 5. Note the two-fold architecture with a thin-bedded lower part and a thick-bedded, amalgamated upper part. (D). Lobe off-axis deposits of lobe 5. Note how the fine-grained turbidite bed (BT 6) is thinning laterally (stippled lines).

The Veidnes outcrop section is characterised by a high percentage of amalgamated turbidite beds (BT 1) suggesting deposition by highly erosive, high-density turbidity flows (Walker, 1966; Mattern, 2002). The lower part of the succession is characterised by frequent scours and channelised lobe axis deposits suggesting deposition in semi-confined settings where flows travel from channelised settings to lobe settings. Additionally, the outcrop section is characterised by a significantly high percentage of thin-bedded turbidite beds (BT 5) suggesting deposition by low-density turbidity currents (Bouma, 1962; Stow & Shanmugam, 1980) and of HEBs (BT 7) suggesting deposition by transitional flows that transform from turbulent to laminar flow conditions (Haughton et al., 2003; Haughton et al., 2009). HEBs are reported from several ancient submarine fans around the world, including the Gottero Sandstone (Fonnesu et al., 2015; Fonnesu et al., 2018), the Karoo Basin (Hodgson, 2009; Spsychala et al., 2017a) and the Marnoso Arenacea Formation (Talling et al., 2004; Amy & Talling, 2006) and typically occur in the most distal areas of the fan systems. The Veidnes outcrop section is therefore interpreted as a representing deposition and stacking of lobes in a relatively distal area.

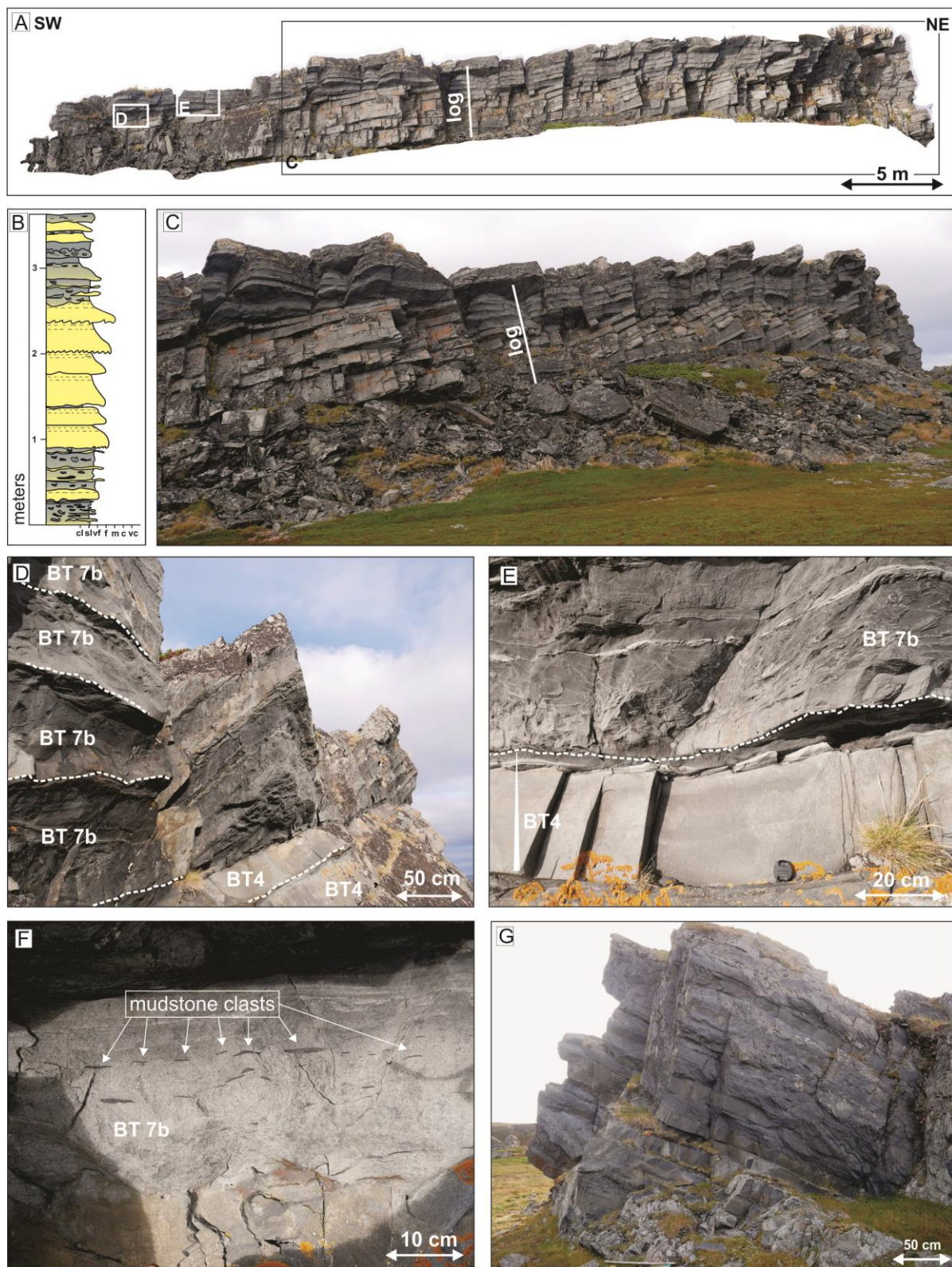


**Figure 4.15:** (A) Digital outcrop model of a small outcrop in the northern part of the Veidnes peninsula. (B) Stratigraphic log through outcrop (C) Photo of the investigated outcrop. (D) Stacked medium-bedded turbidites (BT 4) and HEBs (BT 7b). (E) Medium-bedded turbidite bed (BT 4) and HEB (BT 7b) showing

*a thin basal sandstone division and an upper mud-rich debrite division exhibiting abundant soft-sediment deformation structures. (F) Upper debrite division of a HEB (BT 7b). Note the numerous mudstone clasts dispersed in the mud-rich matrix. (G) Outcrop photo showing lobe off-axis deposits (stacked HEBs).*

#### **4.2.5 Seglodden**

##### *Description*

The studied succession in Seglodden (Fig. 3.1D) consists of a several hundred metres long section of alternating sandstone and mudstone beds exposed along the coast. The sandstone beds commonly stack to form thick amalgamated sandstone units that appear as positive topographic features in the present landscape and are separated by several metres thick heterolithic successions either dominated by thin-bedded turbidite beds, or mudstones (Fig. 4.16A). These units are commonly eroded or scree-covered and typically form topographic depressions or small bays in the present coastal landscape (Fig. 4.16A). About 45 % of the total measured thickness is missing due to erosion and scree cover, indicating that the investigated succession contains a significant amount of thin-bedded and/or fine-grained deposits. The mudstone intervals show well developed cleavage that is attributed to post-depositional deformation and may potentially explain the preferential erosion of these intervals. Other signs of post-depositional deformation such as folding, fractures, and quartz-filled veins are seen through the succession. The remaining, exposed part of the succession consists of 77 % of very fine-grained to medium-grained sandstones and is characterised by the absence of coarse-grained turbidite beds. The section shows a high proportion of thick-bedded turbidite beds (30.9 %), medium-bedded turbidite beds (21.1 %) and amalgamated turbidite beds (20.8 %) (Fig. 4.7). Beds have an average thickness of 48.9 cm.

Two stratigraphic logs allowed the identification of 37 distinct composite units, here referred to as lobes, along a 560 m composite section (Fig. 4.17). Individual lobes are recognised based on their bounding surfaces which exhibit sharp facies breaks between packages of thick-bedded, amalgamated turbidites (BT 1, BT 3) and packages of thin-bedded turbidites (BT 5, BT 6), mudstone or an eroded/scree-covered interval. Most of the lobes show upward thickening/coarsening trends, from lobe fringe deposits in the lowermost part of the lobes to lobe off-axis and lobe axis deposits in the uppermost part of the lobes (Figs. 4.16B and 4.17). However, the following bed thickness patterns are also identified: constant bed thickness; thickening then thinning upward; thinning then thickening upward; and overall thinning upward



(Fig. 4.17). Overall, lobes have highly variable thickness (4 to 27 m) and are 12 m thick on average (see Table 3).



**Figure 4.16:** (A) Outcrop photo showing the lobes exposed along the coast. Note how the eroded/scler covered intervals form small bays in the coastal landscape. Photo: Sten-Andreas Grundvåg. (B) Outcrop photo of lobe 5. Note the two-fold architecture with a thin-bedded lower part (lobe fringe to off-axis deposits) and a thick-bedded upper part (lobe axis deposits). (C) Thick-bedded upper part of a lobe (lobe axis deposits).

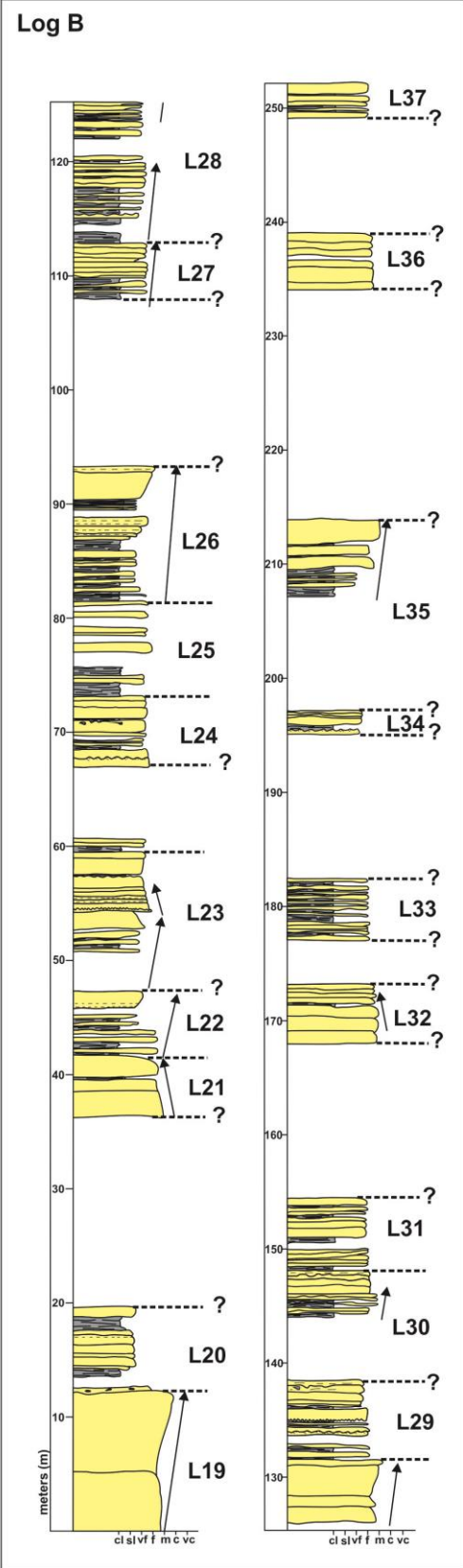
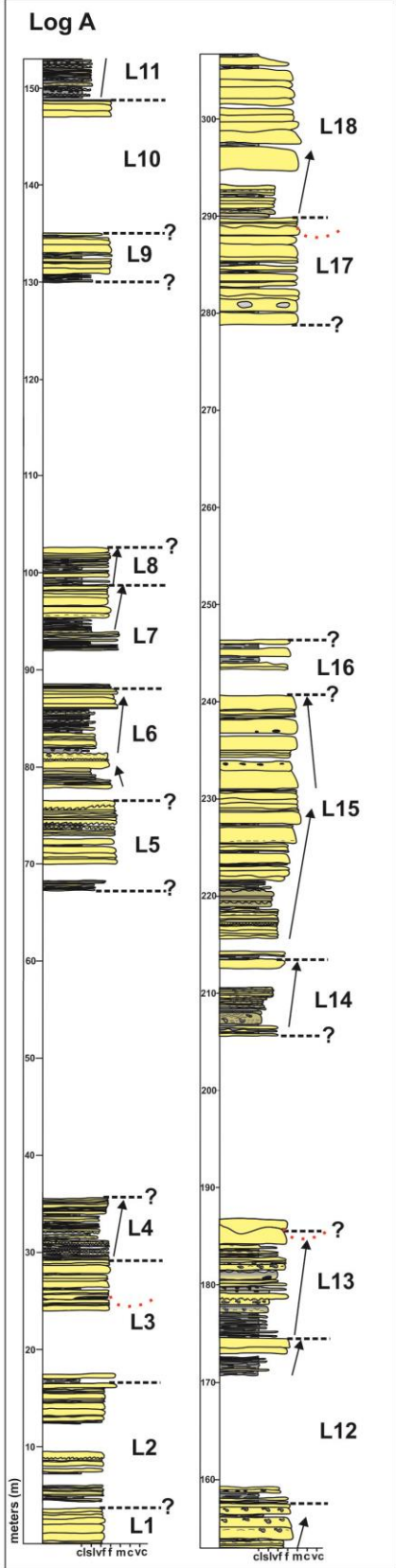
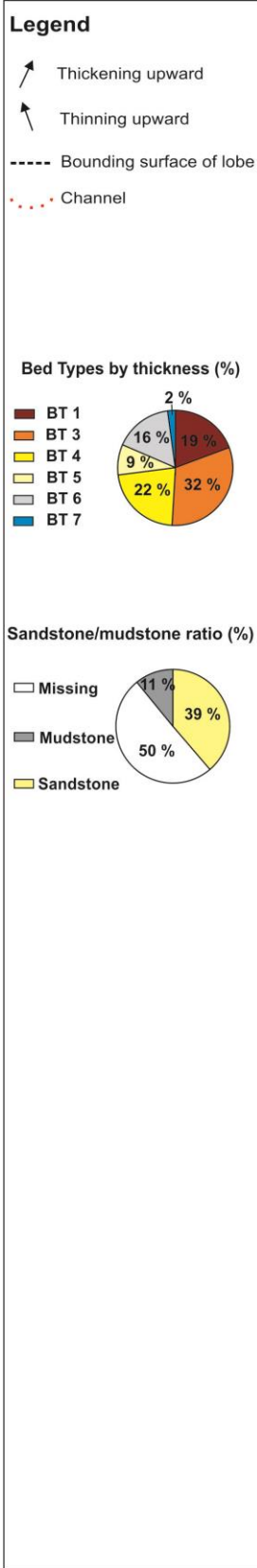


**Figure 4.17:** Stratigraphic logs A and B from the Seglommen outcrop section. Pie charts showing for the two logs (i) the bed type percentage (by thickness), (ii) the sandstone/mudstone percentage. A total of 37 units referred to as lobes are recognised in the succession (L1 to L37).

Many beds are laterally continuous and can be traced across the length of the outcrop. The cyclic stacking of lobes is best observed at a mountain ridge approximately 150 m (in a landward direction) from the coastal section where beds crop out (Fig. 3.1D). A lower portion of missing intervals are evident in the mountain section, and aided by drone and aerial photos, this enabled the correlation between the lobes of the coastal section with those of the mountain section (Fig. 4.18). One or more lobes appear to stack together into 20 to 60 m thick intervals referred to as lobe complexes that are separated by eroded or scree-covered intervals. These missing intervals could represent thick interlobe complex fines (*sensu* Prélat et al., 2009). However, due to the very high proportion of missing intervals in the coastal section and the impossibility to extrapolate on their lithology in the mountain section (thin-bedded turbidite beds versus hemipelagic mudstone), it is difficult to identify these potential architectural elements with certainty.

The Seglommen outcrop section is also characterised by a very high proportion of thick-bedded turbidite beds (BT 3). The BT 3 beds commonly show erosive bases, however no proper channel fill is observed throughout the investigated succession. These beds are often massive to weakly graded and they only rarely develop tractive structures. Additionally, the succession is characterised by the occurrence of very thick turbidite beds (i.e., beds >5 m thick; Fig. 4.19). These beds often show large (>20 cm), isolated mudstone clasts dispersed in the middle of the beds (Fig. 4.19C) representing amalgamation surfaces.

HEBs are rare throughout the succession (only 2% of the section). When occurring, they consist a thick basal sandstone division that exhibit mudstone clast in its upper part and is often overlain by a banded mudstone layer (BT 7a) and an upper debrite division containing abundant large mudstone clasts (Fig. 4.5A, B and C).



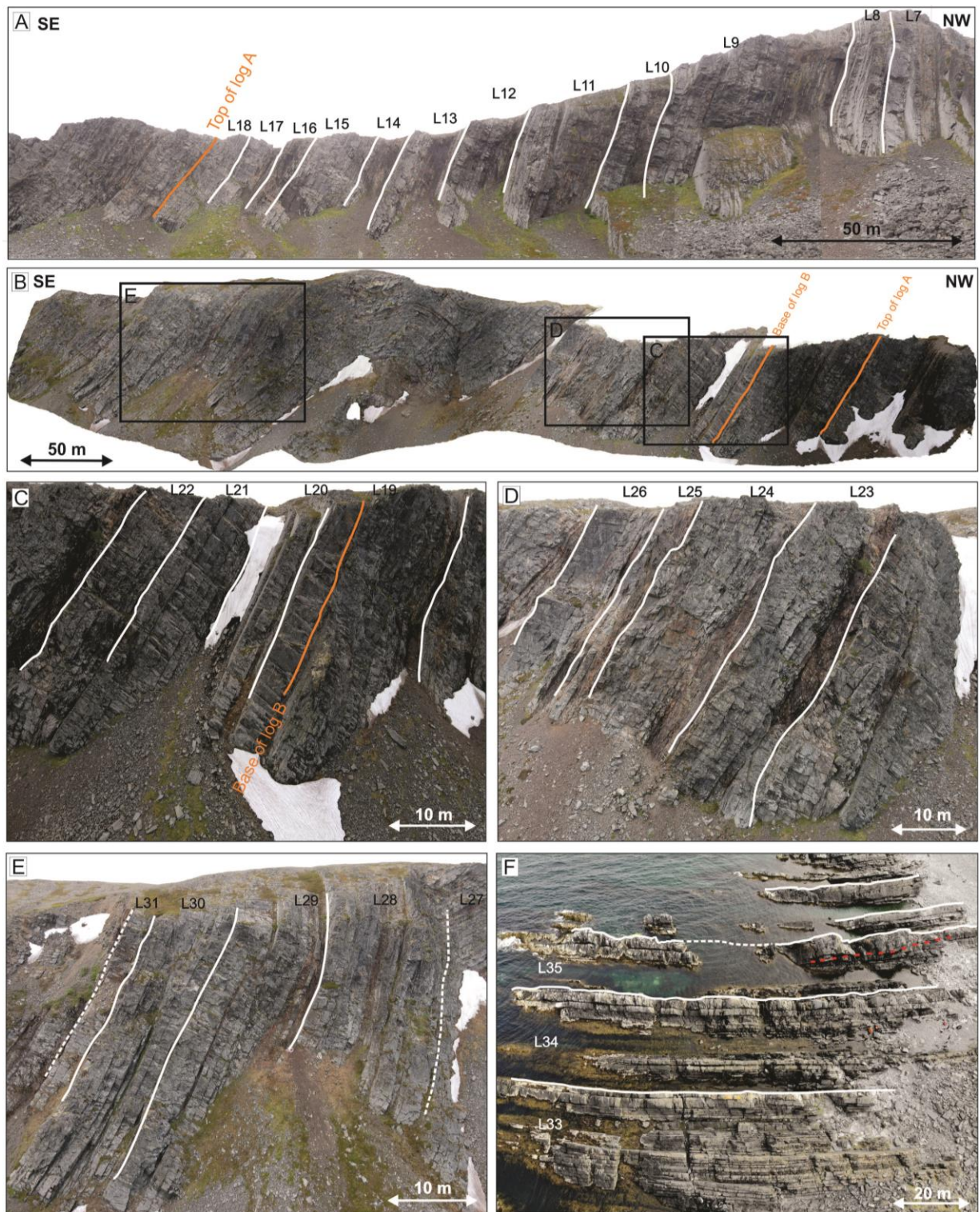


**Figure 4.18:** (A) Overview of the nearby mountain ridge which represent the lateral continuation of the coastal section of log A and tentative correlation with the lobes in log A (lobes 7 to 18; Fig. 4.17). (B) Digital outcrop model of the mountain ridge representing the lateral continuation of the coastal outcrop section of log B (Fig. 4.17). Model by Julian Janocha. (C), (D) and (E) Outcrop photos from the mountain ridge which represent the lateral continuation of the coastal section of log B and tentative correlation with the lobes of log B (lobes 19 to 31; Fig. 4.17). Photos: Julian Janocha. (F) Plan view photo of the

*uppermost part of the coastal succession shown in log B documenting lobes 33 to 35. Note the presence of a channelised bed (red stippled line). Photo: Sten-Andreas Grundvåg.*

### *Interpretation*

In the Seglommen outcrop section, a total of 37 stacked lobes are identified. Typically, each lobe consists of a thin-bedded lower part interpreted as representing deposition in lobe fringe and lobe off-axis settings and a thick-bedded/amalgamated upper part interpreted as representing deposition in lobe axis settings. Thus, the lobes commonly exhibit internal thickening upward trends from lobe fringe deposits to lobe off-axis and lobe axis deposits. Thickening upward trends have commonly been interpreted as resulting from lobe progradation (Macdonald et al., 2011a; Grundvåg et al., 2014; Zhang & Dong, 2020). However, five different types of bed thickness trends are also observed. According to Macdonald et al. (2011a), progradation results in repeated thickening upward packages across the fan system whereas compensational stacking results in varying thickness trends across the fan system. Lobes showing different bed thickness patterns have been observed in several submarine fan systems (e.g., Prélat & Hodgson, 2013; Piazza & Tinterri, 2020). Prélat and Hodgson (2013) showed that the compensational stacking of lobes will produce a full range of bed thickness trends rather than a cyclic thickening upward trend. Therefore, the different stacking trends observed in the lobes of the Seglommen outcrop section are interpreted as representing the compensational stacking of lobes. Additionally, lobes of the Seglommen outcrop section are stacked regularly over a great thickness suggesting high aggradation rates (Bourget et al., 2010).

The Seglommen outcrop section is characterised by a high proportion of amalgamated and thick-bedded turbidite beds suggesting deposition by high-density turbidity flows (Bouma, 1962; Walker, 1966; Lowe, 1982). However, the large proportion of thin-bedded and fine-grained turbidite beds and of missing intervals, probably representing eroded mudstone intervals indicates deposition predominantly by low-density turbidity flows and possibly hemipelagic fallout in a distal area (Bouma, 1962; Stow & Shanmugam, 1980). The overall lack of erosive features, the stacking of depositional lobes and the absence of coarse-grained sandstones (BT 2) indicate deposition in a zone of reduced sediment bypass such as the relatively distal part of lobe complexes (Normark, 1970; Mutti & Ricci Lucchi, 1972).



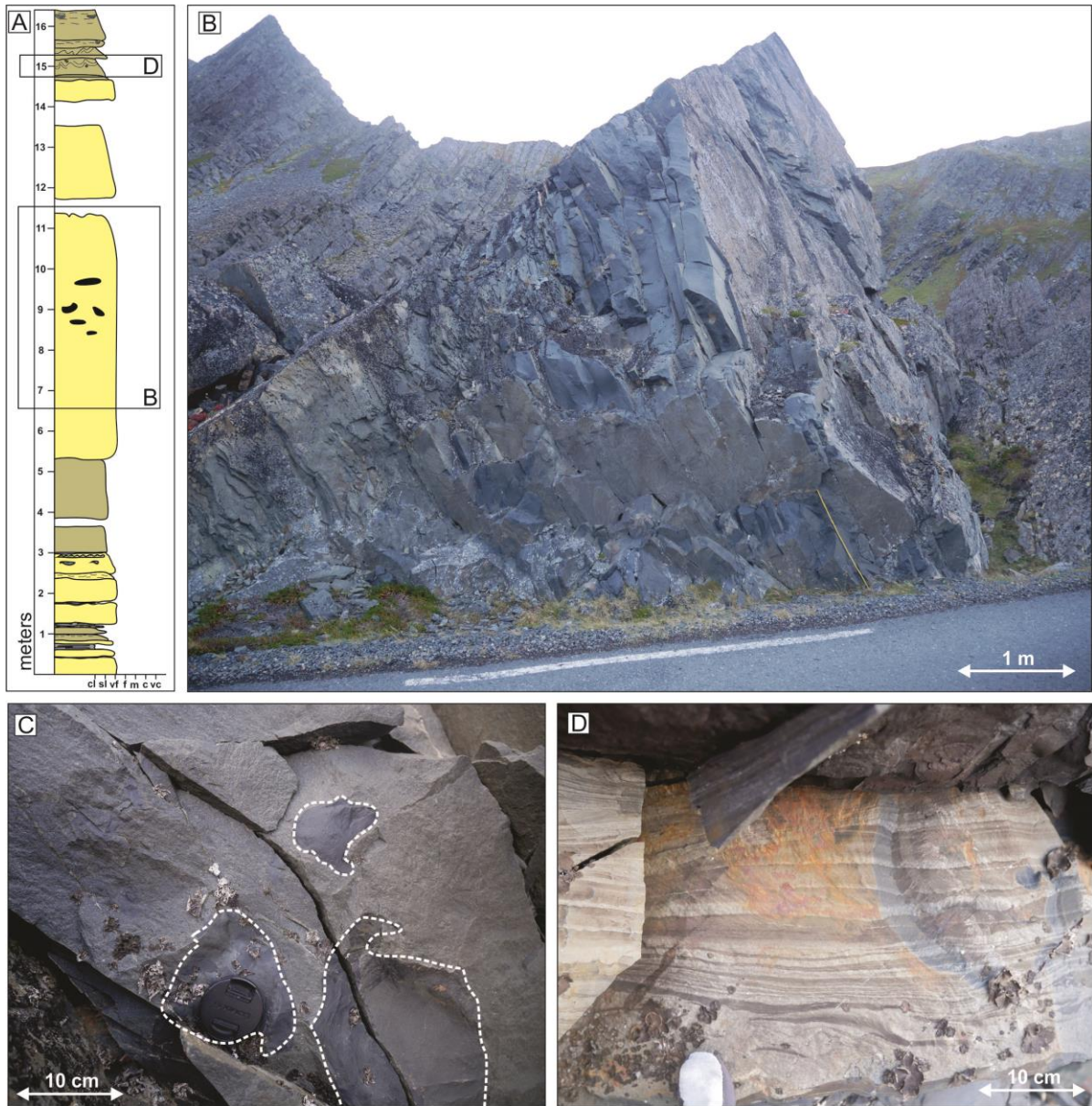


**Figure 4.19:** (A) Stratigraphic log through the upper part of a lobe (not shown in the stratigraphic logs of Fig. 4.17) showing a very thick amalgamated turbidite bed. (B) Very thick (ca. 6 m) amalgamated turbidite bed. (C) Large mudstone clasts dispersed in the middle of the very thick turbidite bed (see stratigraphic log). (D) Plane-parallel and convolute laminations in a medium-bedded turbidite bed (BT 4).

## 5 Discussion

The following chapter discusses the various depositional sub-environments of the Kongsfjord Formation and their constituent architectural elements. Although the formation has been extensively studied and the submarine fan setting is well established (e.g., Pickering, 1979, 1981, 1982a, 1983, 1985; Drinkwater et al., 1996; Drinkwater, 1997; Drinkwater & Pickering, 2001), there are no published work describing bed type variability in detail, and hybrid event beds have not yet been reported from the succession. Pickering (1981) documented different types of lobes in the succession and interpreted them in the context of the most classical submarine fan models that were established at that time (e.g., Mutti & Ricci Lucchi, 1975; Walker, 1978). However, research on lobes have progressed significantly in the last few decades, particularly with the study of their hierarchical elements, dimensions, and stacking patterns (e.g., Deptuck et al., 2008; Pr lat et al., 2009; Pr lat et al., 2010; Pr lat & Hodgson, 2013; Grundv g et al., 2014; Marini et al., 2015; Piazza & Tinterri, 2020). Despite the development, there is still an ever-increasing need for more empiric data from lobes accumulating under different settings to elucidate factors controlling their development and fully appreciate their variability. Therefore, this chapter particularly focuses on the deposition and distribution of hybrid event beds, as well as on lobe dimensions and stacking patterns. The results from this study are further compared to previous studies of the Kongsfjord Formation as well as to studies describing other ancient submarine fan systems.

### 5.1 Depositional sub-environments

#### 5.1.1 Slope-proximal settings

The N lneset section is characterised by a high proportion of amalgamated and thick-bedded turbidite beds (BT 1 and BT 3), frequent scouring, and the occurrence of debrite beds (BT 8; Fig. and 5.1). The high proportion of thick, massive turbidite beds suggests deposition mainly by high-density turbidity currents while the abundant scours and the high amalgamation degree suggest that the area was influenced by frequent erosion and bypass. Altogether, this advocate deposition in slope-proximal settings. In particular, the high amalgamation degree and the frequent scouring suggest enhanced erosive power of the flows (Mattern, 2002; Pohl et al., 2019). In slope-proximal settings, this might be caused by the hydraulic jumps that passing

flows experience when they travel from confined slope channels to unconfined basin floor areas and the break-in slope associated with the abrupt decrease in slope angle at the transition to the basin floor. The occurrence of a hydraulic jump is expected to favour scouring because bed shear and turbulence are increased locally (Komar, 1971; Macdonald et al., 2011b; Sumner et al., 2013). Thus, areas with repeated scours are associated with hydraulic jump arrays due to a decrease in slope gradient or a change in the degree of confinement (Baas et al., 2004; Macdonald et al., 2011b; Sumner et al., 2013; Hamilton et al., 2015; Dorrell et al., 2016). Recent experimental studies showed that enhanced erosion can also occur due to flow relaxation at the terminus of channels without the occurrence of a hydraulic jump (Pohl et al., 2019; Soutter et al., 2021). The loss of confinement upon leaving a channel causes the lowering of the velocity maximum within the flow and thus enhanced friction between the bed and the flow. The area downstream of a channel is therefore characterised by the readjustment of the flow to its new unconfined conditions leading to the development of frequent scours and amalgamation surfaces (Pohl et al., 2019). Bathymetric surveys in modern submarine fan systems showed that such a transition zone characterised by repeated, isolated erosive structures can develop downstream of channels and is referred to as the channel-lobe transition zone (e.g., Wynn et al., 2002; Ito, 2008; Macdonald et al., 2011b; Dorrell et al., 2016; Carvajal et al., 2017). The recognition of channel-lobe transition zones in ancient submarine fan systems is often challenging due to outcrop limitations. However, scours and megaflutes are commonly documented from several systems and interpreted as related to the occurrence of hydraulic jumps in base-of-slope to basin transitions where there are changes in slope gradient and degree of confinement (Elliott, 2000; Ito, 2008; Hofstra et al., 2015; Brooks et al., 2018a; Brooks et al., 2022). In the Nålneiset section, outcrop limitations prevent the recognition of a channel-lobe transition zone. However, the frequent scours and amalgamation surfaces could indicate a change in the degree of confinement or slope gradient in semi-confined, slope-proximal settings.

The Nålneiset outcrop section is also characterised by relatively coarse grain sizes, a high sandstone percentage and the absence of thick hemipelagic mudstone intervals. This indicates that deposition occurred mainly by high-density turbidity currents and that the upper most dilute part of the flow could have bypassed this proximal area. The bypass of the finer grain-size fractions can be explained by grain-size stratification. Flow stratification typically occurs as the flow passes from confined channelised settings to unconfined lobe settings as the flow

incorporates large volumes of sediments through erosion of the substrate (Pohl et al., 2019). The coarse-sediment fraction is concentrated towards the base of the flow whereas the fine and medium grain sizes are distributed more homogeneously over the height of the current (Baas et al., 2004; Eggenhuisen et al., 2020; Spsychala et al., 2021). The denser basal part is deposited immediately upon leaving the channel while the upper more dilute part travels further downcurrent. Drinkwater (1997) suggested that the sparse occurrence of coarse-grained beds indicated source sediment fluctuations controlled by sea level changes or tectonic activity. However, considering that flow stratification occurs predominantly where the sediment concentration in the flow is enhanced by erosion, the sparse occurrence of coarse-grained beds could be linked to the occurrence of repeated hydraulic jumps and deposition of coarser grain fractions further up-dip (which is not exposed in the present case due to outcrop limitations).

The Nålneset section have previously been studied by Drinkwater (1997), who suggested that it could have been part of a perched intraslope basin possibly bounded by a basin-margin parallel-oriented structural high separating the intraslope basin from the basin floor. This assumption was mainly based on paleocurrent data which possibly indicated flow deflection. He also argued that the overall coarse-grained character of the material, the absence of hemipelagic mudstone intervals, and the frequent occurrence of massive turbidite beds indicative of rapid deposition, pointed to deposition in a perched intraslope basin. However, this line of reasoning cannot be viewed as sufficient evidence for basin confinement since these features may as well be characteristic of slope-proximal settings in unconfined basins (e.g., Hofstra et al., 2015; Brooks et al., 2018a). Furthermore, recent studies of intraslope basins (Sinclair & Tomasso, 2002; Spsychala et al., 2015; Rohais et al., 2021) and of tectonically confined basins (Muzzi Magalhaes & Tinterri, 2010; Tinterri & Tagliaferri, 2015; Cunha et al., 2017; Tinterri & Piazza, 2019) emphasised that basin confinement strongly influences the vertical and lateral distribution of facies. These studies showed that ponded basins typically contain a high proportion of contained-reflected beds (i.e., beds exhibiting abundant deformation structures such as convolute laminations and liquefaction structures) and of beds developing tractive structures reflecting flow deceleration due to basin confinement and ponding processes. While beds showing tractive structures are observed in Nålneset, they are not predominant throughout the succession and no occurrence of beds showing liquefaction structures is noted from the 296 analysed beds. Typically, ponded basins show an asymmetric facies distribution due to flow reflection on the lateral margins of the basin (Cunha et al., 2017;

Tinterri et al., 2017). Due to outcrop limitations and the large size of the basin investigated here, it is impossible to infer such trends for the Kongsfjord Formation. Furthermore, intraslope lobes are typically incised by channels due to a lower base level (Spsychala et al., 2015). Even if widespread erosion is suggested by the frequent occurrence of shallow scours, no deep channel fills are observed from the studied succession. Based on the results from this study, it is therefore considered unlikely that the section in Nålneiset represents an intraslope basin bounded by morphological highs because it lacks the typical features and facies distribution observed in confined intraslope basins elsewhere. Rather the data presented here suggests slope-proximal environments of an unconfined basin.

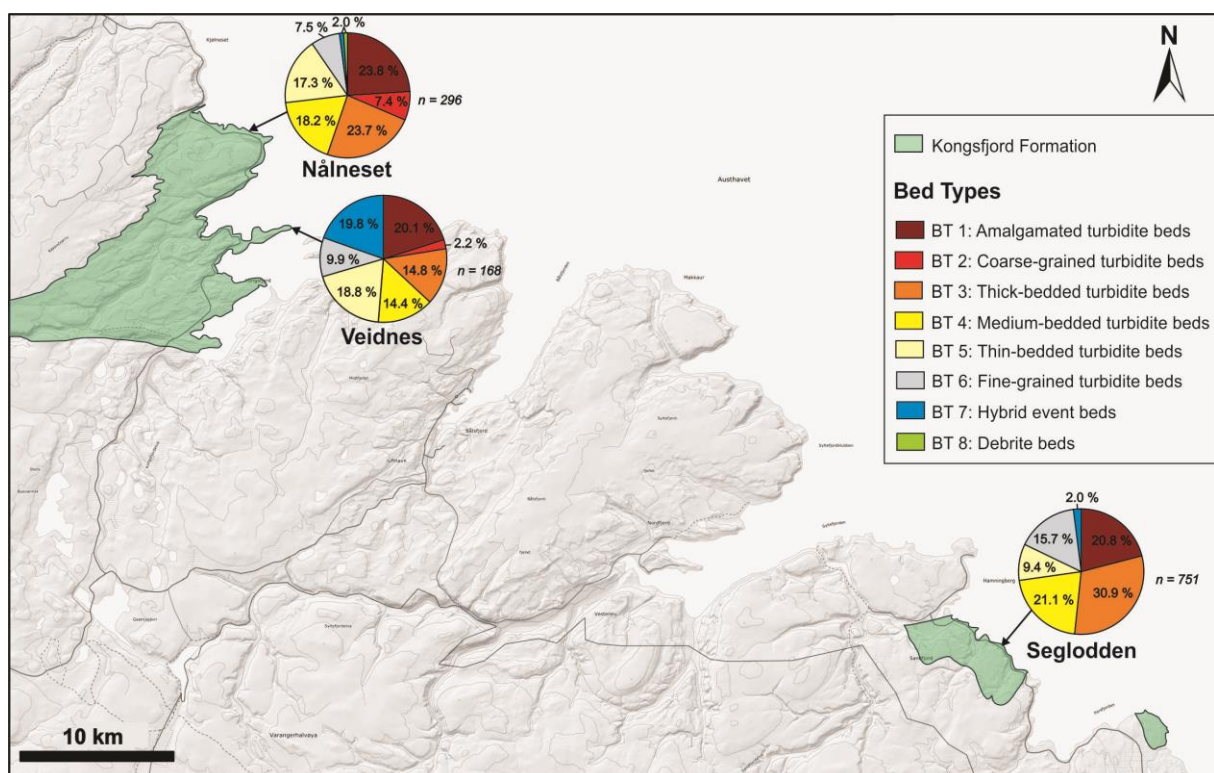


**Figure 5.1:** Summary distribution charts of the recognised bed types in the Kongsfjord Formation showing the total percentage of these (by thickness) for each studied locality. Source map: NMA (2021a).

### 5.1.2 Basin-floor settings

The Veidnes outcrop section has a significantly higher percentage of thin-bedded and fine-grained turbidites (BT 5 and BT 6) and a significantly lower sandstone percentage than the Nålneiset outcrop section (Fig. 5.1), suggesting deposition predominantly by low-density



turbidity currents. This also suggests deposition of a significant amount of fine-grained sediment fractions that bypassed the inferred most proximal area (i.e., the Nålneset outcrop section). Altogether this points to deposition in more distal settings than the Nålneset outcrop section. However, the high percentage of amalgamated turbidite beds (BT 1) and the occurrence of scours and channelised lobe axis deposits in the lower part of the succession (lobe 1; Figs 4.3 and 4.12) suggest that the area was periodically influenced by erosion processes related to the passage of powerful, high-density turbidity currents. The scoured base of the lobe axis deposits of lobe 1 may suggest the presence of shallow distributary channels that incised into and eroded its own off-axis and fringe deposits. This could suggest that the Veidnes outcrop section was fed by unstable, erosive feeder channels. The lowermost part of lobe 2 shows an interesting development consisting of successive thick-bedded and amalgamated turbidite beds deposited by high-density turbidity currents passing upward into coarse-grained turbidite beds exhibiting well developed tractive structures. This could reflect progressive deceleration of the turbidity currents against sea floor morphology created by sediments deposited in the early stage of the lobe development (Piazza & Tinterri, 2020). Rapid flow deceleration is also indicated by the upward increase in load and flame structures (Postma et al., 2009; Tinterri et al., 2016). Finally, an upward increase in thin-bedded turbidite beds indicates the progressive abandonment of the lobe or a lateral switch of the lobe depocenter related to up-dip channel avulsion (Hodgson et al., 2006). Altogether, this suggests that the Veidnes outcrop section represents deposition in relatively distal settings controlled by the avulsion of unstable erosive feeder channels.

Throughout the Veidnes succession, there is an upward increase in mudstone percentage, and in the proportion of thin-bedded and fine-grained turbidites and HEBs (BT 5, BT 6 and BT 7) suggesting a change from deposition predominantly by high-density turbidity currents to deposition by predominantly low-density turbidity currents and transitional flows. This may reflect the progressive decrease of sediment supply to the area controlled by either allogenic (local sea-level and/or climate changes) or autogenic processes (channel avulsion and compensational stacking of lobes; Hodgson et al., 2006). Since lobes of the Veidnes outcrop section show compensational stacking patterns and the upward decrease of sediment supply has not been observed elsewhere in the Formation, this decrease of sediment supply to the area is rather interpreted to be controlled by autogenic processes such as channel avulsion and compensational stacking of lobes. According to Pickering (1981), the Veidnes outcrop section

represents an outer-fan area in which lobes prograded and retreated suggesting source-controlled fluctuations in sediment supply. Here however, the compensational stacking observed in lobes of the Veidnes outcrop section suggesting the influence of autogenic processes controlling lobe deposition.

The Seglommen outcrop section is characterised by a high percentage of thick-bedded turbidite beds (BT 3), medium-bedded turbidite beds (BT 4) and amalgamated turbidite beds (BT 1; Fig. 5.1). The Seglommen outcrop section exhibits the recurrent presence of up to several meters thick mudstone intervals, which are often eroded or scree-covered in outcrop, suggesting that a significant amount of fine-grained sediments reached this depositional area. Furthermore, the Seglommen outcrop section lacks the frequent scours observed in Nålneiset and the channelised units observed in Veidnes. This suggests that deposition in Seglommen occurred in relatively distal basin-floor settings. In such distal settings, the fine sediment fraction that bypass the more proximal areas are generally deposited by low-density turbidity currents (Baas et al., 2004; Spychala et al., 2021). There is, however, a significantly high percentage of thick-bedded turbidite beds (BT 3) in the Seglommen outcrop section (Fig 5.1) and beds are also on average thicker than in the other studied localities (48.9 cm thick on average versus 37.8 cm for the Nålneiset outcrop section and 33.6 cm for the Veidnes outcrop section). The majority of the thick-bedded turbidite beds observed are massive to weakly graded and only very rarely do they exhibit tractive structures, collectively suggesting that deposition occurred from high-density turbidity currents. The origin of massive turbidite beds has long been a matter of debate (e.g., Shanmugam & Moiola, 1995; Lowe, 1997). Their deposition was commonly attributed to surge-type flows with high sediment fallout rates, such that the sediments have insufficient time to be reworked by tractive processes (Middleton & Hampton, 1973; Lowe, 1982). Additionally, Kneller and Branney (1995) proposed that massive turbidite beds are formed by continuous aggradation from sustained high-density currents in which a near bed layer is dominated by grain to grain interaction and hindered settling. Alternatively, en masse deposition by sandy debris flows has been invoked for the deposition of massive turbidite beds (Shanmugam, 1996; Talling et al., 2012; Talling et al., 2013). According to Talling et al. (2013), massive turbidite beds deposited by sandy debris flows have a distinctive swirly fabric (i.e., consisting of sandstone patches of coarser and finer grains) and pinch out abruptly. However, in most outcrops the recognition of these features is not possible, resulting in difficulties in determining how massive turbidite beds are deposited.

Several very abnormally thick beds occur in the Seglommen section (i.e., beds > 5 m thick; Fig. 4.19). Based on the internal occurrence of vague grain size breaks and amalgamation surfaces, these beds are interpreted as amalgamated turbidite beds resulting from successive high-density turbidity flows. Very thick turbidite beds have been reported from several ancient submarine fan systems (e.g., Ricci Lucchi & Valmori, 1980; Ricci Lucchi, 1995; Muzzi Magalhaes & Tinterri, 2010; Tinterri et al., 2022). Typically, they occur in confined settings as a result of flow reflection and dampening of turbulence in over-supplied basins, or they may record seismically triggered events along tectonically active basin margins (Ricci Lucchi & Valmori, 1980). Such turbidite ‘mega-beds’ typically show abundant deformation structures, complex assemblages of tractive structures, and thick mudstone caps (e.g., Felletti et al., 2009; Tinterri et al., 2022), features which have not been observed to any significant extent in the Seglommen succession. According to Pickering (1979), throughout the Seglommen section, the lack of thin mudstone intervals separating thick turbidite beds suggests rapid deposition by successive turbidity currents as a result of retrogressive flow sliding. The transformation of slides into turbulent flows is a common mechanism for initiating turbidity currents (Piper et al., 1999; Piper & Normark, 2009). Retrogressive flow sliding typically occurs when high volumes of unconsolidated sediments are available for successive failures from the same slump scar or canyon head and may also be triggered by breaching in canyons and channels (Van Den Berg et al., 2002). Such long-lived failure events may trigger quasi-steady, sustained-type turbidity currents, which in many turbidite systems have been linked to the deposition of thick, massive sandstone beds (e.g., Kneller & Branney, 1995; Felletti et al., 2009). Therefore, the formation of very thick, massive turbidite beds in the Seglommen outcrop section might suggest deposition by sustained-type turbidity flows.

The Seglommen outcrop section consists of aggradationally to slightly compensationally stacked lobes (Figs. 4.17 and 4.18). The lobes are stacked regularly over an accumulative thickness of > 500 m. There are no major erosional surfaces observed between the lobes, indicating that deposition in the area was most likely governed by relatively stable processes and that all lobes developed under similar conditions. This could reflect that the area was tectonically quiet and that the deposition was mainly controlled autogenic processes such as lobe avulsion (Prélat et al., 2009; Prélat & Hodgson, 2013). According to Pickering (1981), lobes in the Seglommen outcrop section suggest regular and stable deposition controlled by intrabasinal processes such as channel migration and avulsion.



## **5.2 Distribution of hybrid event beds**

This study documents the occurrence of hybrid event beds (HEBs) in the Kongsfjord Formation (Figs. 4.3, 4.5, 4.10 and 4.15). These beds, deposited by composite or transitional flows, comprise a lower sandy division deposited by a high-density turbidity current, and an upper muddy heterogeneous division deposited by a cohesive debris flow. Similar beds have been increasingly recognised in various submarine fan systems in the last few decades (e.g., Lowe & Guy, 2000; Haughton et al., 2003; Amy & Talling, 2006; Hodgson, 2009; Sychala et al., 2017a; Fonnesu et al., 2018; Pierce et al., 2018). HEBs are predominantly reported from lobe off-axis to lobe fringe settings and their formation is commonly associated with lobe progradation during periods of fan growth when the up-dip slope is out of equilibrium (Talling et al., 2004; Hodgson, 2009). However, several studies also show that HEBs may occur in proximal as well distal fan settings and that they may exhibit highly variable lithological expressions within an individual submarine fan system, and that different mechanisms can lead to their formation (Haughton et al., 2009; Kane et al., 2017; Fonnesu et al., 2018; Pierce et al., 2018). Several mechanisms have been invoked for their formation including: (i) co-generation by independent flows (debris flows and turbidity flows are simultaneously triggered by the failure of a slope and juxtaposed to form a HEB; Haughton et al., 2003; Haughton et al., 2009); (ii) the longitudinal evolution of a turbidity current (part of a turbidity current undergoes flow transformation due to entrainment of the substrate, suppressing turbulence and promoting transformation to a cohesive debris flow; Haughton et al., 2003; Talling et al., 2004; Ito, 2008; Haughton et al., 2009; Hodgson, 2009); (iii) vertical grain size segregation and deceleration of mud-enriched turbidity flows (high sediment concentrations lead to the stratification of the flow and the development of a dense basal layer and to the suppression of the turbulence; Sumner et al., 2009; Baas et al., 2011; Kane & Pontén, 2012; Kane et al., 2017).

### **5.2.1 Origin of HEBs**

In the Kongsfjord Formation, HEBs are identified in the three studied localities. However, there is a significant variation in their character and proportion across the study area (Fig. 5.1). Two sub-types of HEBs are recognised and can be differentiated mainly based on differences in

thicknesses, sand percentages and sizes of the mudstone clasts (see Fig. 4.1). HEBs of BT 7a show a higher sand percentage and a thick basal sandy turbidite division that occasionally contain large mudstone clasts in the uppermost part of the unit (Fig. 4.5A, B and C). This could suggest that these types of beds were deposited by flows that carried large volume of sediments which to a large degree bypassed the proximal areas of the fan system (Pierce et al., 2018). Additionally, the large mudstone clasts suggest that flow transformation most likely occurred due to substrate erosion and entrainment of mudstone clasts (Hodgson, 2009; Fongnesu et al., 2018). The disaggregation of the mudstone clasts causes enrichment of mud in the flow and promote transformation from turbulent to laminar flow conditions, with the flow eventually evolving into a cohesive debris flow (Haughton et al., 2003; Haughton et al., 2009; Pierce et al., 2018). These beds are only observed in the Segloddan outcrop section, inferred as the most distal settings, where they are rare (2% of the succession in thickness; Fig. 5.1). BT 7a beds tend to develop a thin banded division between the turbidite and debrite divisions (Fig. 4.5C). The banded division is associated with episodes of near bed turbulence dampening in flows that are intermediate between turbulent and laminar flow behaviour (Lowe & Guy, 2000; Haughton et al., 2009). This suggests that the turbulent flows travelled for a long distance before transforming progressively to laminar flows resulting in the development of a layer of transitional flow conditions depositing the banded division. Similar thin banded divisions have been observed in HEBs across various submarine fan systems elsewhere (e.g., Lowe & Guy, 2000; Haughton et al., 2009; Hodgson, 2009; Sumner et al., 2009; Kane & Pontén, 2012). Here, BT 7a represents the most distal expression of the HEBs observed in the Kongsfjord Formation. Similar beds have been observed in the most distal settings of the Ross Formation fan system by Pierce et al. (2018) (HEB 1 and HEB 2) and interpreted as deposits of large-volume flows that bypassed the up-dip environments.

HEBs of BT 7b show a thin basal turbidite division and a mud-rich debrite division containing abundant soft-sediment deformation and relatively small mudstone clasts (Figs. 4.3B, 4.5D and E, 4.10 and 4.15). At Veidnes, HEBs of BT 7b represent an important proportion of the succession (Fig. 5.1). They occur mostly interbedded with turbidite beds in the lowermost parts of the lobes, recording high concentration of these deposits in lobe fringe and lobe off-axis environments. The mud-rich nature of the matrix of the debrite division of BT 7b and the relatively small and sparse mudstone clasts may suggest that flow transformation occurred due to the progressive deceleration and turbulence dampening of a mud-enriched flow. The

transformation of the flow might be enhanced by the expansion and deceleration of the mud-enriched flow as it transitions from confined to unconfined settings. This may concentrate finer material and mud clasts in the upper flow which hinders turbulence and promote transformation to laminar flow and deposition of HEBs as frontal splays (Hodgson, 2009; Kane et al., 2017). Therefore, HEBs of BT 7b are interpreted as recording the transformation of mud-enriched turbidity flows due to flow deceleration and vertical grain size segregation leading to turbulence dampening and transformation to laminar flow conditions. The fact that HEBs are observed interfingering with turbidite beds suggest temporal and spatial switches in the type of flow (Pierce et al., 2018). Flow transformation can be promoted locally by changes in topography induced by previously deposited lobe deposits or by subtle changes in sea-floor topography. As the turbulent flow decelerates due to a decrease in slope angle or the reflection against some topography, it transforms partially to a laminar flow. The stratigraphic distribution of HEBs in the Veidnes outcrop section is similar to several other ancient submarine fan systems where HEBs have been observed mainly in lobe fringe settings (e.g., Hodgson, 2009; Sychala et al., 2017a; Pierce et al., 2018).

### **5.2.2 Controls on HEBs deposition**

The importance of autogenic versus allogenic factors on the control of HEB distribution has been stressed by several studies (e.g., Haughton et al., 2009; Hodgson, 2009). In the Kongsfjord Formation, the fact that BT 7a and BT 7b occur in different localities and never co-occur possibly suggests the influence of several processes including: (i) proximity to the break-in-slope; (ii) periods of slope disequilibrium due to feeder channel instability or tectonic; (iii) differences in lobe stacking patterns.

At Nålneset, in the inferred most proximal setting, HEBs are rare (1 % of the studied succession in thickness; Fig. 5.1). The rare occurrence of HEBs in the Nålneset outcrop section may reflect that flow transformation occurs more readily further down dip on the basin floor after the progressive entertainment and disaggregation of mudstone clasts, or that transitional flows have great run-out distances and bypass the most proximal fan areas. The Nålneset outcrop section records deposition in slope-proximal settings by flows that undergo a change from confined to unconfined settings. Turbulence can be temporarily increased with the occurrence of a

hydraulic jump in a flow that undergo a change from confined to unconfined settings, preventing the transformation to a cohesive flow (Kane et al., 2017; Fonnesu et al., 2018). HEBs are commonly absent in the most proximal areas of several submarine fan systems (e.g., Hodgson, 2009; Fonnesu et al., 2018). Where HEBs have been observed in proximal settings, their origin was attributed to enhanced erosion of the substrate due to a high degree of confinement of the flow (Haughton et al., 2009; Pierce et al., 2018) or increased tectonic activity (Muzzi Magalhaes & Tinterri, 2010).

Several studies have postulated that HEBs distribution was associated with periods of slope disequilibrium during fan initiation and growth (Haughton et al., 2003; Haughton et al., 2009; Hodgson, 2009; Pierce et al., 2018). Slope disequilibrium might be the result of a variety of factors including increased flow magnitude, mass-transport deposition, tectonic deformation, changes in sea-level, or a steep inherited slope profile (Cronin et al., 2000; Kneller, 2003; Ferry et al., 2005; Haughton et al., 2009; Pierce et al., 2018). The frequent occurrence of HEBs in the Veidnes outcrop section might reflect periods of disequilibrium associated with fan initiation and growth during which there might have been an increase availability of mud due to early phases of erosion. The lowermost part of the succession is characterised by channelised lobe axis deposits that suggests that erosion was enhanced locally by the change from confined to unconfined settings (Pohl et al., 2019; Eggenhuisen et al., 2020). Therefore, the phase of initiation of the lobe complex is associated with increased erosion of the substrate resulting in mud enrichment of the flows leading eventually to flow transformation and the deposition of HEB of BT 7b. Conversely, the rare occurrence of HEBs at Seglommen could suggest deposition on the basin floor under slope-equilibrium conditions.

Some studies proposed that the stratigraphic distribution of HEBs in vertical sections depends on the dominant stacking pattern of lobes and reflects the spatial relationships between lobe sub-environments (Spychala et al., 2017a; Fonnesu et al., 2018). Because HEBs are concentrated in lobe fringe and off-axis environments, where aggradational stacking is dominant, HEBs are distributed in a discrete area. Conversely, where compensational stacking is dominant, lobes sub-environments are stacked in a complex manner resulting in a stochastic distribution of HEBs (Spychala et al., 2017a). Therefore, the distribution of HEBs across the Kongsfjord Formation could indicate differences in lobe stacking patterns. In Seglommen, the dominant aggradational stacking pattern of lobes could result in a low percentage of HEBs in a

vertical section. In Veidnes, where lobes are observed to be compensationally stacked, this could result in a higher proportion of HEBs in a vertical section due to their stochastic distribution. Additionally, high aggradation rates can play a role in reducing basin-floor relief. This could result in flows having shorter slopes on which to accelerate, thus preventing the incorporation of mud from the substrate and the transformation of the flow into a cohesive debris flow (Pierce et al., 2018).

In the Kongsfjord Formation, HEBs are formed by several processes including longitudinal evolution of a turbidity flow into a debris flow by mudstone clasts entertainment and disaggregation (BT 7a) and transformation of a mud-enriched turbidity flow to a cohesive debris flow due to flow deceleration and grain size segregation (BT 7b). HEBs are absent in the most proximal investigated areas. In the distal areas, the occurrence and distribution of HEBs seem to be controlled by either slope disequilibrium during the early phase of development of the lobe complex or by channel avulsion and lobe stacking patterns. However, the paucity of HEBs in the Seglommen outcrop section could also be biased by the fact that the succession is partially eroded, particularly the lobe fringe deposits, and the HEBs could thus be preferentially eroded due to their high mud content leading to a lower proportion of HEBs in the recorded section.

### **5.3 Controls on lobe deposition**

Lobes have been identified in all the three studied localities (Figs. 4.8, 4.11 and 4.17) and are recognised as major architectural elements of the Kongsfjord Formation (see also Pickering, 1981, 1982a; Drinkwater & Pickering, 2001). Lobes have some common characteristics throughout the Kongsfjord Formation which have been used as recognition criteria, such as their tabular-shaped geometry, a two-fold architecture with a lower thin-bedded part and an upper thick-bedded part, and sharp facies breaks representing lobe tops and the bounding surfaces between successive lobes. Despite these common characteristics, the investigated lobes also exhibit significantly different thicknesses, internal hierarchy, degree of amalgamation, and different stacking trends are evident between the three studied localities (see Table 3). In several studies, it has been recognised that lobe deposits can have variable dimensions, stacking patterns and deposits even within an individual submarine fan system

(Deptuck et al., 2008; Prélat et al., 2009; Etienne et al., 2012). Their formation has been interpreted as an interaction of allogenic (tectonic settings, sea-level changes, climate) and autogenic (basin morphology, channel migration and avulsion) processes (Bouma, 2004; Ferguson et al., 2020). The extent to which these processes control the development and dimensions of lobe deposits has been a matter of debate (Prélat et al., 2010; Macdonald et al., 2011a; Marini et al., 2015; Hamilton et al., 2017; Spychala et al., 2020). Therefore, studying the variable expressions of lobe deposits across a system can be a key to understand factors controlling and influencing lobe deposition.

### **5.3.1 Lobe dimensions**

While lateral extent of the lobes could not be determined in the field due to outcrop limitations, significant variations in lobe thicknesses were noted between the three studied localities. Lobes in Nålneset are relatively thin and typically consist of a single lobe element (Fig. 4.8). In Seglodden, lobes form thick composite bodies typically consisting of several stacked lobe elements (*sensu* Prélat et al., 2009; Fig. 4.17). Elsewhere, lobe thicknesses have been observed to vary significantly even within a single submarine fan system (e.g., Deptuck et al., 2008; Prélat et al., 2009; Bourget et al., 2010; Morris et al., 2014) and a variety of factors have been invoked for these differences (Prélat et al., 2010; Hamilton et al., 2017; Spychala et al., 2020). The difference in lobe thicknesses between the studied localities in the Kongsfjord Formation could suggest the interaction of several factors including: (i) relative proximal to distal positions to the break-in-slope, (ii) feeder channel stability and avulsion frequency controlling lobe switching and compensational stacking, (iii) the degree of confinement.

The lobes of the Kongsfjord Formation are interpreted to record deposition in different depositional environments. In slope-proximal settings (i.e., Nålneset), where lobes are relatively thin, flow relaxation or hydraulic jumps at the mouth of up-dip feeder channels or near the break-in-slope can enhance the erosive power of the flows (Wynn et al., 2002; Macdonald et al., 2011b; Sumner et al., 2013; Pohl et al., 2019). Therefore, high-density turbidity flows can erode previously deposited lobes resulting in frequent amalgamation surfaces and overall thinner lobes with unrecognisable lobe elements (Deptuck et al., 2008; Brooks et al., 2018a). Additionally, hydraulic jumps can favour the bypass of the finer sediment

fraction and therefore hamper the development of the muddier lobe fringes in proximal areas (Spychala et al., 2021). Conversely, lobes developing in more distal settings (i.e., Seglommen), where the depositional gradients are gentler, are deposited by flows carrying higher volumes of sediments that bypassed the proximal areas. This could result in the deposition of thicker, composite lobes internally comprising stacked lobe elements. A similar proximal- to distal-thickening of the lobes has been observed in submarine lobes off the margin of East Corsica (see Deptuck et al., 2008), where thin, architecturally simple (typically consisting of a single lobe element) lobes were observed on the slope or near the break-in-slope and thicker, architecturally complex (consisting of several stacked lobe elements) lobes were observed in more distal locations.

The thickness variations within lobes can also reflect variations in feeder channel geometries and stabilities and in rates of sediment supply. Lobe dimensions are related to the number and frequency of flows and their concentration in sediments and therefore lobe deposits formed during low versus high sediment supply have different morphology (Deptuck et al., 2008; Spychala et al., 2020). Typically, increased sediment supply forces lobes to build vertically resulting in thicker deposits (Prélat et al., 2010; Rohais et al., 2021). The thickness differences within lobes of the Kongsfjord Formation might reflect variations in sediment supply rates possibly due to differences in feeder channel geometry or stability. In Nålneiset, the thin lobes could suggest an unstable sediment source, like a short-lived erosive feeder channel with limited sediment supply dominated by surge-type turbidity flows. In Seglommen, the thick composite lobes could suggest relatively constant sediment input by a long-lived feeder system. The occurrence of sustained-type turbidity flows could contribute to the great thickness and architectural complexity of the lobes.

The degree of confinement has been recognised as having a major influence on lobe dimensions and stacking (Prélat et al., 2010; Marini et al., 2015; Spychala et al., 2020). Typically, within unconfined settings the thickness of lobes is relatively restricted because of frequent switching in lobe position (compensational stacking) while in some confined depositional settings, lobes are forced to build vertically (aggradational stacking) forming thicker depositional bodies (Prélat et al., 2010; Spychala et al., 2020). The great thickness of the lobes in Seglommen could therefore reflect an increase in the degree of confinement within the system, possibly supporting the perched intra-slope basin setting of Drinkwater (1997). However, increased confinement

can also arise from other mechanism (see Sinclair & Tomasso, 2002; Lomas et al., 2004) and the data presented here do not favour such a setting.

The differences in lobe dimensions between the investigated localities of the Kongsfjord Formation appear to record differences in flow evolution (increase in transport distance) or in feeder channel stability rather than differences in basin settings (degree of confinement). However, most published studies documenting lobe dimensions also document their lateral extent. Additional information on lobes lateral extent, albeit limited by outcrop limitations, might be needed to confirm the results from this study. Additionally, the high proportion of eroded intervals (particularly in the Seglommen section) can lead to significant uncertainties in determining lobe bounding surfaces and therefore bias the estimated lobe thicknesses.

### **5.3.2 Lobe stacking patterns**

Most of the investigated lobes of the Kongsfjord Formation show cyclicity recorded at lobe element and lobe scale by thickening upward trends from lobe fringe deposits to lobe off-axis and lobe axis deposits. These trends are interpreted as representing lobe progradation and are commonly observed in lobes across a wide range of systems (Gervais et al., 2006; Deptuck et al., 2008; Mulder & Etienne, 2010; Macdonald et al., 2011a; Grundvåg et al., 2014). Thickness variations at the lobe element scale is commonly attributed to compensational stacking (e.g., Prélat et al., 2009; Prélat & Hodgson, 2013). However, there also seem to be differences in stacking trends between the lobes of the three studied localities. While lobes of the Nålneset and Seglommen outcrop sections are stacked continuously, showing an aggradational to slightly compensational style of stacking, lobes of the Veidnes outcrop section are stacked irregularly, showing a compensational style of stacking. There are several possible reasons that could explain the differences in lobes stacking patterns between the studied localities including: (i) the degree of confinement, (ii) sedimentation rates and/or feeder channel stability controlling avulsion and lobe switching.

Aggradational to slightly compensational stacking patterns have been predominantly observed in lobes in confined settings (e.g., Pyles, 2008; Marini et al., 2015; Sychala et al., 2015; Rohais et al., 2021). Typically, in confined settings, lobes are forced to prograde, or more commonly, to build vertically (aggradation) since accommodation space is limited (Prélat et al., 2010).



Lobes in semi-confined to unconfined settings typically show compensational stacking patterns as lobes tend to accumulate in the depressions formed between older lobes (Prélat et al., 2009; Prélat & Hodgson, 2013; Marini et al., 2015). Fully confined lobes are generally observed in relatively small tectonically active basins or in intraslope basins (e.g., Marini et al., 2015; Spychala et al., 2015; Tinterri et al., 2017). All lobes of the Kongsfjord Formation seem to some degree to show compensation cycles suggesting that deposition occurred in a relatively large, unconfined basin. However, the margins of the basin in which the Kongsfjord Formation turbidites accumulated and the relative stratigraphic position of the localities to each other are unknown, although it is undisputed that the Trollfjorden-Komagelva Fault Zone (TKFZ) defined the southernmost margin of the basin and controlled sedimentation and basin development in the region (see Siedlecka, 1985; Drinkwater et al., 1996; Roberts & Siedlecka, 2012). In general, confinement can be subtle and occur on one side of the system only, laterally, frontally or oblique to the main flow direction (Soutter et al., 2021). The aggradational to compensational stacking pattern of the lobes of the Seglommen outcrop section may suggest the influence of a lateral basin margin or a mid-basin high within the system. Confinement can also occur from a variety of processes such as inherited basin-floor topography, topography created by previous deposits (including mass transport complexes), and syn-depositional tectonic deformation (Hodgson & Haughton, 2004; Lomas et al., 2004; Kane et al., 2010). However, these processes are not supported by the results from this study.

Increased sediment supply to the basin (as a response to increased sediment flux governed by tectonism and climatic fluctuations, relative sea-level fall, or progressive confinement) is expected to force progradation of the turbidite system into the basin (Gardner et al., 2003; Hodgson et al., 2016; Spychala et al., 2020). The aggradational stacking pattern of lobes in Seglommen could reflect rather steady sediment supply in unconfined settings leading to aggradation and compensational stacking of lobes on the basin floor (e.g. Prélat et al., 2009). Pickering (1981) have previously noted the difference in lobes stacking patterns in the Kongsfjord Formation between the Seglommen and the Veidnes sections. He suggested that the differences in lobe stacking patterns could reflect differences in sediment distribution processes with lobes in Seglommen representing stable deposition controlled by autogenic processes such as channel migration and avulsion, and lobes in Veidnes reflecting source-controlled sediment distribution in sediment supply. The Seglommen area could be down-dip of a major feeder channel/canyon bringing continuously large volume of sediments into the system and forcing

lobes to aggrade and eventually to switch position. The Veidnes area could be fed by a less stable, short-lived feeder-channels occasionally bringing lower, yet significant volumes of sediments onto the basin floor resulting in lobe progradation followed by abandonment. At outcrop scale, observing stacking patterns is often limited by the two-dimensional nature of the outcrops. In Seglodden, where the stacking trends have been observed based on only one vertical section, this could lead to significant errors. Moreover, the high proportion of eroded/missing intervals, and the high degree of amalgamation can also induce errors in the interpretation of lobe deposits.

#### **5.4 Depositional model for the Kongsfjord Formation**

Based on the results from this study, a conceptual model for the development of the Kongsfjord Formation is proposed (Fig. 5.2). Since the base of the Kongsfjord Formation is not exposed and that large scale and regionally extensive tectonic deformation do not allow stratigraphic correlations between outcrop sections, it is not possible to reconstruct the full extent of the Kongsfjord Formation submarine fan system. However, this study provides insights to the different depositional environments and their architectural elements within the system. Differences in bed type percentages and lobe thicknesses and stacking patterns suggest that the deposition in the Kongsfjord Formation is most likely controlled by the interaction of several autogenic processes including feeder channel geometry and stability, flow transport distances, and sedimentation rates controlling lobe avulsions. The Nålneset outcrop section was possibly deposited in relatively slope-proximal settings, whereas the Veidnes outcrop section was deposited in more distal basin-floor settings influenced by unstable erosive distributary channels. This resulted in frequent flow transformation and deposition of HEBs in lobe off-axis and fringe settings. The Seglodden outcrop section was possibly deposited in stable, relatively distal basin-floor settings and fed continuously by a stable sediment source. Steady sediment supply resulted in the deposition of thick, aggradationally to compensationally stacked lobes. Additionally, high sedimentation rates can trigger slope failures that trigger both surge- and sustained-type flows at the shelf edge, adding to the complex architecture of the corresponding lobes.

The Kongsfjord Formation accumulated during the Late Precambrian as part of the shallowing upward succession of the Barents Sea Group that filled a deep, regionally extensive rift basin along the northeastern margin of Baltica (Drinkwater et al., 1996; Roberts & Siedlecka, 2002). The margin of the basin was delimited by the TKFZ to the south, which played a major role in the early basin development (Drinkwater et al., 1996; Nystuen et al., 2008). Siedlecka (1985) suggested that the Kongsfjord Formation basin might have been part of a graben or half-graben with at least one steep, fault-controlled margin. Fault-controlled basins can offer significant accommodation space induced by fault-controlled subsidence (e.g., Hiscott et al., 1990; Gawthorpe et al., 1997). In the case of the Kongsfjord Formation, this could possibly explain the great thickness of the formation (> 3200 m). Additionally, episodes of fault activity can play a major role in slope instability and in triggering sediment failure (Piper et al., 1999; Piper & Normark, 2009).

The Kongsfjord Formation is part of a N–NE prograding slope to basin-floor system that includes the overlying Båsnæringen Formation consisting of prodelta, delta front, delta top and associated fluvial deposits (Pickering, 1982b, 1984; Siedlecka et al., 1989). The lower part of the Båsnæringen Formation consists of slope and prodelta deposits showing abundant soft-sediment deformation as slides, slumps and liquefaction indicating a slope driven by high instability and frequent mass wasting processes (Siedlecka & Edwards, 1980; Pickering, 1982b; Siedlecka et al., 1989). Additionally, Siedlecka et al. (1989) reported gully-shaped depressions and channel-fills indicating high sediment bypass. This suggests that slope instability possibly due to high sedimentation rates and/or fault activity was an important process for triggering sediment failure and initiating turbidity currents. Furthermore, the delta top and fluvial deposits of the Båsnæringen formation are characterised by distributary channel fills of a high-energy braided fluvio-deltaic system (Hjellbakk, 1993; Hjellbakk, 1997). Sediment provenance studies suggest that a Mesoproterozoic terrane, which is not preserved today, was exposed to erosion and provided much of the infill for the Kongsfjord and Båsnæringen Formations (Roberts & Siedlecka, 2012). The uniform and relatively fine-grained nature of the sediments of the Kongsfjord Formation may indicate a recycled sediment source. Therefore, well-exposed sediment sources in the non-vegetated settings of the Precambrian resulted in a high discharge fluvio-deltaic system with rapid runoff and unstable flash-flood dominated channels (Hjellbakk, 1993; Hjellbakk, 1997). According to Hjellbakk (1997), the Båsnæringen fluvial system had an exceptionally wide braidplain due to the absence of stabilised vegetated banks

forcing channels to expand laterally. This suggests that considerable volumes of sediments regularly reached the shelf edge from multiple sources due to the braided and unstable nature of the fluvio-deltaic system. This possibly resulted in the bypass of the sediments to the basin-floor in several erosional gullies, channels and/or canyons and the deposition of coalescing lobes on the basin-floor. Therefore, the sediment delivery system probably resembled a multiple-sourced sand-rich system and resulted in the deposition of the Kongsfjord Formation as sand-rich slope aprons or a sand-rich submarine ramp (see classification of Reading & Richards, 1994). Such multiple-sourced systems form when considerable volumes of sediments are available for failing from several sources and feeders resulting in the deposition of coalescing lobes on the basin floor (Reading & Richards, 1994; Richards et al., 1998). Typically, submarine ramps are associated with stable feeder systems (see Heller & Dickinson, 1985), while slope aprons are associated with unstable feeder systems and slope failure (e.g., Wynn et al., 2000). Therefore, the suggested 'flash-flood' nature of the Båsnæringen feeder system and the evidence of frequent slope failure rather points to a slope apron-type of system for the Kongsfjord Formation turbidite system. This shows that the classical submarine fan models (e.g., Normark, 1970; Mutti & Ricci Lucchi, 1972; Walker, 1978) are difficult to apply to the Kongsfjord Formation and should only be used with caution. These facies models were developed mainly based on relatively small, point-sourced submarine fan systems that were significantly different from the large Kongsfjord Formation turbidite system.

## **5.5 Comparison with other submarine fan systems**

Lobes of the Kongsfjord Formation show a similar architectural hierarchy (bed, lobe element, lobe, lobe complex), sub-environments (lobe axis, lobe off-axis and lobe fringe) and stacking trends (aggradational to compensational) to lobes of several submarine fan systems including lobes of the Karoo Basin, South Africa (Johnson et al., 2001; Prélat et al., 2009; Groenenberg et al., 2010; Spychala et al., 2017b); and the Ross Formation, western Ireland (Pyles, 2008; Pyles & Jennette, 2009; Macdonald et al., 2011a; Pyles et al., 2014; Pierce et al., 2018; Zhang & Li, 2020).

In particular, the Kongsfjord Formation shows great similarities to the Skoorsteenbergh Formation in the Karoo Basin that consist mainly of fine-grained turbidite deposits (Hodgson

et al., 2006; Prélat et al., 2009). The lobes of the Skoorsteenberg Formation show a wide range of thickness trends interpreted as representing compensational stacking and deposition in unconfined settings (Prélat et al., 2009; Prélat & Hodgson, 2013). The distribution of HEBs in the Karoo Basin has been interpreted to be controlled by autogenic processes such as channel avulsion and the stacking patterns of lobes (Spsychala et al., 2017a). In the Kongsfjord Formation, lobe stacking patterns also possibly controlled the distribution of HEBs. However, in contrast with the Kongsfjord Formation, the Skoorsteenberg Formation has a limited thickness (ca. 450 m thick; Johnson et al., 2001), reflecting different key parameters. The submarine fans of the Karoo Basin developed in a retro-arc foreland basin as part of shallowing upward basin-floor-slope succession (Johnson et al., 2001). The Kongsfjord Formation accumulated in a passive margin formerly subjected to rifting. Late syn-rift to post-rift subsidence and/or long-term relative sea-level rise created significant amounts of accommodation space for the Kongsfjord Formation turbidites to accumulate. Additionally, high sedimentation rates at the shelf edge resulted in frequent sediment failure and promoted the aggradational and compensational stacking of the coalescent lobes which eventually resulted in the great thickness of the succession. Other well studied submarine fan systems are generally recording deposition along active margins, whereas there are really few documented example of submarine fans associated to large, passive margins because such systems are severely affected by orogenic processes and rarely preserved.

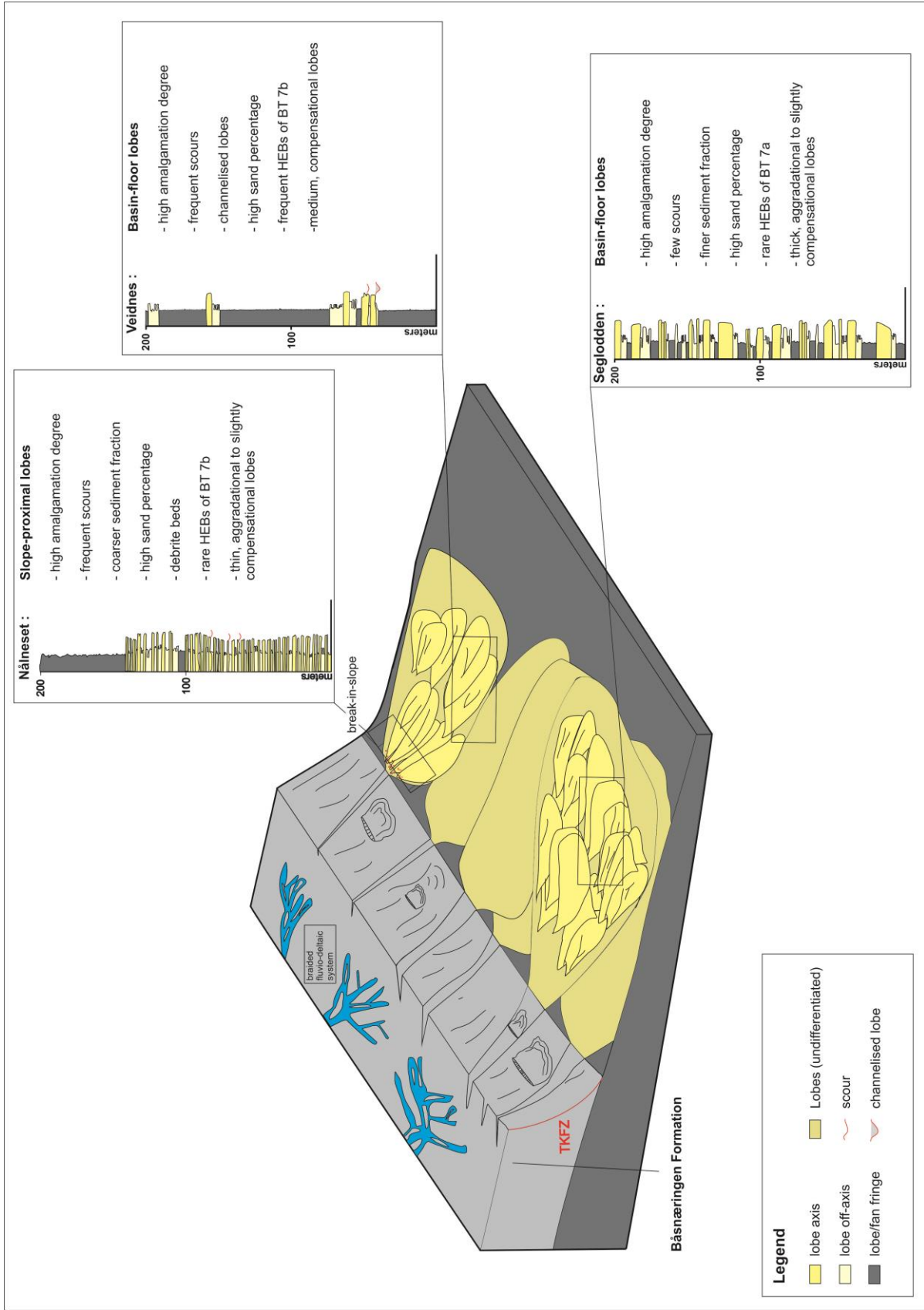


**Figure 5.2:** Conceptual model for the deposition of the Kongsfjord Formation (not to scale) showing the inferred location of each investigated outcrop section (i.e., Nålneset, Veidnes and Seglodden) within the Kongsfjord Formation turbidite system and their related deposits. Theoretical logs show typical section through the studied areas and the main recognition criteria for the depositional sub-environments.



## 6 Conclusions

This study documents the sedimentology and depositional architecture of the Kongsfjord Formation, northern Norway. Detailed facies and bed by bed analyses from stratigraphic logs and digital outcrop models in three main outcrop areas allowed to identify architectural elements and depositional sub-environments and resulted in the following conclusions:

- A total of eight bed types were recognised within the investigated outcrop sections of the Kongsfjord Formation. Amalgamated, coarse-grained, thick-, medium- and thin-bedded and fine-grained turbidite beds (BT 1 to BT 6) record deposition by high- and low-density turbidity flows. Hybrid event beds (BT 7) record deposition by transitional flows. Debrite beds (BT 8) record en masse deposition by cohesive debris flows.
- Two types of architectural elements were recognised within the investigated sections: channels and lobes. Channels have shallow (<1 m erosional relief) erosive bases and comprise a high proportion of amalgamated beds that record deposition in confined settings. Lobes are tabular-shaped units that record deposition in unconfined settings in front of channels. Lobes have a two-fold architecture with a thin-bedded lower part and a thick-bedded upper part. Based on their characteristic bed type associations, three distinct lobes sub-environments have been recognised: lobe axis, lobe off-axis and lobe fringe deposits.
- Lobes exhibit a four-order hierarchy: beds stack into lobe elements, lobe elements stack into lobes and lobes stack into lobe complexes. Thickness variations at lobe elements scale are attributed to compensational stacking. Lobe elements and lobes often show thickening upward trends interpreted as recording lobe progradation.
- Based on the vertical and lateral distribution of bed types, different sub-environments have been recognised. The frequent scouring and amalgamation surfaces in the Nålneiset outcrop section record deposition in semi-confined slope-proximal settings. The Veidnes outcrop section records deposition in unconfined relatively distal basin-floor settings. The Seglodden outcrop section records deposition in distal basin-floor settings

by large-volume flows that bypass up-dip areas. Sustained-turbidity currents possibly result in the deposition of thick massive to weakly graded turbidite beds.

- Hybrid event beds (HEBs) comprise a lower turbidite sandstone division and an upper clast-rich heterogeneous debrite division. Thick, clast-rich HEBs are deposited by turbidity flows that transform to cohesive debris flows due to the entrainment and disaggregation of mudstone clasts. They represent the most distal expression of HEBs. Thin HEBs with a mud-rich matrix are deposited by mud-enriched turbidity flows that transform to cohesive debris flows due to flow deceleration and grain size segregation. They occur in lobe fringe and lobe off-axis deposits in distal settings. The distribution of HEBs in the Kongsfjord Formation reflects slope disequilibrium during the early phase of development of lobe complexes or channel avulsion and lobe stacking patterns.
- Lobes show differences in thicknesses, internal hierarchy, degree of amalgamation and stacking trends between the studied outcrop sections of the Kongsfjord Formation suggesting that lobe deposition is controlled by the interaction of several autogenic processes. The Kongsfjord Formation accumulated in a rift basin as part of a slope to basin-floor system comprising the overlying Båsnæringen Formation. High sedimentation rates and sediment failure are likely to be the main controls for the deposition of the Kongsfjord Formation turbidite system as coalescent lobes on the basin-floor.

## 7 Future research

The large outcrop areas of the Kongsfjord Formation offer many possibilities for further investigations and analyses. As the recognition of the architectural elements was often limited by the two-dimensional nature of the outcrops, further research should focus on the identification of the geometries of the architectural elements and on regional correlations between sections using aerial images and digital outcrop models (using a drone for large scale and high-resolution image acquisition). This should be accompanied by a detailed study of the tectonic deformations across the Formation in order to gain a better understanding of the stratigraphic positions of each locality. Additional information on the petrography and geochemistry of the successions may provide better understanding to the provenance of the Kongsfjord Formation and therefore allow better paleogeographic reconstructions.

Additionally, as the deposition of the Kongsfjord Formation was controlled by the progradation of the Båsnæringen fluvio-deltaic system, a detailed study of the Båsnæringen Formation may provide a better understanding of the factors controlling sediment deposition within the slope to basin-floor system.

## References

- Amy, L. A., & Talling, P. J. (2006). Anatomy of turbidites and linked debrites based on long distance (120 × 30 km) bed correlation, Marnoso Arenacea Formation, Northern Apennines, Italy. *Sedimentology*, 53(1), 161-212. <https://doi.org/10.1111/j.1365-3091.2005.00756.x>
- Beckinsale, R. D., Reading, H. G., & Rex, D. C. (1976). Potassium-argon ages for basic dykes from East Finnmark: stratigraphical and structural implications. *Scottish Journal of Geology*, 12(1), 51. <https://doi.org/10.1144/sjg12010051>
- Bogdanova, S. V., Pisarevsky, S. A., & Li, Z. X. (2009). Assembly and Breakup of Rodinia (Some results of IGCP project 440). *Stratigraphy and Geological Correlation*, 17(3), 259. <https://doi.org/10.1134/S0869593809030022>
- Bouma, A. H. (1962). Sedimentology of Some Flysch Deposits. A Graphic Approach to Facies Interpretation. *Elsevier, Amsterdam*, 168.
- Bouma, A. H. (2004). Key controls on the characteristics of turbidite systems. In S. A. Lomas & P. Joseph (Eds.), *Confined Turbidite Systems* (Vol. 222, pp. 0): Geological Society of London.
- Bouma, A. H., Normark, W. R., & Barnes, N. E. (1985). *Submarine Fans and Related Turbidite Systems*. New York: Springer Verlag.
- Bourget, J., Zaragosi, S., Mulder, T., Schneider, J. L., Garlan, T., Van Toer, A., Mas, V., & Ellouz-Zimmermann, N. (2010). Hyperpycnal-fed turbidite lobe architecture and recent sedimentary processes: A case study from the Al Batha turbidite system, Oman margin. *Sedimentary Geology*, 229(3), 144-159. <https://doi.org/10.1016/j.sedgeo.2009.03.009>
- Brooks, H. L., Hodgson, D. M., Brunt, R. L., Peakall, J., Hofstra, M., & Flint, S. S. (2018a). Deep-water channel-lobe transition zone dynamics: Processes and depositional architecture, an example from the Karoo Basin, South Africa. *GSA Bulletin*, 130(9-10), 1723-1746. <https://doi.org/10.1130/b31714.1>
- Brooks, H. L., Hodgson, D. M., Brunt, R. L., Peakall, J., Poyatos-Moré, M., & Flint, S. S. (2018b). Disconnected submarine lobes as a record of stepped slope evolution over multiple sea-level cycles. *Geosphere*, 14(4), 1753-1779. <https://doi.org/10.1130/ges01618.1>
- Brooks, H. L., Ito, M., Zuchuat, V., Peakall, J., & Hodgson, D. M. (2022). Channel-lobe transition zone development in tectonically active settings: Implications for hybrid bed development. *The Depositional Record*, 00, 1-40. <https://doi.org/10.1002/dep2.180>
- Bylund, G. (1994). Palaeomagnetism of the Late Precambrian Vadsø and Barents Sea Groups, Varanger Peninsula, Norway. *Precambrian Research*, 69(1), 81-93. [https://doi.org/10.1016/0301-9268\(94\)90080-9](https://doi.org/10.1016/0301-9268(94)90080-9)
- Baas, J. H., & Best, J. L. (2008). The dynamics of turbulent, transitional and laminar clay-laden flow over a fixed current ripple. *Sedimentology*, 55(3), 635-666. <https://doi.org/10.1111/j.1365-3091.2007.00916.x>
- Baas, J. H., Best, J. L., & Peakall, J. (2011). Depositional processes, bedform development and hybrid bed formation in rapidly decelerated cohesive (mud-sand) sediment flows. *Sedimentology*, 58(7), 1953-1987. <https://doi.org/10.1111/j.1365-3091.2011.01247.x>
- Baas, J. H., Van Kesteren, W., & Postma, G. (2004). Deposits of depletive high-density turbidity currents: a flume analogue of bed geometry, structure and texture. *Sedimentology*, 51(5), 1053-1088. <https://doi.org/10.1111/j.1365-3091.2004.00660.x>

- Campbell, C. V. (1967). Lamina, Laminaset, Bed and Bedset. *Sedimentology*, 8(1), 7-26. <https://doi.org/10.1111/j.1365-3091.1967.tb01301.x>
- Carter, R. M. (1975). A discussion and classification of subaqueous mass-transport with particular application to grain-flow, slurry-flow, and fluxoturbidites. *Earth-Science Reviews*, 11(2), 145-177. [https://doi.org/10.1016/0012-8252\(75\)90098-7](https://doi.org/10.1016/0012-8252(75)90098-7)
- Cartigny, M. J. B., Eggenhuisen, J. T., Hansen, E. W. M., & Postma, G. (2013). Concentration-Dependent Flow Stratification In Experimental High-Density Turbidity Currents and Their Relevance To Turbidite Facies Models. *Journal of Sedimentary Research*, 83(12), 1047-1065. <https://doi.org/10.2110/jsr.2013.71>
- Carvajal, C., Paull, C. K., Caress, D. W., Fildani, A., Lundsten, E., Anderson, K., Maier, K. L., McGann, M., Gwiazda, R., & Herguera, J. C. (2017). Unraveling the Channel–Lobe Transition Zone With High-Resolution AUV Bathymetry: Navy Fan, Offshore Baja California, Mexico. *Journal of Sedimentary Research*, 87(10), 1049-1059. <https://doi.org/10.2110/jsr.2017.58>
- Cronin, B. T., Hartley, A. J., Celik, H., Hurst, A., Türkmen, I., & Kerey, E. (2000). Equilibrium profile development in graded deep-water slopes: Eocene, Eastern Turkey. *Journal of the Geological Society*, 157(5), 943-955. <https://doi.org/10.1144/jgs.157.5.943>
- Cullis, S., Colombera, L., Patacci, M., & McCaffrey, W. D. (2018). Hierarchical classifications of the sedimentary architecture of deep-marine depositional systems. *Earth-Science Reviews*, 179, 38-71. <https://doi.org/10.1016/j.earscirev.2018.01.016>
- Cunha, R. S., Tinterri, R., & Muzzi Magalhaes, P. (2017). Annot Sandstone in the Peira Cava basin: An example of an asymmetric facies distribution in a confined turbidite system (SE France). *Marine and Petroleum Geology*, 87, 60-79. <https://doi.org/10.1016/j.marpetgeo.2017.04.013>
- Deptuck, M. E., Piper, D. J. W., Savoye, B., & Gervais, A. (2008). Dimensions and architecture of late Pleistocene submarine lobes off the northern margin of East Corsica. *Sedimentology*, 55(4), 869-898. <https://doi.org/10.1111/j.1365-3091.2007.00926.x>
- Dorrell, R. M., Peakall, J., Sumner, E. J., Parsons, D. R., Darby, S. E., Wynn, R. B., Özsoy, E., & Tezcan, D. (2016). Flow dynamics and mixing processes in hydraulic jump arrays: Implications for channel-lobe transition zones. *Marine Geology*, 381, 181-193. <https://doi.org/10.1016/j.margeo.2016.09.009>
- Drinkwater, N. J. (1997). *Architecture of deep-water systems in a rift-basin fill: the Kongsfjord Formation, Finnmark, north Norway*. (Doctoral dissertation). University of London, London, United Kingdom. ProQuest Dissertations and Theses Global.
- Drinkwater, N. J., & Pickering, K. T. (2001). Architectural elements in a high-continuity sand-prone turbidite system, late Precambrian Kongsfjord Formation, northern Norway: Application to hydrocarbon reservoir characterization. *AAPG Bulletin*, 85(10), 1731-1757. <https://doi.org/10.1306/8626D059-173B-11D7-8645000102C1865D>
- Drinkwater, N. J., Pickering, K. T., & Siedlecka, A. (1996). Deep-water fault-controlled sedimentation, Arctic Norway and Russia: response to Late Proterozoic rifting and the opening of the Iapetus Ocean. *Journal of the Geological Society*, 153(3), 427-436. <https://doi.org/10.1144/gsjgs.153.3.0427>
- Eggenhuisen, J. T., McCaffrey, W. D., Houghton, P. D. W., & Butler, R. W. H. (2011). Shallow erosion beneath turbidity currents and its impact on the architectural

- development of turbidite sheet systems. *Sedimentology*, 58(4), 936-959.  
<https://doi.org/10.1111/j.1365-3091.2010.01190.x>
- Eggenhuisen, J. T., Tilston, M. C., de Leeuw, J., Pohl, F., & Cartigny, M. J. B. (2020). Turbulent diffusion modelling of sediment in turbidity currents: An experimental validation of the Rouse approach. *The Depositional Record*, 6(1), 203-216.  
<https://doi.org/10.1002/dep2.86>
- Elliott, T. (2000). Megaflute erosion surfaces and the initiation of turbidite channels. *Geology*, 28(2), 119-122.
- Eschard, R., Albouy, E., Deschamps, R., Euzen, T., & Ayub, A. (2003). Downstream evolution of turbiditic channel complexes in the Pab Range outcrops (Maastrichtian, Pakistan). *Marine and Petroleum Geology*, 20(6), 691-710.  
<https://doi.org/10.1016/j.marpetgeo.2003.02.004>
- Etienne, S., Mulder, T., Bez, M., Desaubliaux, G., Kwasniewski, A., Parize, O., Dujoncquoy, E., & Salles, T. (2012). Multiple scale characterization of sand-rich distal lobe deposit variability: Examples from the Annot Sandstones Formation, Eocene–Oligocene, SE France. *Sedimentary Geology*, 273-274, 1-18.  
<https://doi.org/10.1016/j.sedgeo.2012.05.003>
- Felletti, F., Carruba, S., Casnedi, R., Kneller, B., Martinsen, O. J., & McCaffrey, B. (2009). Sustained Turbidity Currents: Evidence from the Pliocene Periadriatic Foredeep (Cellino Basin, Central Italy). In *External Controls on Deep-Water Depositional Systems* (Vol. 92, pp. 0): SEPM Society for Sedimentary Geology.
- Ferguson, R. A., Kane, I. A., Eggenhuisen, J. T., Pohl, F., Tilston, M., Spychala, Y. T., & Brunt, R. L. (2020). Entangled external and internal controls on submarine fan evolution: an experimental perspective. *The Depositional Record*, 6(3), 605-624.  
<https://doi.org/10.1002/dep2.109>
- Ferry, J.-N., Mulder, T., Parize, O., Raillard, S., Hodgson, D. M., & Flint, S. S. (2005). Concept of equilibrium profile in deep-water turbidite systems: effects of local physiographic changes on the nature of sedimentary process and the geometries of deposits. In *Submarine Slope Systems: Processes and Products* (Vol. 244, pp. 0): Geological Society of London.
- Fonnesu, M., Felletti, F., Haughton, P., Patacci, M., & McCaffrey, W. (2018). Hybrid event bed character and distribution linked to turbidite system sub-environments: The North Apennine Gottero Sandstone (north-west Italy). *Sedimentology*, 65(1), 151-190.  
<https://doi.org/10.1111/sed.12376>
- Fonnesu, M., Haughton, P., Felletti, F., & McCaffrey, W. (2015). Short length-scale variability of hybrid event beds and its applied significance. *Marine and Petroleum Geology*, 67, 583-603. <https://doi.org/10.1016/j.marpetgeo.2015.03.028>
- Gabrielsen, R. H., Faerseth, R. B., & Townsend, C. (1987). The inner shelf of North Cape, Norway and its implications for the Barents Shelf-Finnmark Caledonide boundary. *Norsk Geologisk Tidsskrift*, 67, 151-153.
- Gardner, M. H., Borer, J. M., Melick, J. J., Mavilla, N., Dechesne, M., & Wagerle, R. N. (2003). Stratigraphic process-response model for submarine channels and related features from studies of Permian Brushy Canyon outcrops, West Texas. *Marine and Petroleum Geology*, 20(6), 757-787. <https://doi.org/10.1016/j.marpetgeo.2003.07.004>
- Gawthorpe, R. L., Sharp, I., Underhill, J. R., & Gupta, S. (1997). Linked sequence stratigraphic and structural evolution of propagating normal faults. *Geology*, 25(9), 795-798.



- Gee, D. G., Fossen, H., Henriksen, N., & Higgins, A. K. (2008). From the Early Paleozoic Platforms of Baltica and Laurentia to the Caledonide Orogen of Scandinavia and Greenland. *International Union of Geological Sciences*, 31(1), 44-51.  
<https://doi.org/10.18814/epiiugs/2008/v31i1/007>
- Gee, M. J. R., Masson, D. G., Watts, A. B., & Allen, P. A. (1999). The Saharan debris flow: an insight into the mechanics of long runout submarine debris flows. *Sedimentology*, 46(2), 317-335. <https://doi.org/10.1046/j.1365-3091.1999.00215.x>
- Gervais, A., Mulder, T., Savoye, B., & Gonthier, E. (2006). Sediment distribution and evolution of sedimentary processes in a small sandy turbidite system (Golo system, Mediterranean Sea): implications for various geometries based on core framework. *Geo-Marine Letters*, 26(6), 373. <https://doi.org/10.1007/s00367-006-0045-z>
- Gladstone, C., McClelland, H. L. O., Woodcock, N. H., Pritchard, D., & Hunt, J. E. (2018). The formation of convolute lamination in mud-rich turbidites. *Sedimentology*, 65(5), 1800-1825. <https://doi.org/10.1111/sed.12447>
- Groenenberg, R. M., Hodgson, D. M., Pr elat, A., Luthi, S. M., & Flint, S. S. (2010). Flow–Deposit Interaction in Submarine Lobes: Insights from Outcrop Observations and Realizations of a Process-Based Numerical Model. *Journal of Sedimentary Research*, 80(3), 252-267. <https://doi.org/10.2110/jsr.2010.028>
- Grundv ag, S.-A., Johannessen, E. P., Helland-Hansen, W., & Plink-Bj orklund, P. (2014). Depositional architecture and evolution of progradationally stacked lobe complexes in the Eocene Central Basin of Spitsbergen. *Sedimentology*, 61(2), 535-569.  
<https://doi.org/10.1111/sed.12067>
- Hamilton, P., Gaillot, G., Strom, K., Fedele, J., & Hoyal, D. (2017). Linking Hydraulic Properties In Supercritical Submarine Distributary Channels To Depositional-Lobe Geometry. *Journal of Sedimentary Research*, 87(9), 935-950.  
<https://doi.org/10.2110/jsr.2017.53>
- Hamilton, P., Strom, K., & Hoyal, D. (2015). Hydraulic and sediment transport properties of autogenic avulsion cycles on submarine fans with supercritical distributaries. *Journal of Geophysical Research: Earth Surface*, 120(7), 1369-1389.  
<https://doi.org/10.1002/2014JF003414>
- Haughton, P. D., Barker, S. P., & McCaffrey, W. D. (2003). ‘Linked’ debrites in sand-rich turbidite systems – origin and significance. *Sedimentology*, 50(3), 459-482.  
<https://doi.org/10.1046/j.1365-3091.2003.00560.x>
- Haughton, P. D., McCaffrey, W. D., & Barker, S. P. (2009). Hybrid sediment gravity flow deposits – Classification, origin and significance. *Marine and Petroleum Geology*, 26(10), 1900-1918. <https://doi.org/10.1016/j.marpetgeo.2009.02.012>
- Heller, P. L., & Dickinson, W. R. (1985). Submarine Ramp Facies Model for Delta-Fed, Sand-Rich Turbidite Systems1. *AAPG Bulletin*, 69(6), 960-976.  
<https://doi.org/10.1306/ad462b37-16f7-11d7-8645000102c1865d>
- Herrevold, T., Gabrielsen, R. H., & Roberts, D. (2009). Structural geology of the southeastern part of the Trollfjorden-Komagelva Fault Zone, Varanger Peninsula, Finnmark, North Norway. *Nowegian Journal of Geology*, 89, 305-325.
- Hiscott, R. N., & Ghibaudo, G. (1981). Deep-sea fan deposits in the Macigno Formation (middle-upper Oligocene) of the Gordana Valley, Northern Apennines, Italy; discussion and reply. *Journal of Sedimentary Research*, 51(3), 1015-1026.  
<https://doi.org/10.1306/212f7e00-2b24-11d7-8648000102c1865d>

- Hiscott, R. N., & Middleton, G. V. (1979). *Depositional Mechanics of Thick-Bedded Sandstones at the Base of A Submarine Slope, Tourelle Formation (Lower Ordovician), Quebec, Canada.*
- Hiscott, R. N., & Middleton, G. V. (1980). Fabric of coarse deep-water sandstones, Tourelle Formation, Quebec, Canada. *Journal of Sedimentary Research*, 50(3), 703-721. <https://doi.org/10.1306/212f7ac7-2b24-11d7-8648000102c1865d>
- Hiscott, R. N., Wilson, R. C. L., Gradstein, F. M., Pujalte, V., García-Mondéjar, J., Boudreau, R. R., & Wishart, H. A. (1990). Comparative Stratigraphy and Subsidence History of Mesozoic Rift Basins of North Atlantic1. *AAPG Bulletin*, 74(1), 60-76. <https://doi.org/10.1306/0c9b2213-1710-11d7-8645000102c1865d>
- Hjellbakk, A. (1993). A 'flash-flood' dominated braid delta in the upper Proterozoic Næringselva Member, Varanger Peninsula, northern Norway. *Norsk Geologisk Tidsskrift*, 73, 63-80.
- Hjellbakk, A. (1997). Facies and fluvial architecture of a high-energy braided river: the Upper Proterozoic Seglodden Member, Varanger Peninsula, northern Norway. *Sedimentary Geology*, 114(1), 131-161. [https://doi.org/10.1016/S0037-0738\(97\)00075-4](https://doi.org/10.1016/S0037-0738(97)00075-4)
- Ho, V. L., Dorrell, R. M., Keevil, G. M., Burns, A. D., & McCaffrey, W. D. (2018). Pulse propagation in turbidity currents. *Sedimentology*, 65(2), 620-637. <https://doi.org/10.1111/sed.12397>
- Hodgson, D. M. (2009). Distribution and origin of hybrid beds in sand-rich submarine fans of the Tanqua depocentre, Karoo Basin, South Africa. *Marine and Petroleum Geology*, 26(10), 1940-1956. <https://doi.org/10.1016/j.marpetgeo.2009.02.011>
- Hodgson, D. M., Flint, S. S., Hodgetts, D., Drinkwater, N. J., Johannessen, E. P., & Luthi, S. M. (2006). Stratigraphic Evolution of Fine-Grained Submarine Fan Systems, Tanqua Depocenter, Karoo Basin, South Africa. *Journal of Sedimentary Research*, 76(1), 20-40. <https://doi.org/10.2110/jsr.2006.03>
- Hodgson, D. M., & Haughton, P. D. (2004). Impact of syndepositional faulting on gravity current behaviour and deep-water stratigraphy: Tabernas-Sorbas Basin, SE Spain. *Geological Society, London, Special Publications*, 222(1), 135-158.
- Hodgson, D. M., Kane, I. A., Flint, S. S., Brunt, R. L., & Ortiz-Karpf, A. (2016). Time-transgressive Confinement On the Slope and the Progradation of Basin-floor Fans: Implications For the Sequence Stratigraphy of Deep-water Deposits. *Journal of Sedimentary Research*, 86(1), 73-86. <https://doi.org/10.2110/jsr.2016.3>
- Hofstra, M., Hodgson, D. M., Peakall, J., & Flint, S. S. (2015). Giant scour-fills in ancient channel-lobe transition zones: Formative processes and depositional architecture. *Sedimentary Geology*, 329, 98-114. <https://doi.org/10.1016/j.sedgeo.2015.09.004>
- Holtedahl, O. (1918). Bidrag til Finnmarkens geologi. *Norges geologiske undersøkelse*, 84, 314.
- Hsu, S. K., Kuo, J., Lo, C. L., Tsai, C. H., Doo, W. B., Ku, C. Y., & Sibuet, J. C. (2008). Turbidity currents, submarine landslides and the 2006 Pingtung earthquake off SW Taiwan. *Terr. Atmos. Ocean. Sci.*, 19, 767-772. [https://doi.org/10.3319/TAO.2008.19.6.767\(PT\)](https://doi.org/10.3319/TAO.2008.19.6.767(PT))
- Hubbard, S. M., Romans, B. W., & Graham, S. A. (2008). Deep-water foreland basin deposits of the Cerro Toro Formation, Magallanes basin, Chile: architectural elements of a sinuous basin axial channel belt. *Sedimentology*, 55(5), 1333-1359. <https://doi.org/10.1111/j.1365-3091.2007.00948.x>
- Ito, M. (2008). Downfan Transformation from Turbidity Currents to Debris Flows at a Channel-to-Lobe Transitional Zone: The Lower Pleistocene Otadai Formation, Boso

- Peninsula, Japan. *Journal of Sedimentary Research*, 78(10), 668-682.  
<https://doi.org/10.2110/jsr.2008.076>
- Johnson, S. D., Flint, S., Hinds, D., & De Ville Wickens, H. (2001). Anatomy, geometry and sequence stratigraphy of basin floor to slope turbidite systems, Tanqua Karoo, South Africa. *Sedimentology*, 48(5), 987-1023. <https://doi.org/10.1046/j.1365-3091.2001.00405.x>
- Kane, I. A., Catterall, V., McCaffrey, W. D., & Martinsen, O. J. (2010). Submarine channel response to intrabasinal tectonics: The influence of lateral tilt. *AAPG Bulletin*, 94(2), 189-219.
- Kane, I. A., & Pontén, A. S. M. (2012). Submarine transitional flow deposits in the Paleogene Gulf of Mexico. *Geology*, 40(12), 1119-1122. <https://doi.org/10.1130/g33410.1>
- Kane, I. A., Pontén, A. S. M., Vangdal, B., Eggenhuisen, J. T., Hodgson, D. M., & Spychala, Y. T. (2017). The stratigraphic record and processes of turbidity current transformation across deep-marine lobes. *Sedimentology*, 64(5), 1236-1273.  
<https://doi.org/10.1111/sed.12346>
- Kirkland, C., Daly, J. S., Chew, D., & Page, L. (2008). The Finnmarkian Orogeny revisited: An isotopic investigation in eastern Finnmark, Arctic Norway. *Tectonophysics*, 460, 158-177. <https://doi.org/10.1016/j.tecto.2008.08.001>
- Kjødde, J., Støretvedt, K. M., Roberts, D., & Gidskehaug, A. (1978). Palaeomagnetic evidence for large-scale dextral movement along the Trollfjord-Komagelv Fault, Finnmark, north Norway. *Physics of the Earth and Planetary Interiors*, 16(2), 132-144.  
[https://doi.org/10.1016/0031-9201\(78\)90084-5](https://doi.org/10.1016/0031-9201(78)90084-5)
- Kneller, B. (2003). The influence of flow parameters on turbidite slope channel architecture. *Marine and Petroleum Geology*, 20(6), 901-910.  
<https://doi.org/10.1016/j.marpetgeo.2003.03.001>
- Kneller, B. C., & Branney, M. J. (1995). Sustained high-density turbidity currents and the deposition of thick massive sands. *Sedimentology*, 42(4), 607-616.  
<https://doi.org/10.1111/j.1365-3091.1995.tb00395.x>
- Komar, P. D. (1971). Hydraulic Jumps in Turbidity Currents. *GSA Bulletin*, 82(6), 1477-1488. [https://doi.org/10.1130/0016-7606\(1971\)82\[1477:Hjtc\]2.0.Co;2](https://doi.org/10.1130/0016-7606(1971)82[1477:Hjtc]2.0.Co;2)
- Kuenen, P. H. (1957). Sole Markings of Graded Graywacke Beds. *The Journal of Geology*, 65(3), 231-258. <https://doi.org/10.1086/626429>
- Kuenen, P. H., & Migliorini, C. I. (1950). Turbidity Currents as a Cause of Graded Bedding. *The Journal of Geology*, 58(2), 91-127. <https://doi.org/10.1086/625710>
- Li, Z. X., Bogdanova, S. V., Collins, A. S., Davidson, A., De Waele, B., Ernst, R. E., Fitzsimons, I. C. W., Fuck, R. A., Gladkochub, D. P., Jacobs, J., Karlstrom, K. E., Lu, S., Natapov, L. M., Pease, V., Pisarevsky, S. A., Thrane, K., & Vernikovskiy, V. (2008). Assembly, configuration, and break-up history of Rodinia: A synthesis. *Precambrian Research*, 160(1), 179-210.  
<https://doi.org/10.1016/j.precamres.2007.04.021>
- Li, Z. X., Li, X. H., Kinny, P. D., & Wang, J. (1999). The breakup of Rodinia: did it start with a mantle plume beneath South China? *Earth and Planetary Science Letters*, 173(3), 171-181. [https://doi.org/10.1016/S0012-821X\(99\)00240-X](https://doi.org/10.1016/S0012-821X(99)00240-X)
- Lomas, S. A., Joseph, P., Lomas, S. A., & Joseph, P. (2004). Confined turbidite systems. In *Confined Turbidite Systems* (Vol. 222, pp. 0): Geological Society of London.
- Lowe, D. R. (1982). Sediment gravity flows; II, Depositional models with special reference to the deposits of high-density turbidity currents. *Journal of Sedimentary Research*, 52(1), 279-297. <https://doi.org/10.1306/212f7f31-2b24-11d7-8648000102c1865d>

- Lowe, D. R. (1997). Reinterpretation of depositional processes in a classic flysch sequence (Pennsylvanian Jackfork Group), Ouachita Mountains, Arkansas and Oklahoma: Discussion. *AAPG Bulletin*, 81(3), 460-465.
- Lowe, D. R., & Guy, M. (2000). Slurry-flow deposits in the Britannia Formation (Lower Cretaceous), North Sea: a new perspective on the turbidity current and debris flow problem. *Sedimentology*, 47(1), 31-70. <https://doi.org/10.1046/j.1365-3091.2000.00276.x>
- Macdonald, H. A., Peakall, J., Wignall, P. B., & Best, J. (2011a). Sedimentation in deep-sea lobe-elements: implications for the origin of thickening-upward sequences. *Journal of the Geological Society*, 168(2), 319-332. <https://doi.org/10.1144/0016-76492010-036>
- Macdonald, H. A., Wynn, R. B., Huvenne, V. A. I., Peakall, J., Masson, D. G., Weaver, P. P. E., & McPhail, S. D. (2011b). New insights into the morphology, fill, and remarkable longevity (>0.2 m.y.) of modern deep-water erosional scours along the northeast Atlantic margin. *Geosphere*, 7(4), 845-867. <https://doi.org/10.1130/ges00611.1>
- Marini, M., Maron, M., Petrizzo, M. R., Felletti, F., & Muttoni, G. (2020). Magnetostratigraphy applied to assess tempo of turbidite deposition: A case study of ponded sheet-like turbidites from the lower Miocene of the northern Apennines (Italy). *Sedimentary Geology*, 403, 105654. <https://doi.org/10.1016/j.sedgeo.2020.105654>
- Marini, M., Milli, S., Ravnås, R., & Moscatelli, M. (2015). A comparative study of confined vs. semi-confined turbidite lobes from the Lower Messinian Laga Basin (Central Apennines, Italy): Implications for assessment of reservoir architecture. *Marine and Petroleum Geology*, 63, 142-165. <https://doi.org/10.1016/j.marpetgeo.2015.02.015>
- Mattern, F. (2002). Amalgamation surfaces, bed thicknesses, and dish structures in sand-rich submarine fans: numeric differences in channelized and unchannelized deposits and their diagnostic value. *Sedimentary Geology*, 150(3), 203-228. [https://doi.org/10.1016/S0037-0738\(01\)00180-4](https://doi.org/10.1016/S0037-0738(01)00180-4)
- Middleton, G. V., & Hampton, M. A. (1973). *Part I. Sediment Gravity Flows: Mechanics of Flow and Deposition*.
- Morris, E. A., Hodgson, D. M., Flint, S. S., Brunt, R. L., Butterworth, P. J., & Verhaeghe, J. (2014). Sedimentology, Stratigraphic Architecture, and Depositional Context of Submarine Frontal-Lobe Complexes. *Journal of Sedimentary Research*, 84(9), 763-780. <https://doi.org/10.2110/jsr.2014.61>
- Mulder, T., & Alexander, J. (2001). The physical character of subaqueous sedimentary density flows and their deposits. *Sedimentology*, 48(2), 269-299. <https://doi.org/10.1046/j.1365-3091.2001.00360.x>
- Mulder, T., & Etienne, S. (2010). Lobes in deep-sea turbidite systems: State of the art. *Sedimentary Geology*, 229(3), 75-80. <https://doi.org/10.1016/j.sedgeo.2010.06.011>
- Mulder, T., Savoye, B., & Syvitski, J. P. M. (1997). Numerical modelling of a mid-sized gravity flow: the 1979 Nice turbidity current (dynamics, processes, sediment budget and seafloor impact). *Sedimentology*, 44(2), 305-326. <https://doi.org/10.1111/j.1365-3091.1997.tb01526.x>
- Mutti, E. (1979). Turbidites et cones sous-marins profonds. *Sédimentation détritique (fluviale, littorale et marine)*, 1, 353-419.
- Mutti, E., Bernoulli, D., Ricci Lucchi, F., & Tinterri, R. (2009). Turbidites and turbidity currents from Alpine 'flysch' to the exploration of continental margins. *Sedimentology*, 56(1), 267-318. <https://doi.org/10.1111/j.1365-3091.2008.01019.x>



- Mutti, E., & Normark, W. R. (1987). Comparing Examples of Modern and Ancient Turbidite Systems: Problems and Concepts. In J. K. Leggett & G. G. Zuffa (Eds.), *Marine Clastic Sedimentology: Concepts and Case Studies* (pp. 1-38). Dordrecht: Springer Netherlands.
- Mutti, E., & Normark, W. R. (1991). An Integrated Approach to the Study of Turbidite Systems. In P. Weimer & M. H. Link (Eds.), *Seismic Facies and Sedimentary Processes of Submarine Fans and Turbidite Systems* (pp. 75-106). New York, NY: Springer New York.
- Mutti, E., & Ricci Lucchi, F. (1972). Le torbiditi dell'Appennino settentrionale : introduzione all'analisi di facies. *Memorie della Società geologica italiana.*, 11, 161-199.
- Mutti, E., & Ricci Lucchi, F. (1975). *Turbidite facies and facies associations*: Verlag nicht ermittelbar.
- Mutti, E., & Ricci Lucchi, F. (1978). Turbidites of the northern Apennines: introduction to facies analysis. *International Geology Review*, 20, 125-166.  
<https://doi.org/10.1080/00206817809471524>
- Mutti, E., & Sonnino, M. (1981). *Compensation cycles: a diagnostic feature of turbidite sandstone lobes*. IAS 2nd European Meeting, Bologna, Italy, pp. 120–123.
- Muzzi Magalhaes, P., & Tinterri, R. (2010). Stratigraphy and depositional setting of slurry and contained (reflected) beds in the Marnoso-arenacea Formation (Langhian-Serravallian) Northern Apennines, Italy. *Sedimentology*, 57(7), 1685-1720.  
<https://doi.org/10.1111/j.1365-3091.2010.01160.x>
- Nasuti, A., Roberts, D., & Gernigon, L. (2015). Multiphase mafic dykes in the Caledonides of northern Finnmark revealed by a new high-resolution aeromagnetic dataset. *Norwegian Journal of Geology*, 95, 285-297.
- NMA. (2021a). *Topografisk Norgeskart 4 gråtone WMS*. Norwegian Mapping Authority. Retrieved from <https://kartkatalog.geonorge.no/>
- NMA. (2021b). *Topografisk Norgeskart 4 WMS*. Norwegian Mapping Authority. Retrieved from <https://kartkatalog.geonorge.no/>
- Normark, W. R. (1970). Growth patterns of deep-sea fans. *AAPG Bulletin*, 54(11), 2170-2195.
- Normark, W. R. (1978). Fan Valleys, Channels, and Depositional Lobes on Modern Submarine Fans: Characters for Recognition of Sandy Turbidite Environments. *AAPG Bulletin*, 62(6), 912-931. <https://doi.org/10.1306/c1ea4f72-16c9-11d7-8645000102c1865d>
- Nystuen, J. P. (2008). Break-up of the Precambrian continent - Late Precambrian, from Precambrian to Palaeozoic; 850-542 Ma. In I. B. Ramberg, I. Bryhni, A. Nøttvedt, & K. Rangnes (Eds.), *The Making of a Land: Geology of Norway* (pp. 120-147): Norsk Geologisk Forening.
- Nystuen, J. P., Andresen, A., Kumpulainen, R., & Siedlecka, A. (2008). Neoproterozoic basin evolution in Fennoscandia, East Greenland and Svalbard. *Episodes*, 31.  
<https://doi.org/10.18814/epiiugs/2008/v31i1/006>
- Piazza, A., & Tinterri, R. (2020). Cyclic stacking pattern, architecture and facies of the turbidite lobes in the Macigno Sandstones Formation (Chattian-Aquitania, northern Apennines, Italy). *Marine and Petroleum Geology*, 122, 104704.  
<https://doi.org/10.1016/j.marpetgeo.2020.104704>
- Pickering, K. (1979). Possible retrogressive flow slide deposits from the Kongsfjord Formation: a Precambrian submarine fan, Finnmark, N. Norway. *Sedimentology*, 26, 295-306. <https://doi.org/10.1111/j.1365-3091.1979.tb00356.x>

- Pickering, K. (1981). Two Types of Outer Fan Lobe Sequence, from the Late Precambrian Kongsfjord Formation Submarine Fan, Finnmark, North Norway. *SEPM Journal of Sedimentary Research*, Vol. 51. <https://doi.org/10.1306/212F7E87-2B24-11D7-8648000102C1865D>
- Pickering, K. (1982a). Middle-fan deposits from the late Precambrian Kongsfjord Formation submarine fan, northeast Finnmark, northern Norway. *Sedimentary Geology* 33, 79-110. [https://doi.org/10.1016/0037-0738\(82\)90044-6](https://doi.org/10.1016/0037-0738(82)90044-6)
- Pickering, K. (1982b). A Precambrian upper basin-slope and prodelta in Northeast Finnmark, North Norway; a possible ancient upper continental slope. *Journal of Sedimentary Research*, 52, 171-186. <https://doi.org/10.1306/212F7F04-2B24-11D7-8648000102C1865D>
- Pickering, K. (1983). Transitional submarine fan deposits from the Late Precambrian Kongsfjord Formation submarine fan, NE Finnmark, N Norway. *Sedimentology*, 30. <https://doi.org/10.1111/j.1365-3091.1983.tb00664.x>
- Pickering, K. (1984). Facies, facies-associations and sediment transport/deposition processes in a late Precambrian upper basin-slope/pro-delta, Finnmark, N. Norway. *Geological Society, London, Special Publications*, 15(1), 343-362. <https://doi.org/10.1144/gsl.Sp.1984.015.01.23>
- Pickering, K. (1985). Kongsfjord Turbidite System, Norway. In A. H. Bouma, Normark, W.R. Barnes, N.E. (Ed.), *Submarine fans and related turbidite systems* (pp. 267-273). New York: Springer.
- Pickering, K., Clark, J., Smith, R., Hiscott, R., Ricci Lucchi, F., & Kenyon, N. (1995). Architectural element analysis of turbidite systems, and selected topical problems for sand-prone deep-water systems. In K. T. Pickering, R. N. Hiscott, N. H. Kenyon, F. Ricci Lucchi, & R. D. A. Smith (Eds.), *Atlas of Deep Water Environments: Architectural style in turbidite systems* (pp. 1-10). Dordrecht: Springer Netherlands.
- Pierce, C. S., Houghton, P. D. W., Shannon, P. M., Pulham, A. J., Barker, S. P., & Martinsen, O. J. (2018). Variable character and diverse origin of hybrid event beds in a sandy submarine fan system, Pennsylvanian Ross Sandstone Formation, western Ireland. *Sedimentology*, 65(3), 952-992. <https://doi.org/10.1111/sed.12412>
- Piper, D. J. W., Cochonat, P., & Morrison, M. L. (1999). The sequence of events around the epicentre of the 1929 Grand Banks earthquake: initiation of debris flows and turbidity current inferred from sidescan sonar. *Sedimentology*, 46(1), 79-97. <https://doi.org/10.1046/j.1365-3091.1999.00204.x>
- Piper, D. J. W., & Normark, W. R. (2001). Sandy Fans-From Amazon to Hueneme and Beyond. *AAPG Bulletin*, 85(8), 1407-1438. <https://doi.org/10.1306/8626cacad-173b-11d7-8645000102c1865d>
- Piper, D. J. W., & Normark, W. R. (2009). Processes That Initiate Turbidity Currents and Their Influence on Turbidites: A Marine Geology Perspective. *Journal of Sedimentary Research*, 79(6), 347-362. <https://doi.org/10.2110/jsr.2009.046>
- Pohl, F., Eggenhuisen, J. T., Tilston, M., & Cartigny, M. J. B. (2019). New flow relaxation mechanism explains scour fields at the end of submarine channels. *Nature Communications*, 10(1), 4425. <https://doi.org/10.1038/s41467-019-12389-x>
- Postma, G., Cartigny, M., & Kleverlaan, K. (2009). Structureless, coarse-tail graded Bouma Ta formed by internal hydraulic jump of the turbidity current? *Sedimentary Geology*, 219(1), 1-6. <https://doi.org/10.1016/j.sedgeo.2009.05.018>



- Postma, G., & Cartigny, M. J. B. (2014). Supercritical and subcritical turbidity currents and their deposits—A synthesis. *Geology*, 42(11), 987-990. <https://doi.org/10.1130/g35957.1>
- Postma, G., Nemec, W., & Kleinspehn, K. L. (1988). Large floating clasts in turbidites: a mechanism for their emplacement. *Sedimentary Geology*, 58(1), 47-61. [https://doi.org/10.1016/0037-0738\(88\)90005-X](https://doi.org/10.1016/0037-0738(88)90005-X)
- Prather, B. E., Keller, F. B., Chapin, M. A., & Weimer, P. (2000). Hierarchy of Deep-Water Architectural Elements With Reference to Seismic Resolution: Implications for Reservoir Prediction and Modeling. In *Deep-Water Reservoirs of the World* (Vol. 20, pp. 0): SEPM Society for Sedimentary Geology.
- Prélat, A., Covault, J. A., Hodgson, D. M., Fildani, A., & Flint, S. S. (2010). Intrinsic controls on the range of volumes, morphologies, and dimensions of submarine lobes. *Sedimentary Geology*, 232(1), 66-76. <https://doi.org/10.1016/j.sedgeo.2010.09.010>
- Prélat, A., & Hodgson, D. M. (2013). The full range of turbidite bed thickness patterns in submarine lobes: controls and implications. *Journal of the Geological Society*, 170(1), 209-214. <https://doi.org/10.1144/jgs2012-056>
- Prélat, A., Hodgson, D. M., & Flint, S. S. (2009). Evolution, architecture and hierarchy of distributary deep-water deposits: a high-resolution outcrop investigation from the Permian Karoo Basin, South Africa. *Sedimentology*, 56(7), 2132-2154. <https://doi.org/10.1111/j.1365-3091.2009.01073.x>
- Pyles, D. R. (2008). Multiscale stratigraphic analysis of a structurally confined submarine fan: Carboniferous Ross Sandstone, Ireland. *AAPG Bulletin*, 92(5), 557-587. <https://doi.org/10.1306/01110807042>
- Pyles, D. R., & Jennette, D. C. (2009). Geometry and architectural associations of co-genetic debrite–turbidite beds in basin-margin strata, Carboniferous Ross Sandstone (Ireland): Applications to reservoirs located on the margins of structurally confined submarine fans. *Marine and Petroleum Geology*, 26(10), 1974-1996. <https://doi.org/10.1016/j.marpetgeo.2009.02.018>
- Pyles, D. R., Strachan, L. J., & Jennette, D. C. (2014). Lateral juxtapositions of channel and lobe elements in distributive submarine fans: Three-dimensional outcrop study of the Ross Sandstone and geometric model. *Geosphere*, 10(6), 1104-1122. <https://doi.org/10.1130/ges01042.1>
- Reading, H. G., & Richards, M. (1994). Turbidite Systems in Deep-Water Basin Margins Classified by Grain Size and Feeder System 1. *AAPG Bulletin*, 78(5), 792-822. <https://doi.org/10.1306/a25fe3bf-171b-11d7-8645000102c1865d>
- Ricci Lucchi, F. (1975). Depositional cycles in two turbidite formations of northern Apennines. *Journal of Sedimentary Research*, 45, 3-43.
- Ricci Lucchi, F. (1995). Contessa and associated megaturbidites: long distance (120× 25 km) correlation of individual beds in a Miocene foredeep. In *Atlas of Deep Water Environments* (pp. 300-302): Springer.
- Ricci Lucchi, F., & Valmori, E. (1980). Basin - wide turbidites in a Miocene, over - supplied deep - sea plain: a geometrical analysis. *Sedimentology*, 27(3), 241-270.
- Rice, A. H. N. (1994). Stratigraphic overlap of the late Proterozoic Vadsø and Barents Sea Groups and correlation across the Trollfjorden-Komagelva Fault, Finnmark, North Norway. *Norsk Geologisk Tidsskrift*, 74, 48-57.
- Rice, A. H. N., & Frank, W. (2003). The early Caledonian (Finnmarkian) event reassessed in Finnmark: 40Ar/39Ar cleavage age data from NW Varangerhalvøya, N. Norway. *Tectonophysics*, 374(3), 219-236. [https://doi.org/10.1016/S0040-1951\(03\)00240-3](https://doi.org/10.1016/S0040-1951(03)00240-3)

- Rice, A. H. N., Gayer, R. A., Robinson, D., & Bevins, R. E. (1989). Strike-slip restoration of the Barents Sea Caledonides Terrane, Finnmark, north Norway. *Tectonics*, 8(2), 247-264. <https://doi.org/10.1029/TC008i002p00247>
- Rice, A. H. N., Ntaflos, T., Gayer, R. A., & Beckinsale, R. D. (2004). Metadolerite geochronology and dolerite geochemistry from East Finnmark, northern Scandinavian Caledonides. *Geological Magazine*, 141(3), 301-318. <https://doi.org/10.1017/s001675680300788x>
- Richards, M., Bowman, M., & Reading, H. (1998). Submarine-fan systems i: characterization and stratigraphic prediction. *Marine and Petroleum Geology*, 15(7), 689-717. [https://doi.org/10.1016/S0264-8172\(98\)00036-1](https://doi.org/10.1016/S0264-8172(98)00036-1)
- Roberts, D. (1995). Principal features of the structural geology of Rybachi and Sredni Peninsulas, Northwest Russia, and some comparisons with Varanger Peninsula, North Norway. *Norges geologiske undersøkelse, Special Publication*, 7, 247-258.
- Roberts, D. (2011). Age of the Hamningberg dolerite dyke, Varanger Peninsula, Finnmark: Devonian rather than Vendian – a revised interpretation. *Norges geologiske undersøkelse Bulletin*, 451, 32-36.
- Roberts, D., Olovyanishnikov, V., Gee, D. G., & Pease, V. (2004). Structural and tectonic development of the Timanide orogen. In *The Neoproterozoic Timanide Orogen of Eastern Baltica* (Vol. 30, pp. 0): Geological Society of London.
- Roberts, D., & Siedlecka, A. (2002). Timanian orogenic deformation along the northeastern margin of Baltica, Northwest Russia and Northeast Norway, and Avalonian–Cadomian connections. *Tectonophysics*, 352(1), 169-184. [https://doi.org/10.1016/S0040-1951\(02\)00195-6](https://doi.org/10.1016/S0040-1951(02)00195-6)
- Roberts, D., & Siedlecka, A. (2012). Provenance and sediment routing of Neoproterozoic formations on the Varanger, Nordkinn, Rybachi and Sredni peninsulas, North Norway and Northwest Russia: a review. *Norges geologiske undersøkelse, Bulletin*, 452, 1-19.
- Rohais, S., Bailleul, J., Brocheray, S., Schmitz, J., Paron, P., Kezirian, F., & Barrier, P. (2021). Depositional Model for Turbidite Lobes in Complex Slope Settings Along Transform Margins: The Motta San Giovanni Formation (Miocene—Calabria, Italy). *Frontiers in Earth Science*, 9. <https://doi.org/10.3389/feart.2021.766946>
- Røe, S. L. (2003). Neoproterozoic peripheral-basin deposits in eastern Finnmark, N. Norway: Stratigraphic revision and palaeotectonic implications. *Norsk Geologisk Tidsskrift*, 83, 259-274.
- Satur, N., Hurst, A., Cronin, B. T., Kelling, G., & Gürbüz, K. (2000). Sand body geometry in a sand-rich, deep-water clastic system, Miocene Cingöz Formation of southern Turkey. *Marine and Petroleum Geology*, 17(2), 239-252. [https://doi.org/10.1016/S0264-8172\(99\)00005-7](https://doi.org/10.1016/S0264-8172(99)00005-7)
- Shanmugam, G. (1996). High-density turbidity currents; are they sandy debris flows? *Journal of Sedimentary Research*, 66(1), 2-10. <https://doi.org/10.1306/d426828e-2b26-11d7-8648000102c1865d>
- Shanmugam, G., & Moiola, R. J. (1995). Reinterpretation of Depositional Processes in a Classic Flysch Sequence (Pennsylvanian Jackfork Group), Ouachita Mountains, Arkansas and Oklahoma. *AAPG Bulletin*, 79(5), 672-695. <https://doi.org/10.1306/8d2b1b6a-171e-11d7-8645000102c1865d>
- Siedlecka, A. (1972). Kongsfjord Formation - a late Precambrian flysch sequence from the Varanger Peninsula, Finnmark. *Norges geologiske undersøkelse*, 278, 41-80.

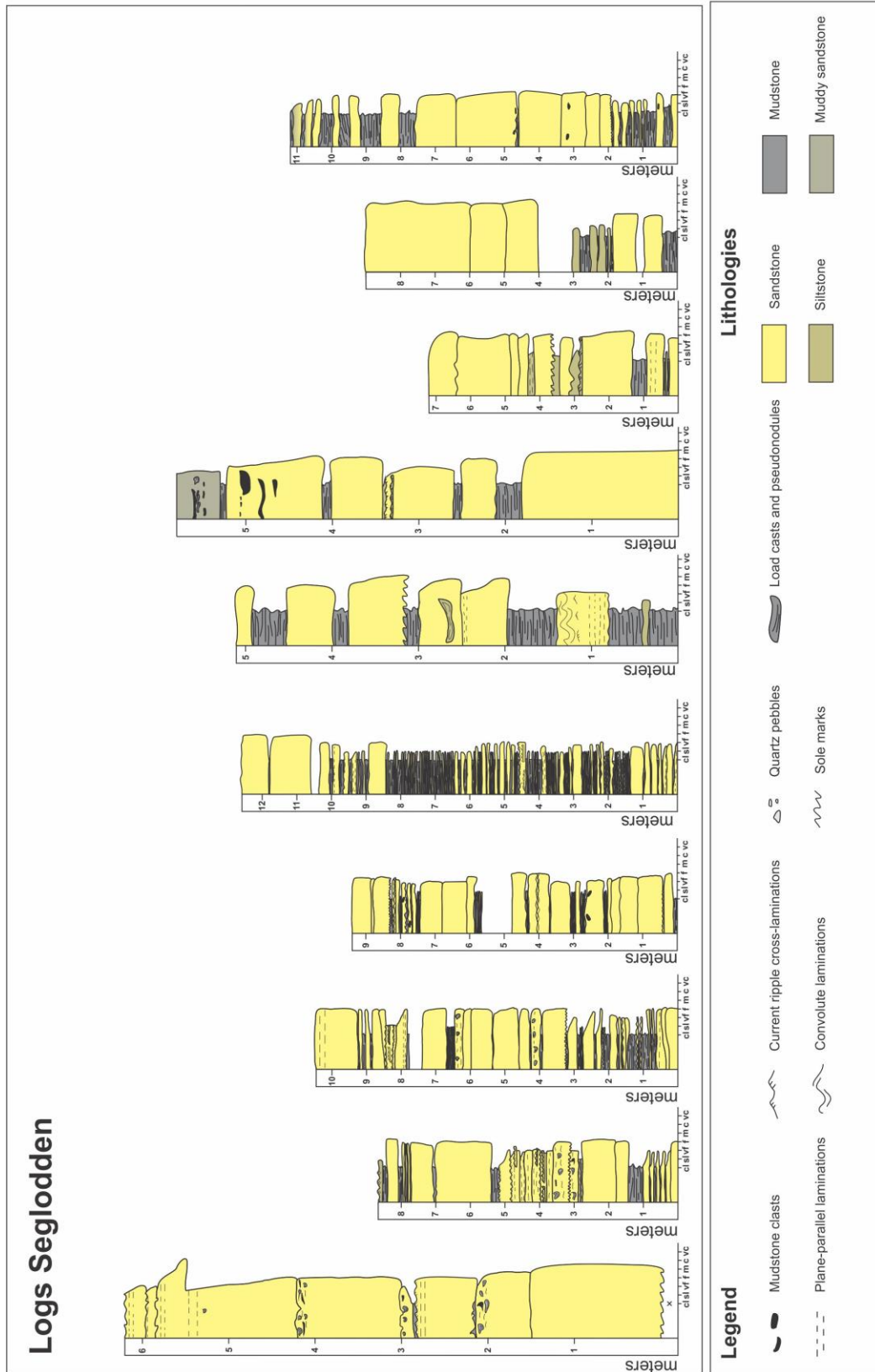
- Siedlecka, A. (1985). Development of Upper Proterozoic sedimentary basins of the Varanger Peninsula, East Finnmark, North Norway. *Geological Survey of Finland, Bulletin*, 331, 175-185.
- Siedlecka, A., & Edwards, M. B. (1980). Lithostratigraphy and sedimentation of the Riphean Båsnæring Formation, Varanger Peninsula, North Norway. *Norges geologiske undersøkelse*, 355, 27-47.
- Siedlecka, A., Pickering, K. T., & Edwards, M. B. (1989). Upper Proterozoic passive margin deltaic complex, Finnmark, N Norway. *Geological Society, London, Special Publications*, 41(1), 205-219. <https://doi.org/10.1144/gsl.Sp.1989.041.01.15>
- Siedlecka, A., & Roberts, D. (1992). *The bedrock geology of Varanger Peninsula, Finnmark, North Norway: an excursion guide*. Trondheim: Norges geologiske undersøkelse.
- Siedlecka, A., Roberts, D., Nystuen, J. P., & Olovyanishnikov, V. G. (2004). Northeastern and northwestern margins of Baltica in Neoproterozoic time: evidence from the Timanian and Caledonian Orogens. *Geological Society, London, Memoirs*, 30(1), 169. <https://doi.org/10.1144/GSL.MEM.2004.030.01.15>
- Siedlecka, A., & Siedlecki, S. (1967). Some new aspects of the geology of Varanger peninsula (Northern Norway). Preliminary report. *Norges geologiske undersøkelse*, 247, 288-306.
- Siedlecki, S., & Levell, B. K. (1978). Lithostratigraphy of the Late Precambrian Løkvikfjell Group on Varanger Peninsula, East Finnmark, North Norway. *Norges geologiske undersøkelse*, 343, 73-85.
- Sinclair, H. D., & Tomasso, M. (2002). Depositional Evolution of Confined Turbidite Basins. *Journal of Sedimentary Research*, 72(4), 451-456. <https://doi.org/10.1306/111501720451>
- Soutter, E. L., Bell, D., Cumberpatch, Z. A., Ferguson, R. A., Spychala, Y. T., Kane, I. A., & Eggenhuisen, J. T. (2021). The Influence of Confining Topography Orientation on Experimental Turbidity Currents and Geological Implications. *Frontiers in Earth Science*, 8. <https://doi.org/10.3389/feart.2020.540633>
- Sprague, A., Garfield, T., Goulding, F., Beaubouef, R., Sullivan, M., Rossen, C., Champion, K., Sickafoose, D., Abreu, V., & Schellpeper, M. (2005). Integrated slope channel depositional models: the key to successful prediction of reservoir presence and quality in offshore West Africa. *Veracruz, Mexico, Colegio de Ingenieros Petroleros de México*, 1-13.
- Spychala, Y. T., Eggenhuisen, J. T., Tilston, M., & Pohl, F. (2020). The influence of basin setting and turbidity current properties on the dimensions of submarine lobe elements. *Sedimentology*, 67(7), 3471-3491. <https://doi.org/10.1111/sed.12751>
- Spychala, Y. T., Hodgson, D. M., Flint, S. S., & Mountney, N. P. (2015). Constraining the sedimentology and stratigraphy of submarine intraslope lobe deposits using exhumed examples from the Karoo Basin, South Africa. *Sedimentary Geology*, 322, 67-81. <https://doi.org/10.1016/j.sedgeo.2015.03.013>
- Spychala, Y. T., Hodgson, D. M., & Lee, D. R. (2017a). Autogenic controls on hybrid bed distribution in submarine lobe complexes. *Marine and Petroleum Geology*, 88, 1078-1093. <https://doi.org/10.1016/j.marpetgeo.2017.09.005>
- Spychala, Y. T., Hodgson, D. M., Prélat, A., Kane, I. A., Flint, S. S., & Mountney, N. P. (2017b). Frontal and Lateral Submarine Lobe Fringes: Comparing Sedimentary Facies, Architecture and Flow Processes. *Journal of Sedimentary Research*, 87(1), 75-96. <https://doi.org/10.2110/jsr.2017.2>

- Spychala, Y. T., Ramaaker, T. A. B., Eggenhuisen, J. T., Grundvåg, S.-A., Pohl, F., & Wróblewska, S. (2021). Proximal to distal grain-size distribution of basin-floor lobes: A study from the Battfjellet Formation, Central Tertiary Basin, Svalbard. *The Depositional Record*, 00, 1-21. <https://doi.org/10.1002/dep2.167>
- Stow, D. A. V., & Shanmugam, G. (1980). Sequence of structures in fine-grained turbidites: Comparison of recent deep-sea and ancient flysch sediments. *Sedimentary Geology*, 25(1), 23-42. [https://doi.org/10.1016/0037-0738\(80\)90052-4](https://doi.org/10.1016/0037-0738(80)90052-4)
- Sumner, E. J., Peakall, J., Parsons, D. R., Wynn, R. B., Darby, S. E., Dorrell, R. M., McPhail, S. D., Perrett, J., Webb, A., & White, D. (2013). First direct measurements of hydraulic jumps in an active submarine density current. *Geophysical Research Letters*, 40(22), 5904-5908. <https://doi.org/10.1002/2013GL057862>
- Sumner, E. J., Talling, P. J., & Amy, L. A. (2009). Deposits of flows transitional between turbidity current and debris flow. *Geology*, 37(11), 991-994. <https://doi.org/10.1130/g30059a.1>
- Talling, P. J., Allin, J., Armitage, D. A., Arnott, R. W. C., Cartigny, M. J. B., Clare, M. A., Felletti, F., Covault, J. A., Girardclos, S., Hansen, E., Hill, P. R., Hiscott, R. N., Hogg, A. J., Clarke, J. H., Jobe, Z. R., Malgesini, G., Mozzato, A., Naruse, H., Parkinson, S., . . . Xu, J. (2015). Key Future Directions For Research On Turbidity Currents and Their Deposits. *Journal of Sedimentary Research*, 85(2), 153-169. <https://doi.org/10.2110/jsr.2015.03>
- Talling, P. J., Amy, L. A., Wynn, R. B., Peakall, J., & Robinson, M. (2004). Beds comprising debrite sandwiched within co-genetic turbidite: origin and widespread occurrence in distal depositional environments. *Sedimentology*, 51(1), 163-194. <https://doi.org/10.1111/j.1365-3091.2004.00617.x>
- Talling, P. J., Malgesini, G., & Felletti, F. (2013). Can liquefied debris flows deposit clean sand over large areas of sea floor? Field evidence from the Marnoso-arenacea Formation, Italian Apennines. *Sedimentology*, 60(3), 720-762. <https://doi.org/10.1111/j.1365-3091.2012.01358.x>
- Talling, P. J., Masson, D. G., Sumner, E. J., & Malgesini, G. (2012). Subaqueous sediment density flows: Depositional processes and deposit types. *Sedimentology*, 59(7), 1937-2003. <https://doi.org/10.1111/j.1365-3091.2012.01353.x>
- Tinterri, R., Laporta, M., & Ogata, K. (2017). Asymmetrical cross-current turbidite facies tract in a structurally-confined mini-basin (Priabonian-Rupelian, Ranzano Sandstone, northern Apennines, Italy). *Sedimentary Geology*, 352, 63-87. <https://doi.org/10.1016/j.sedgeo.2016.12.005>
- Tinterri, R., Mazza, T., & Magalhaes, P. M. (2022). Contained-Reflected Megaturbidites of the Marnoso-arenacea Formation (Contessa Key Bed) and Helminthoid Flysches (Northern Apennines, Italy) and Hecho Group (South-Western Pyrenees). *Frontiers in Earth Science*, 10. <https://doi.org/10.3389/feart.2022.817012>
- Tinterri, R., Muzzi Magalhaes, P., Tagliaferri, A., & Cunha, R. S. (2016). Convolute laminations and load structures in turbidites as indicators of flow reflections and decelerations against bounding slopes. Examples from the Marnoso-arenacea Formation (northern Italy) and Annot Sandstones (south eastern France). *Sedimentary Geology*, 344, 382-407. <https://doi.org/10.1016/j.sedgeo.2016.01.023>
- Tinterri, R., & Piazza, A. (2019). Turbidites facies response to the morphological confinement of a foredeep (Cervarola Sandstones Formation, Miocene, northern Apennines, Italy). *Sedimentology*, 66(2), 636-674. <https://doi.org/10.1111/sed.12501>

- Tinterri, R., & Tagliaferri, A. (2015). The syntectonic evolution of foredeep turbidites related to basin segmentation: Facies response to the increase in tectonic confinement (Marnoso-arenacea Formation, Miocene, Northern Apennines, Italy). *Marine and Petroleum Geology*, 67, 81-110. <https://doi.org/10.1016/j.marpetgeo.2015.04.006>
- Van Den Berg, J. H., Van Gelder, A., & Mastbergen, D. R. (2002). The importance of breaching as a mechanism of subaqueous slope failure in fine sand. *Sedimentology*, 49(1), 81-95. <https://doi.org/10.1111/j.1525-139X.2006.00168.x-i1>
- Walker, R. G. (1966). Shale Grit and Grindslow shales; transition from turbidite to shallow water sediments in the upper Carboniferous of northern England. *Journal of Sedimentary Research*, 36(1), 90-114. <https://doi.org/10.1306/74d71415-2b21-11d7-8648000102c1865d>
- Walker, R. G. (1978). Deep-water sandstone facies and ancient submarine fans: models for exploration for stratigraphic traps. *AAPG Bulletin*, 62, 932-966.
- Wynn, R., Kenyon, N., Masson, D., Stow, D., & Weaver, P. (2002). Characterization and Recognition of Deep-Water Channel-Lobe Transition Zones. *AAPG Bulletin*, 86. <https://doi.org/10.1306/61EEDCC4-173E-11D7-8645000102C1865D>
- Wynn, R. B., Masson, D. G., Stow, D. A. v., & Weaver, P. P. e. (2000). The Northwest African slope apron: a modern analogue for deep-water systems with complex seafloor topography. *Marine and Petroleum Geology*, 17(2), 253-265. [https://doi.org/10.1016/S0264-8172\(99\)00014-8](https://doi.org/10.1016/S0264-8172(99)00014-8)
- Zhang, L.-F., & Dong, D.-Z. (2020). Thickening-upward cycles in deep-marine and deep-lacustrine turbidite lobes: examples from the Clare Basin and the Ordos Basin. *Journal of Palaeogeography*, 9(1), 11. <https://doi.org/10.1186/s42501-020-00059-9>
- Zhang, L., & Li, Y. (2020). Architecture of deepwater turbidite lobes: A case study of Carboniferous turbidite outcrop in the Clare Basin, Ireland. *Petroleum Exploration and Development*, 47(5), 990-1000. [https://doi.org/10.1016/S1876-3804\(20\)60111-2](https://doi.org/10.1016/S1876-3804(20)60111-2)

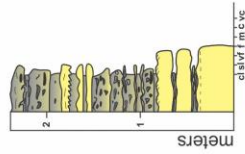
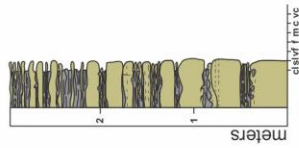


# Appendix 1: Stratigraphic logs

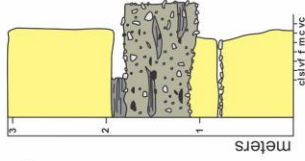
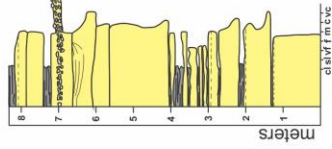
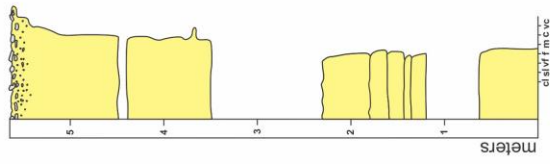
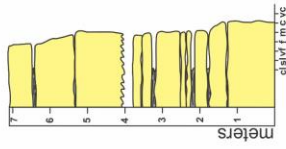
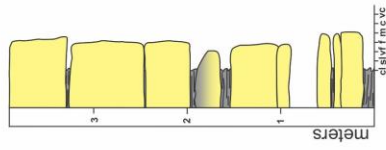
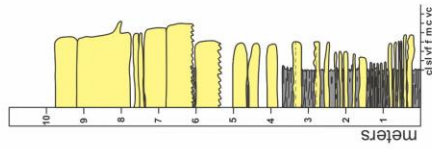




## Logs Veidnes



## Logs Nålneset



### Legend

- Mudstone clasts
- Plane-parallel laminations

### Lithologies

- Sandstone
- Mudstone
- Siltstone
- Muddy sandstone

- Load casts and pseudonodules
- Quartz pebbles

- Current ripple cross-laminations
- Convolute laminations
- Sole marks

# Appendix 2: Digital outcrop models

